Tampere University

Anca Andreea Telembeci

SURFACE FUNCTIONALIZATION OF A SILICON NANOWIRE FIELD-EFFECT TRANSISTOR (SINW-FET) FOR miRNA DETECTION

Faculty of Computing and
Electrical Engineering
Master's Thesis
May 2019

ABSTRACT

Anca Andreea Telembeci: Surface functionalization of a silicon nanowire field-effect transistor (SiNW-FET) for miRNA detection
Master of Science Thesis
Tampere University
Master's Degree Programme in Computing and Electrical Engineering
Major: Biomedical Engineering
May 2019

Micro RNAs (miRNAs) are promising biomarkers of various physiological and pathological processes. Since miRNAs are found in very low concentrations (e.g., attomolar), their detection requires highly sensitive devices. Recently, silicon nanowire field-effect transistors (SiNW-FETs) have drawn attention due to their high sensitivity and low detection limits. SiNW-FETs can be tailored to detect miRNA by employing surface functionalization strategies. The miRNA recognition event that occurs at the sensor surface is transduced by the SiNW-FET in a detectable electronic signal.

The main goals of the thesis are to propose and discuss different possibilities to functionalize a SiNW-FET for miRNA detection, and to experimentally evaluate the potential to detect miRNA with provided SiNW-FET devices. Additionally, different methods for regeneration of a SiNW-FET for miRNA detection are proposed and discussed since, in the future, the SiNW-FETs are meant to be integrated in *in vitro* cell culture platforms. Ideally, sensors for *in vitro* cell platforms would allow multiple sampling that can be enabled through surface regeneration.

The thesis is divided into two major parts: a theoretical and an experimental approach. In the theoretical part, four functionalization methods are proposed. Two methods involve treating SiNW-FETs with (3-aminopropyl)triethoxysilane (APTES) and attaching DNA probes via glutaraldehyde (GA) or L- ascorbic acid (AA) crosslinkers. AA-based functionalization is a novel method that has not been yet reported for design of miRNA biosensor. The other two methods allow DNA probes to be directly attached to (3-glycidoxypropyl)trimethoxysilane- (GPTMS) or 1,1´-carbonyldiimidazole- (CDI) modified silicon nanowires (SiNWs).

To enable miRNA SiNW-FET reusability, the thesis proposes thermal-, chemical-, and enzymes-based methods to detach the miRNA molecules from the DNA probes. The enzyme-based regeneration proposed in the thesis is a novel approach that has not been yet reported in miRNA SiNW-FET regeneration.

Next, the provided SiNW-FET devices were electrically characterized in order to evaluate their performance. In addition, the main environmental disturbances were tested to understand how the external factors affect the sensors.

For miRNA detection experiments, the functionalization method based on APTES and GA was employed to attach DNA probes on the surface of SiNW-FETs. Even though the final miRNA tests revealed possible positive results, a clear statement about whether miRNA was detected cannot be made due to the challenges related to the SiNW-FETs (e.g., gate current leakages) and uncertainties of the functionalization scheme (e.g., hydrophobicity of the resulted surface). Nevertheless, the thesis's proposed functionalization and regeneration approaches, the miRNA handling and experiments protocols, and the test observations offer valuable information for future research.

Keywords: microRNA, silicon nanowire field-effect transistors (SiNW-FET), surface functionalization, regeneration, biomarker, DNA probe.

PREFACE

This master's thesis was conducted in the Faculty of Medicine and Health Technology of Tampere University, in the Micro- and Nanosystem Research group, as a part of the Woodbone project financed by Academy of Finland.

I wish to express my sincere gratitude to my supervisors Project Researcher Mariaana Savia and Professor Pasi Kallio for their guidance and patience during the thesis process, and most importantly for the opportunity to work in this project. Additionally, I would like to also thank the researchers who advised me during this work including Jarmo Verho, Anne Skogberg, Sagar Bhalerao, Joni Leivo, and Joose Kreutzer.

Finally, my special thanks and gratefulness to my partner, Tommi Halonen, for his constant support, love, and encouragement.

Tampere, Finland, 15 May 2019

Anca Andreea Telembeci

CONTENTS

LIST OF FIGURES

LIST OF TABLES

LIST OF SYMBOLS AND ABBREVIATIONS

A	Adenine
AA	L-ascorbic acid
APTES	(3-aminopropyl)triethoxysilane
AT	Adenine-Thymine
ATP	Adenosine triphosphate
AuNPs	Gold nanoparticles
C	Cytosine
CDI	1,1´-carbonyldiimidazole
CMOS	Complementary metal oxide semiconductor
CVD	Chemical vapor deposition
DI water	Deionized water
DMSO	Dimethyl sulfoxide
DNA	Deoxyribonucleic acid
EDTA	Ethylenediaminetetraacetic acid
EIS	Electrochemical impedance spectroscopy
G	Guanine
GA	Glutaraldehyde
GC	Guanine-cytosine
GPTMS	(3-glycidoxypropyl)trimethoxysilane
hASCs	Human adipose-derived stem cells
HCl	Hydrochloric acid
I_{DS}	Drain-source current
I_G	Gate current
ISFET	Ion selective field-effect transistor
LNA	Locked-nucleic acid
LOD	Limit of detection
miR-218	miRNA molecule upregulated during osteogenic differentiation
miRNA	Micro ribonucleic acid
MOSFET	Metal-oxide-semiconductor field effect transistor
mRNA	Messenger RNA
mRNA	Messenger RNA
PBS	Phosphate buffer saline
PEC	Photoelectrochemical
PNA	Peptide nucleic acid
POC	Point-of-care
pri-miRNAs	Primary miRNA
qRT-PCR	Qualitative reverse transcription-polymerase chain reaction
R	Resistance
RISC	RNA-induced silencing complex
RNA pol II	RNA polymerase II
RNA	Ribonucleic acid
RNase H	Ribonucleases H
SERS	Surface-Enhanced Raman Spectroscopy
SiNW	Silicon nanowire
SPR	Surface plasmon resonance
ssDNA	Single-stranded DNA
T	Thymine
T_m	Melting temperature
UTR	Untranslated region
V_{DS}	Drain-source voltage
V_G	Gate voltage
λ_D	Debye length

1. INTRODUCTION

Recently, research on microRNAs (miRNAs) has expanded rapidly due to the discovery that miRNAs engage in various regulatory functions and are involved in different physiological and pathological processes. For example, specific miRNAs have been identified as modulators of cell proliferation and apoptosis and of stem cell maintenance and differentiation (Huang, 2017). Additionally, in disease research, miRNAs have been discovered to be involved in cancers and in cardiovascular, autoimmune, and neurodegenerative diseases (Almeida, 2011). MicroRNA molecules are found intracellularly, but also circulate in various body fluids, including blood plasma, serum, urine, and saliva (Chen, 2008; Mitchell, 2008; Lautner & Gyurcsányi, 2014). They are, therefore, considered valuable biomarkers in molecular diagnostics and prognostics (Bartel, 2004; Chen, 2018; Lautner & Gyurcsányi, 2014).

Biosensor systems allow the identification of miRNAs from cell cultures or body fluids. Generally, biosensors integrate a specific bioreceptor probe with a physicochemical transducer. The integration of the bioreceptor probes into transducers is done by employing different chemical functionalization schemes. Through functionalization, the properties of the transducer surface are altered by the introduction of various chemical reactive groups that allow immobilization of the bioreceptor molecules on the transducer surface. The bioreceptor molecules suitable for miRNA detection are complementary oligonucleotide probes, such as deoxyribonucleic acid (DNA), ribonucleic acid (RNA), peptide nucleic acid (PNA), or locked-nucleic acid (LNA) molecules. The interaction between the miRNA target analyte and its complementary DNA probe can be transduced into a readable electronic signal.

Since circulating miRNAs are found in very low concentrations, attomolar (aM) to picomolar (pM) levels (Tsujiura, 2010), the detection method employed must be very sensitive. Silicon nanowire field-effect transistors (SiNW-FETs) have drawn a great deal of attention in the field of biosensors for their high sensitivity and low limits of detection (LOD), real-time detection ability, possibility of being integrated into arrays, and multiplex detection capabilities. Additionally, SiNW-FET-based measurement is non-invasive, thus

it may be suitable for cell studies, for example, monitoring cell differentiation. The differentiation of cells can be monitored by detecting miRNA biomarkers involved in this process (e.g., miR-218 was found to be upregulated during osteogenic differentiation).

The high surface-to-volume ratios of the NW structures make the SiNW-FETs extremely sensitive sensors. Thus, SiNW-FETs offer the possibility of miRNA detection down to the aM (10^{-18}) or even zeptomolar (zM = 10^{-21}) range, as previously reported by several research groups (Gao, 2013a; Gao, 2013b; Lu, 2014a, Lu, 2014b; Shen, 2013; Zhang, 2009; Zhang, 2011). Therefore, for this thesis, a SiNW-FET was chosen as transducer. The SiNW-FET sensors used in the experimental part of the thesis were obtained from Shanghai Institute of Microsystem and Information Technology, China.

The aims of this thesis are divided into two major components: a theoretical background and an experimental approach. The theoretical component includes the review of miRNAs, the proposal of various methods suitable for chemical functionalization of the SiNW-FETs for detection of miRNA, and the proposal of possible regeneration methods of the miRNA SiNW-FET sensors. Since the SiNW-FETs for miRNA detection represent a relatively new field of research, the information about the methods used for functionalization and regeneration is scarce. Therefore, the functionalization and regeneration methods proposed in this thesis are either reported from miRNA biosensor research, or represent novel approaches previously used in different types of applications.

The rest of the thesis is organized as follows. Chapter 2 presents miRNA's structure, its biogenesis, its involvement in physiological and pathological processes, and the types of the bioreceptors used in detecting it. The most relevant methods for miRNA detection are reviewed as well. Chapter 3 introduces the SiNW-FET sensor operation principle, the fabrication methods, and the specific performance parameters, while Chapter 4 discusses four functionalization methods proposed for miRNA SiNW-FET biosensors. Chapter 5 presents the primary regeneration aspects of an oligonucleotide-based biosensor and discusses four regeneration methods for a miRNA SiNW-FET biosensor.

The experimental part focuses on the electrical characterization of SiNW-FET devices, testing of the effects of different disturbances on the operation of the sensors, testing of a chosen functionalization method, and measurements of miRNA. The materials and the methods used in the experiments are presented in Chapter 6, and in Chapter 7 the results obtained are presented and discussed. Lastly, the conclusions of the thesis are presented in Chapter 8.

2. MIRNA AS BIOMARKER

This chapter presents microRNAs (miRNAs), their structure, and their biogenesis. Section 2.1 introduces various ways in which miRNAs are involved in cell physiology processes, and Section 2.2 briefly discusses miR-218, a specific miRNA molecule, or biomarker, that is involved in osteogenesis. A biomarker can be defined as a measurable indicator of a particular disease state or some other physiological state of an organism (Chen, 2018). Since biosensing applications typically require the use of bioreceptor molecules, Section 2.3 presents bioreceptors for miRNA. There are various ways to measure miRNAs, thus Section 2.4 introduces the primary methods used in research.

2.1 miRNAs and their role in cell physiology

MicroRNAs, in their mature shape, are a class of small, non-coding (i.e., not translated into a protein), single-stranded ribonucleic acid (RNA) molecules of about 18–25 nucleotides that can be found in plants, animals, and even viruses (Lautner & Gyurcsányi, 2014; Peng, 2016). miRNA was first described in the early 1990s by Lee *et al.,* who identified the short lin-4 RNA that is today recognized as a member of a large class of miRNAs that have important regulatory roles (Lee, 1993; Wahid, 2010). The main function of miRNAs is to inhibit protein synthesis of protein-coding genes, either by degrading messengerRNA (mRNA) or by inhibiting the translation process (Almeida, 2011).

In recent years, the importance of gene regulation directed by miRNAs has drawn attention as more types of miRNAs and their regulatory targets have been discovered. Recent discoveries about miRNA show that they exhibit various regulatory functions, including control of cell proliferation, apoptosis, and differentiation and are associated with multiple pathologies, such as cancers, cardiovascular diseases, and inflammatory diseases. (Bartel, 2004; Lautner & Gyurcsányi, 2014.) Therefore, their value as specific biomarkers in molecular diagnostics and prognostics raised considerable interest (Lautner & Gyurcsányi, 2014).

Although most miRNAs are found intracellularly, there is evidence that some can be found in body fluids (blood plasma, serum, urine, saliva) as circulating miRNAs (i.e., extracellular miRNAs) (Chen, 2008; Mitchell, 2008; Lautner & Gyurcsányi, 2014). In the presence of nucleases, RNA molecules are rapidly degraded, but the fact that circulating miRNAs are stable in blood indicates that these are somehow protected (Mitchell, 2008).

Evidence has indicated that circulating miRNAs are encapsulated in exosomes (diameter of 40–100 nm), microvesicles (diameter of 0.1–1 μm), or apoptotic bodies (diameter of 0.5–2 μm) formed during the process of apoptosis, or cell death (Bhome, 2018; Rayner & Hennessy, 2013). Estimates are that concentration of circulating miRNAs are at attomolar (aM) – to picomolar (pM) levels (Tsujiura, 2010). Thus, the miRNA detection or quantification method must have high sensitivity.

2.1.1 Biogenesis of miRNA

The biogenesis of miRNAs is a unique process in the cell physiology. As a starting point, miRNAs are produced inside the cell nucleus by a transcription process mediated by a multiprotein complex called RNA polymerase II (RNA pol II) into a long primary miRNA transcript (pri-miRNAs) (see Figure 1). After transcription, pri-miRNAs are further processed inside the nucleus and cleaved by the Drosha enzyme. (Huang, 2017). The pre-miRNAs are then transported outside the nucleus into the cytoplasm by the protein exportin-5 (EXP-5) shuttle system. Once in the cytoplasm, they are processed further into mature single-stranded miRNAs by Dicer proteins and loaded onto Argonaute (ago) proteins to produce RNA-induced silencing complex (RISC). (Wahid, 2010.) These mature miRNAs bind to the 3´ untranslated region (3´UTR) of specific mRNAs through partial or complete complementary pairing between the mRNA and miRNA sequences. Thus, the silencing system formed by imperfect or perfect base pairing between mRNA and miRNA enables miRNAs to induce inhibition of the translational process and degrade the target mRNA (Huang, 2017).

The miRNA-RISC complex binds to the complementary mRNA sequence, followed by the enzymatic cleavage of the target mRNA. The term “silenced” refers to the process of rendering the mRNA as nonfunctional or downregulation of gene expression. (Wahid, 2010.)

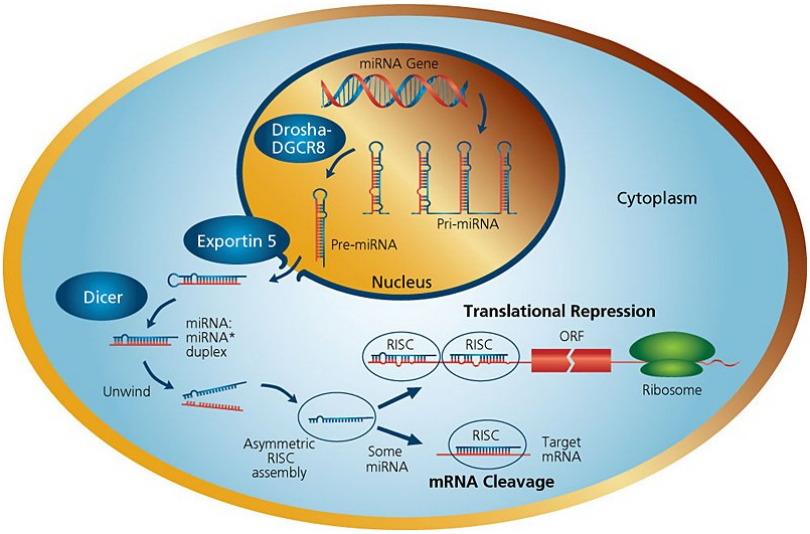

Figure 1. *Biogenesis of miRNA (Sigma-Aldrich, 2019b)*

Currently, thousands of miRNAs have been identified in humans and other species, and data related to them are stored in online databases such as miRBase (miRbase, 2019). As mentioned before, miRNAs are involved in different physiological and pathological processes. Specific miRNAs have been implicated as the modulators of cell proliferation and apoptosis and of stem cell maintenance and differentiation (Huang, 2017). In disease research, miRNAs have been identified as related to different pathologies such as different cancers, cardiovascular diseases (i.e., heart failure, cardiac hypertrophy, and atherosclerosis), autoimmune diseases (i.e., psoriasis, rheumatoid arthritis, and lupus), and neurodegenerative diseases (i.e., Alzheimer's, Parkinson's, and Huntington's disease). (Almeida, 2011.)

2.2 miRNA involvement in osteogenesis

Osteogenesis is a very complex and multi-step process that involves the differentiation of mesenchymal stem cells into osteoblasts and osteocytes and the crosstalk between different cell types for formation and remodeling of bone. Generally, the regulatory signaling pathway during osteogenesis includes a wide variety of components, such as growth factors, transcription factors, and miRNAs, which can control osteogenic differentiation through positive or negative regulation. (Peng, 2016.) While the importance of growth factors in osteogenic differentiation has long been known, recently miRNAs have been found to be important regulators as well, being involved in multiple signaling pathways.

In previous studies, Hassan *et al.* found that miR-218 is an enhancer of osteogenic differentiation in bone marrow-derived mesenchymal stem cells, while Zhang *et al.* found it

to be upregulated during osteogenic differentiation of human adipose-derived stem cells (hASCs) (Hassan, 2012; Zhang, 2014). More details about the mechanism through which miR-218 enhances the osteogenesis of hASCs can be found in the study of Zhang *et al.* (Zhang, 2014). For this thesis, miR-218 was chosen as the biomarker of osteogenic differentiation.

2.3 miRNA bioreceptors

Generally, hybridization is a process used in biology for detecting specific nucleotide sequences, but the process can also be useful in the field of nucleic acid-based biosensors (Alberts, 2002). As miRNA is a single-stranded nucleotide, it can be detected with different sensor systems based on its ability to hybridize with a complementary bioreceptor. The probe molecules used as these bioreceptors can be designed complementary deoxyribonucleic acid (DNA) or RNA or even synthetic molecules analogous to the natural nucleic acids, such as peptide nucleic acid (PNA) or locked-nucleic acid (LNA) molecules. In this section, the structures and differences among DNA, RNA, PNA, and LNA molecules are presented.

2.3.1 Natural bioreceptor molecules: DNA and RNA

A DNA molecule has a three-dimensional structure composed of two long strands that coil around each other forming a double helix (see Figure 2) (Lodish, 2008). Each strand of the DNA molecule is composed of individual units linked together called nucleotides. A nucleotide unit is composed of a five-carbon sugar (pentose) to which one or more phosphate groups (PO_4) and a nitrogen-containing base are attached. The sugar in DNA's structure is a deoxyribose attached to a single phosphate group, hence the name deoxyribonucleic acid. (Alberts, 2002.)

There are two types of bases in the DNA structure: purines (adenine, A, and guanine, G) and pyrimidines (cytosine, C, and thymine, T). These bases can bind to each other, or hybridize, in a very specific manner, as described by the Watson-Crick base pairing model, such that adenine always binds thymine, and guanine always binds cytosine, hence the term complementary base pairing (see Figure 2). (Glick, 2010.) The nucleotides with these bases are covalently linked together in chains through their sugars and phosphates, forming the backbone of the DNA strand. The complementary base-pairing enables an arrangement in which each base-pair has a similar width, thus holding the phosphate backbones at constant distance from each other along the DNA molecule. (Alberts, 2002.) While the backbone of each DNA strand is formed through covalent

bonding of nucleotides, the two strands are held together through hydrogen bonds, namely the three hydrogen bonds between G and C, and the two hydrogen bonds formed between A and T.

Additionally, for DNA strands to form the double helix, the two strands need to be anti-parallel, meaning that the polarity of one strand is oriented opposite to that of the other strand. The polarity in the DNA chain is indicated by referring to one end as the 3'-end (the hydroxyl end) and the other as the 5'-end (the phosphate end). Hence, the sequence of nucleotides is exactly complementary to the nucleotide sequence of its opposite strand (Alberts, 2002). DNA can be used as bioreceptor in biosensor development either in double-standed form, or as a single strand, called single-stranded DNA (ssDNA).

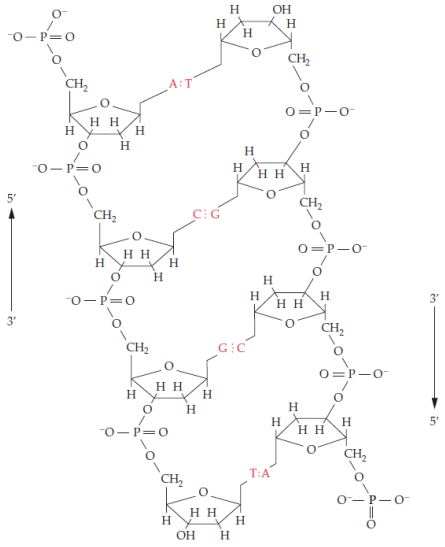

Figure 2. *Chemical structure of DNA double strand, and the complementary (Watson-Crick) base pairing (A-T and C-G) that held the strands together. (Glick, 2010)*

In contrast with the DNA molecule, RNA contains the sugar ribose (hence the name ribonucleic acid), which differs from deoxyribose by the presence of an additional hydroxyl (-OH) group. Additionally, RNA contains a different base than DNA, uracil (U). Uracil is the equivalent of thymine from DNA but differs only by the lack of a -CH_3 group. (Alberts, 2002.) As their primary roles, DNA holds the genetic material of an organism, and RNA is involved in RNA synthesis (transcription) and protein synthesis (translation). Step-wise, a structural gene synthesizes a messenger RNA molecule (mRNA), then the mRNA molecule interacts with ribosomes, transfer RNAs, and enzymes to produce a protein molecule. In contrast with standard RNA, miRNA is not involved in protein translation. (Glick, 2010.) Due to the presence of the phosphate components in their backbones, DNA, RNA, and miRNA are negatively charged molecules.

2.3.2 Synthetic bioreceptor molecules: PNA and LNA

Peptide nucleic acid molecules (PNA) (see Figure 3A) are nucleic acid analogs of DNA molecules in which the phosphate backbone is replaced by a synthetic backbone composed of (2-aminoethyl)glycine repeating units linked by peptide bonds (Egholm, 1992). The nucleotide bases known from the natural DNA molecule (A, C, G, and T) are joined to the backbone of PNA by methylene carbonyl linkages. However, unlike DNA, PNA does not contain any phosphate groups or pentose sugar moieties, which renders PNA as electrically neutral molecules (Egholm, 1992; Shakeel, 2006). The 5´ and 3´ ends of the DNA molecule correspond to the PNA molecule's as N-terminus (or amine terminus) and C terminus (or carboxy terminus), respectively (Shakeel, 2006). Due to the structural similarity between DNA and PNA, PNA can bind to its complementary nucleic acid sequence, obeying the Watson-Crick base-pairing rules (Singh, 2010).

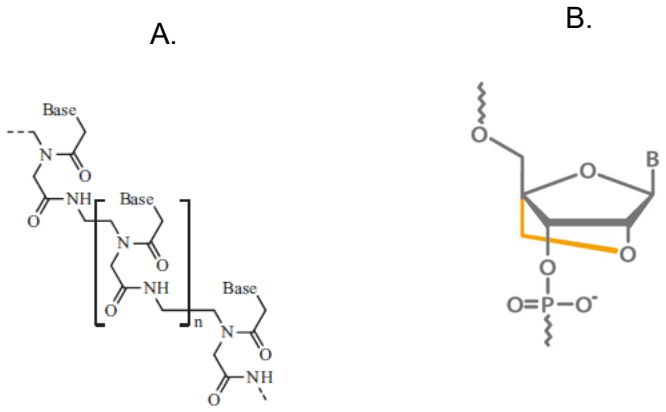

Figure 3. *Structure of PNA (A), and LNA (B) molecules. (B)The ribose ring is connected or locked by the methylene bridge (orange) between 2´-O and 4´-C atoms. (Gupta, 2017; Exiqon, 2009)*

As with the above-mentioned PNA molecule, the LNA molecules is also a synthetic oligonucleotide (see Figure 3B) that was developed in the late 1990s and is characterized by the presence of a methylene bridge between the 2´-oxygen and 4´-carbon atoms in the furanose ring. This conformation has a locking effect and restricts the flexibility of the furanose ring, which is the reason for PNA's enhanced hybridization properties.

Because the sugar moiety is locked in an N-type sugar ring conformation through the bridge, the LNA molecule has a structure similar to that of RNA. This conformational restriction has an effect in the preorganization of the LNA backbone that results in an energetically favorable duplex formation. The melting temperature of an LNA molecule is raised by 2–8°C for each nucleotide incorporated into it in comparison to native-state

DNA oligonucleotides, making it highly suitable for applications where high affinity is desirable. (Lundin, 2013.)

Compared to natural DNA and RNA molecules, the synthetic PNA molecule is electrically neutral (due to its lack of the anionic phosphate backbone), thus the repulsion between PNA and miRNA molecules is less than that between DNA and miRNA, resulting in an enhanced hybridization efficiency. Additionally, PNA–DNA and PNA–RNA duplexes have higher thermal stability than DNA–DNA and DNA – RNA duplexes (Shakeel, 2006). Similarly, LNA molecules show increased hybridization stability, specifically due to their locked structure, and high selectivity, being capable of single nucleotide discrimination. Therefore, PNA and LNA are both attractive as candidate complementary probes for a miRNA biosensor. Additionally, since they are synthetic molecules, they have increased resistance to the activity of different exo- and endonucleases (Exiqon, 2009; Zhang & Apella, 2010), which is in contrast to natural DNA and RNA molecules, which are susceptible to enzymatic degradation. However, the higher costs and the long time needed to synthesize PNA and LNA are some of the main disadvantages of these molecules.

2.4 miRNA detection methods

Owing to their important role in biological and pathological processes, miRNAs have generated great interest in the field of research and diagnostics, thus opening a vast field for biosensors or other methods for detecting miRNA. The methods for miRNA detection that have been developed in the recent years have been grouped and categorized by Kilic *et al.* as follows: conventional methods (e.g., Northern blotting, qualitative reverse transcription-polymerase chain reaction (qRT-PCR), and microarray technology), electrochemical methods (e.g., amperometric, voltametric, impedimetric, and NW-based FETs), optical methods (e.g., SPR), and other emerging technologies (Kilic, 2018). These main methods are summarized in Table 1, and this section describes the most used techniques and categories.

Generally, as the initial step in the detection of miRNA, oligonucleotides are first extracted from sources such as whole organisms, cell cultures, tumors, or body fluids (e.g., plasma or serum) (see Figure 4). These are then quantified and amplified if the amounts obtained from original sources are very low. MicroRNAs have properties that make the processes of extraction (or isolation), amplification, and detection quite challenging (Kilic, 2018). These processes of isolation and amplification increase the assay time, thus direct detection in serum or other biological samples is desired. It is important to keep in mind, however, that in real biological samples, the quantity of miRNA molecules can be

extremely low (e.g., at the aM level), therefore the method of detection has to be highly sensitive. Additionally, these types of samples contain a mixture of pre-miRNAs and mature miRNAs such that the complementary oligonucleotide probe can hybridize nonspecifically with the pre-miRNAs, therefore leading to false-positive detection of mature miRNA. (Hamidi-Asl, 2013.)

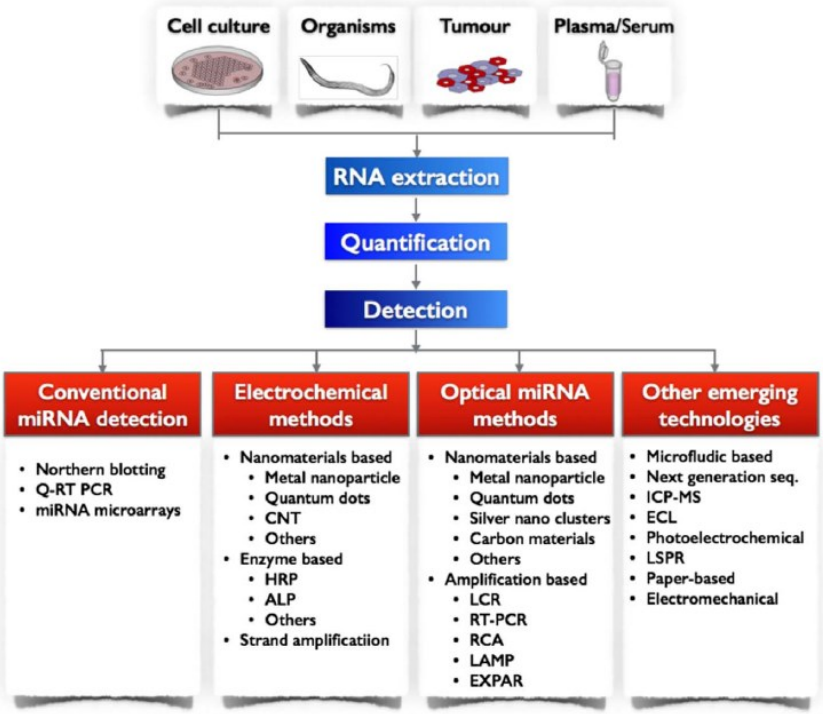

Figure 4. *miRNA detection methods and the steps prior detection: extraction from different sources (cells, organisms, tumors, plasma/serum), quantification, and detection. (Killic, 2018)*

Table 1. *miRNA detection methods. (reproduced from Kilic, 2018)*

Methods	Technologies	Sensitivity	Advantages	Disadvantages	Approaches	References
Conventional	Northern Blotting	nM-fM	○ cheap	○ sample degradation ○ low sensitivity ○ requires high amount of miRNA	○ LNA based detection ○ Cross-linked RNA probes to nylon membranes	
	qRT-PCR	nM-fM	○ sensitive to 1 nucleotide difference	○ low selectivity ○ low throughput ○ expensive instrumentation	○ TaqMan miRNA assay ○ TagManqRT-PCR	
	Microarrays	fM-pM	○ high throughput	○ low selectivity and specificity ○ need of fluorescent labels	○ Fluorescent labelling of miRNAs ○ Quantum dots (QDs) labelling	
Electrochemical	Amperometric & voltammetric	fM-aM	○ easy to use ○ high sensitivity ○ miniaturization possibility	○ need of labels ○ difficulties with real-time detection		Kilic, 2012; Kilic, 2013; Labib & Berezovski, 2015
	Potentiometric	20 pM		○ might need RT-PCR prior electrochemical sensing		Rothberg, 2011
	Conductometric	5 fM	○ sensitivity	○ use of enzymes		Fang, 2017
	Impedimetric	fM - pM	○ label free		○ EIS	Gao & Peng, 2011; Gao, 2013b; Shen, 2013
	FET-based biosensors	aM - fM	○ label free ○ real-time		○ SiNW-FETs ○ Carbon nanotube-based FETs	Zhang, 2009; Zhang, 2011; Gao, 2013a; Ramnani, 2013; Lu, 2014a; Lu, 2014b

Methods	Technologies	Sensitivity	Advantages	Disadvantages	Approaches	References
Optical	SPR	fM - pM	○ simple	○ low sensitivity ○ low selectivity ○ need of amplification strategies	○ Au nanoparticles ○ hairpin assembly (CHA) ○ Hybridization chain reaction (HCR) ○ Streptavidin-biotin enhancement ○ DNA-RNA-Ab assay	Fang, 2006; Li, 2014; Li, 2016; Šípová, 2010; Wang, 2016
	Fluorescence-based	fM - aM	○ measurement inside cells	○ low sensitivity ○ low selectivity	○ QDs ○ Au nanoparticles ○ Graphene-oxide quenchers ○ Organic dyes	Dong, 2012; Geißler, 2010
	SERS	fM	○ specificity ○ high sensitivity	○ lack of spectral reproducibility ○ not real-time detection	○ Silver nanorods arrays	Driskell, 2008; Kim, 2019
Other methods	Photoelectrochemical (PEC)	fM	○ sensitive	○ needs labeling ○ need of enzyme	○ Au nanoparticles ○ QDs	Yin, 2014
	Paper-based or "lab-on-paper"	pM	○ low-cost	○ low selectivity and sensitivity	○ Dipstick ○ Lateral flow assays	Deng 2017; Gao, 2014; Yildiz, 2013
	Eelectromechanical	pM - aM	○ high sensitivity	○ low selectivity	○ AFM (atomic force microscopy) ○ piezoelectric cantilever	Husale, 2009; Johnson & Mutharasan, 2012

Conventional Northern blotting, qRT-PCR, and microarrays are the most established methods for miRNA detection, but they are generally used in the study of gene expression and are not considered biosensors. Despite their robustness and well-established operation, the conventional methods have a few drawbacks such as low throughput, low sensitivity, and the possibility of sample contamination with RNAses. They are also time consuming and require expensive equipment, large miRNA samples, and trained personnel. However, since these methods are not included in the biosensor categorization, they will not be discussed in this work, and the focus is instead on presentation of electrochemical, optical, and other possible technologies.

In contrast with the above-mentioned conventional miRNA detection methods, biosensors have the advantage of being more sensitive and selective, having higher throughput and lower costs, and offering the possibility of miniaturization, which allows portability. Generally, a biosensor is composed of two elements: a target capture element, such as a biological complementary probe that can catch and hybridize with the target miRNA, and a transducer that converts the biological signal resulting from, for example, hybridization, into a measurable electrical or optical signal. Electrochemical and optical transducers are the main types of transducers used in miRNA biosensors and are introduced in the following sections.

2.4.1 Electrochemical methods

Compared to conventional methods for miRNA detection, electrochemical methods (see Table 1) have the advantages of their lower costs, higher sensitivity and selectivity, and faster response time, while also offering the possibility of miniaturization, which makes them suitable for point-of-care (POC) applications. The principle of detection in this approach is related to the measurement of changes in the electrode properties that occur upon hybridization of the target miRNA with its complementary probe. Based on which electrical properties are measured, the electrochemical methods can be further classified as amperometric, voltammetric, potentiometric, impedimetric, or FET-based. (Kilic, 2018.)

In amperometry, the detection of the analyte is accomplished by measuring the current resulting from hybridization while a constant potential is applied, while in voltammetry the current is measured as the potential is ramped up at different rates (Labib & Berezovski, 2015; Kilic, 2018).

Potentiometry is performed by measuring the potential of a solution between two electrodes to determine the concentration of the analyte of interest. This method was first

implemented by Goda *et al.* in 2012 for miRNA detection from exosomes, as a part of a system that included an RT-PCR (Goda, 2012).

As the name suggests, conductometric biosensors involve the measurement of electrolytic conductivity, from which the progress of a chemical reaction can be assessed (Labib & Berezovski, 2015). An example of this type of sensor is a nanogap interdigitated microelectrode with PNA probes and polyaniline nanowires. Upon hybridization, the polyaniline nanowires are deposited onto miRNA, a process mediated by the electrostatic interaction between the aniline and the phosphate groups of the miRNA molecules. The conductance of the nanowires is then linearly correlated with the quantity of miRNA. (Fan, 2007.)

The most well-known impedimetric method for detection of miRNA is electrochemical impedance spectroscopy (EIS). Through EIS, the effective resistance or impedance of an electrical component is measured over a range of potential frequencies. From changes in the frequency-domain response, one can analyze the physico-chemical changes taking place between the probe and analyte (e.g., miRNA hybridization). Another interesting impedimetric miRNA biosensor was described by Shen *et al.* in 2013 (Shen, 2013). The biosensor included a self-assembled monolayer of oligonucleotide capture probes on a gold electrode. The capture probes that remained intact after miRNA hybridization were removed with enzymes (nucleases), and a second hybridization was performed with a DNAzyme having an oligonucleotide tail. Upon incubation with a mixture of dymethoxybenzidine and hydrogen peroxide (H_2O_2), the DNAzyme triggered the deposition of polydimethoxybenzidine (PDB) on the surface. The deposited PDB layer altered the impedance of the sensor, which was read using EIS methods. (Shen, 2013; Labib & Berezovski, 2015.)

The final electrochemical method presented here is based on FETs. In brief, these devices consist of three electrodes (source, drain, and gate). The electrical field induced by charges from the environment alter the conductivity of the source-drain channel, which provides information about the events happening at the sensor surface. Recently, interest has been directed to FETs constructed with nanomaterials such as silicon nanowires (SiNWs) or carbon nanotubes, as the building blocks of the source-drain channel. The small sizes and the one-dimensional structure, for example, the NWs, allow a greater sensitivity and selectivity. Their limits of detection (LOD) down to aM (Ramnani, 2013) or even 1 zeptomolar (1 zM) (Lu, 2014b) make them good candidates for miRNA biosensors. A more detailed description of SiNW-FETs and their properties is presented in Chapter 3.

2.4.2 Optical methods

Generally, the principle of an optical biosensor for detection of miRNA molecules relies on transduction of an optical signal, such as absorbance or fluorescence, resulting from the hybridization event between the target miRNA and the capture probes, which may be labeled with an optically active reporter. These labels can be either dyes or quantum dots. (Kilic, 2018.) The detection strategy, however, may vary depending on the optical method chosen. The most well-known methods are surface plasmon resonance (SPR), fluorescence-based biosensors, and surface-enhanced Raman spectroscopy (SERS).

SPR is the most commonly used optical method, and it can be described as a charge-density oscillation that takes place at the interface between two media (metal and dielectric) having different dielectric constants. The resulting oscillation generates a surface plasmon wave that has a constant propagation speed. (Zhang, 2015; Homola; 2008.) Compared to, for example, fluorescence-based biosensors, SPR is a label-free method. The chip surface is coated with bioreceptor molecules, and the introduced miRNA sample hybridizes. Upon hybridization, the refractive index of the surface changes, which leads to a change of the SPR angle, which in turn, is optically detected (Mahdiannasser & Karami, 2018). In recent years, multiple methods based on SPR technology have been developed. Three examples include 1) signal amplification strategies based on, for example, gold nanoparticles (AuNPs), 2) hairpin assemblies in which the amplification results from streptavidin-aptamer coupling, or 3) DNA-RNA-antibody assays where thiolated DNA probes couple with miRNA following antibody recognition. (Kilic, 2018.)

Even though SPR is a robust and fast method with wide applicability, its LODs are too high for use with the analyte levels in physiological samples (Homola, 2018). Other drawbacks of this method include the high prices of the chips, the non-specific bindings, and difficulties in interpreting the resulting data (Mahdiannasser & Karami, 2018).

In fluorescent-based biosensors, detection is generally achieved through signal generation or signal quenching after the hybridization of miRNA with the receptor probe. These sensors have the miRNA molecules and/or the capture probes modified with organic dyes, quantum dots or Au nanoparticles. Even though the method is widely used, it has as its main disadvantage a lack of robustness due to high background noise and low sensitivity. (Kilic, 2018.)

SERS is a method based on Raman scattering, in which the molecular fingerprints of molecules are detected as spectral bands. SERS has potential in biosensing, as it is a label-free and highly sensitive method capable of distinguishing between spectra from molecules with very similar structures and functions. (Bantz, 2011.) Kim *et al.* proposed

a multiplexed and label-free SERS method to detect different types miRNAs at LODs down to the fM from serum-like solutions, therefore SERS could be a good option for POC applications (Kim, 2019).

2.4.3 Other detection methods

Although many miRNA biosensors based on electrochemical and optical transducers have been developed, some groups have directed their research toward more novel or hybrid approaches that could introduce new advantages or overcome the drawbacks of the above-mentioned methods. Some such methods are listed in Table 1 and include photoelectrochemical and electromechanical biosensors.

The photoelectrochemical method was developed to exploit the advantages of both electrochemical and fluorescence methods. A photoelectrochemical (PEC) biosensor was recently developed by Yin *et al.*, and its operation relies on the quantification of miRNA according to the magnitude of current induced by light (Yin, 2014). Electromechanical miRNA biosensors have transduction mechanisms that can detect the changes induced by hybridization in a static or dynamic way. For measuring of static properties, an atomic force microscopy method is used to evaluate the stiffness maps resulting from hybridization of DNA capture probes and miRNA molecules (Husale, 2009). In contrast, for measurement of dynamic changes, piezoelectric cantilevers have been used by Johnson and Mutharasan for successful detection of miRNA down to 10 aM (Johnson & Mutharasan, 2012).

Despite the current state of miRNA research, there is still a need for standardized and reliable methods for detection of miRNAs that can overcome the drawbacks of existing technologies.

3. SILICON NANOWIRE FIELD-EFFECT TRANSISTORS (SINW-FETS)

This chapter introduces a short history of field-effect transistor (FET) sensors, their operation principle, and some of the performance parameters related to the use of silicon nanowires (SiNWs) in FET devices. Section 3.1 introduces some general concepts related to the development history of FET devices, and Section 3.2 presents the general operation principle of a FET sensor. The SiNW-FETs, as their name depicts, include in their structure nanowires (NW) as building blocks, thus Section 3.3 presents the manufacturing methods for SiNW-FET devices. Integrating SiNWs in FET sensors introduces new parameters that must be considered in the manufacturing and operation of SiNW-FET devices, so Section 3.4 introduces these specific parameters.

3.1 General aspects of FETs

Early in the 1970s, Bergveld was the first to introduce the novel concept of interfacing an electrical transistor with a liquid environment meant for electrochemical or biological sensing. He proposed a device called an ion-sensitive field effect transistor (ISFET), which was based on the conventional metal-oxide-semiconductor FET (MOSFET) but with the gate metallization removed, leaving the gate oxide in direct contact with the biological environment. The device was capable of selective ion detection as the basis for pH measurement, and later its use was extended to intracellular recordings of Na^+ and K^+ ions. (Bergveld, 1970; Bergveld, 1972.)

The development of ISFETs led other research groups to direct their research to the detection of charged biomolecules. Already by 1980, Caras and Janata had proposed an ISFET called an EnzymeFET of EnFET with its surface modified with immobilized enzymes that catalyze a reaction causing a change in pH, which is then seen as a change in the sensor signal. (Caras & Janata, 1980.) In the same year, Schenck released a patent for an ISFET immunosensor (ImmunoFET) in which antibodies were immobilized on the gate surface, and antibody-antigen reactions could be detected (Schenck, 1980). However, problems related to low sensitivity (the magnitude of the output signal with respect to the change in concentration) and selectivity (the ability of the device to detect a specific analyte in a sample containing other admixtures (Bhalla, 2016)) drove new developments that would have the potential to overcome these drawbacks. In 1997,

Goldhaber-Gordon *et al.* wrote a review about research developments int the area of nanometer-scale electronic devices (Goldhaber-Gordon, 1997). Although their paper was related to computer applications, in 2001 Cui and Lieber developed FET sensors that integrated silicon nanowires in their structure (the first SiNW-FETs) (Cui & Lieber, 2001). In the same year, Cui *et al.* proposed the use of SiNW-FETs as pH sensors, biotin modified SiNWs for detection of streptavidin down to the picomolar (pM) range, and immunosensor applications with an antigen-functionalized SiNW for reversible antigen-antibody interaction (Cui, 2001). Patolsky and Lieber predicted that the small size of NWs could open possibilities for array-based screening, making possible detection down to the level of a single molecule (Patolsky, 2004; Patolsky & Lieber, 2005).

In recent years, SiNW-FETs have drawn much attention as biosensors due to their high sensitivity and selectivity, low LODs (the lowest concentration that the sensor can detect), ability for real-time detection, possibility of integration into arrays, low production costs, and not least possibility of a label-free and multiplex detection (simultaneous measurement of multiple analytes in an experiment). Additionally, the already developed processing and fabrication technologies for silicon offer possibilities for precise tailoring of SiNWs in different shapes and sizes and with different dopants. All of these advantages make SiNW-FETs highly relevant for point-of-care applications and lab-on-chip platforms. (Chen, 2011; Veigas, 2015.) As concentration levels of miRNA in the cell medium are generally quite low (aM range), and SiNW-FETs offer the possibility of LODs down to this aM range due to their high surface-to-volume ratio, they are suitable as transducers for detecting miR-218, which was proposed as part of this thesis work.

3.2 Operation principle

As an introduction to the operation principle of SiNW-FETs, we first explain the general working principle of a classic MOSFET. An SiNW-FET sensor is derived from a standard planar MOSFET sensor and has a three-electrode system, having source, drain, and gate electrodes. While the source and drain have the role of bridging the semiconductor channel between them, the gate electrode is used to modulate the conductivity of that channel. (Chen, 2011.) Compared with the planar FET, in SiNW-FETs the doped semiconductor channel is replaced with a nanowire (NW) and employs bioreceptors as a gate (see Figure 5A). Although the structure of the SiNW-FET differs from that of a MOSFET, the functional concept remains the same: the external charged species approaching the NW affects its conductivity, leading to a change in the channel current. (Wang, 2016.) However, the original silicon surface is not responsive to the charged biomolecules,

meaning that their accumulation near the isolation layer does not affect the NW's conductivity; to make the NW responsive to these biomolecules, its surface needs to be functionalized and bound to capturing biological probes (Cui, 2001; Wang, 2016). The biological probes are immobilized on the surface of the semiconductor channel via surface chemistry, and they have the role of recognizing the target analytes that are delivered to the sensor through a buffer solution. These biological probes, therefore, should possess high specificity and strong binding affinities. During the interaction between the probe and the target analyte, the surface potential of the semiconductor channel is altered, leading to a change in the nanowire channel's conductance, which is, in turn, collected by a detection system as a change in the electrical current. (Chen, 2011.)

A.

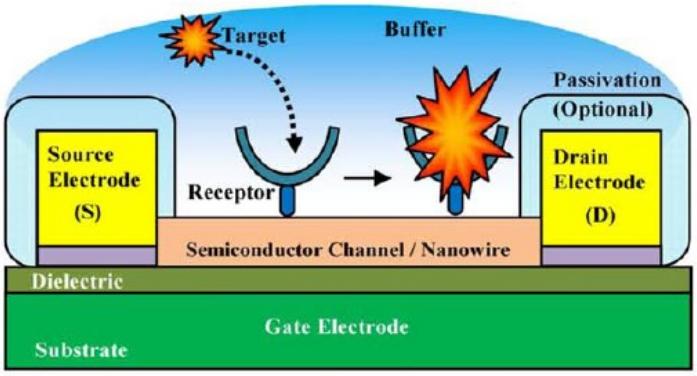

B.

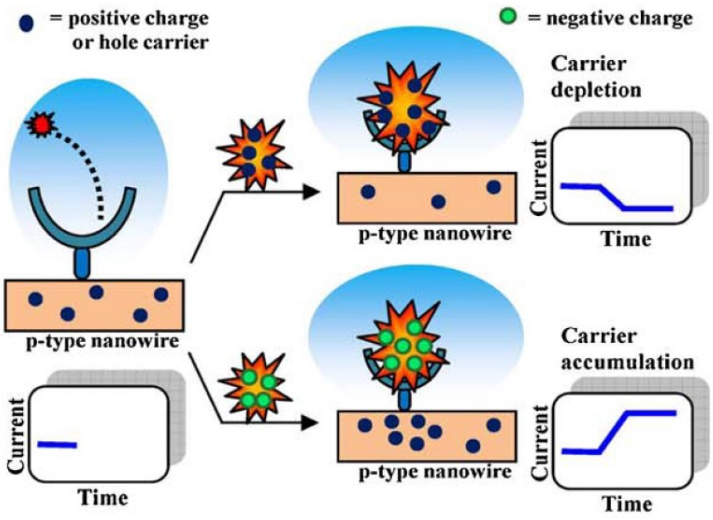

Figure 5. *Schematic of a SiNW-FET (A), and the SiNW-FET response when the NW is approached by a negative or positive charge (B). (reproduced from Chen, 2011)*

Depending on the charge carriers in the semiconductor channel or nanowire (given by the doping elements), an SiNW-FET can be of two types: p-type or n-type. In a p-type FET, the charge carriers are holes, and when a positively charged molecule binds to the

immobilized probe at the NW surface, a charge carrier depletion occurs, which leads to a decrease in the device's conductivity. In contrast, when a negative charge accumulates at the NW surface, the charge carriers accumulates in the channel, and the channel's conductivity increases (see Figure 5B). In an n-type FET, on the other hand, the charge carriers are electrons. When positive charges accumulate at the NW surface, the conductance of the channel increases, whereas a negative charge accumulation decreases the conductance. (Chen, 2011.)

3.3 Manufacturing of SiNW-FETs

As mentioned before, due to their high surface-to-volume ratios and high sensitivity, the SiNWs have raised interest in many fields as good candidates for biosensor applications. The production of SiNW-FET devices is not yet fully standardized as it is in the case of MOSFETS, but several research groups (Yang, 2018; Whang, 2003; Zhang, 2001) have proposed different manufacturing methods for this type of devices.

In this work, the SiNW-FET devices used were designed by Yang *et al.* using a low-cost and highly efficient fabrication process with (111) SOI wafers that are compatible with complementary metal oxide semiconductor or CMOS technology. In the manufacturing steps, traditional microfabrication technologies are used, such as lithography, reactive ion etching, and wet etching. (Yang, 2018.)

There are two main methods for manufacturing SiNWs-FETs, there are two main methods: top-down and bottom-up. While the top-down methods use corrosive liquids to etch silicon wafers to fabricate the aligned SiNWs, the bottom-up approaches involve a deposition method, such as template-assisted chemical vapor deposition (CVD) or CVD combined with Langmuir-Blodgett technology (Whang, 2003; Zhang, 2001). The bottom-up method is laborious, and its primary disadvantage is the difficulty of precisely controlling the dimensions and alignment of the SiNWs, leading to batch-to-batch variations. With a top-down method, however, Yang *et al.* have been able to precisely control the NWs position and to provide better device reproducibility. With their method, Yang *et al.*, were able to produce 3.000 p-type SiNW-FET devices, with 120 SiNW arrays on a chip. (Yang, 2018.)

3.4 FET characterization

The characteristics of a FET device are represented by a series of curves that define its operation. Generally, these characteristics are known as the current-voltage (I-V) characteristic curves and show the relationship between the current flow through the device and the voltage applied through the terminals. To characterize a FET device, the I-V curves can be represented as the drain current versus drain-source voltage (I_D-V_{DS}) or as the drain current versus gate-source voltage (I_D-V_{GS}) (see Figure 6).

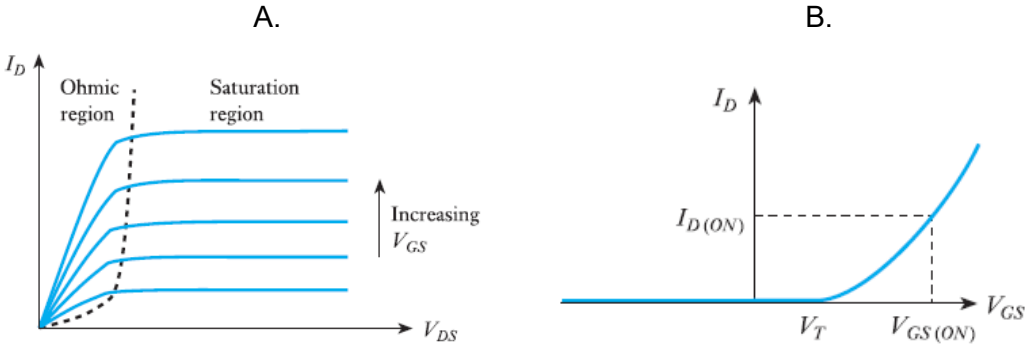

Figure 6. *General I-V output characteristics form of a FET: (A) the drain current (I_D) versus drain source voltage (V_{DS}), (B) and the drain current (I_D) versus gate-source voltage (V_{GS}). (Storey, 2009)*

The I_D-V_{DS} characteristic curves are named the output characteristics or drain characteristics and describe how the output voltage (the voltage that flows between the source and drain terminals) affects the output current (the current that flows between the source and drain terminals). In this case the gate-source voltage (V_{GS}) is kept constant while the drain-source voltage (V_{DS}) is increased, and the resulting change in drain current (I_D) is measured. In Figure 6A, it can be observed that the characteristic curve has two regions: the ohmic region and the saturation region. In the ohmic region, the behavior of the FET resembles that of a voltage-controlled resistor, with the drain current proportional to the drain-source voltage. In the saturation region, the drain current remains effectively constant even as the drain voltage is further increased. In this region, the gate voltage is the only parameter that can change the resistance of the channel. (Storey, 2009)

As mentioned above, another way of characterizing the FET device is by representation of the drain current versus gate-source voltage (I_D-V_{GS}), also named the transfer characteristic (Figure 6B). This describes the relationship between the input and the output parameters of the device; thus, by maintaining a constant drain-source voltage (V_{DS}), the drain current (I_D) can be measured as a function of the applied gate-source voltages (V_{GS}). (Storey, 2009)

3.5 Performance parameters for SiNW FET

The building of nanowires in SiNW-FET sensors introduces new factors or parameters that must be considered in the design and operation of this type of devices. These parameters are the Debye length and the size of the nanowires. Each has an important role in defining the overall sensitivity of the device, thus their impact is explained below.

3.5.1 Charge screening and Debye length

The specific binding between bioreceptors (DNA or PNA probes) and charged molecules (miRNA) modifies the conductivity of NWs, but in practical applications, other phenomena also occur near the isolation layer that can further modify the conductivity of NWs. (Stern, 2007; Wang, 2016.) In FET sensors for measurements of biomolecules, the solution environment or the buffer is a key element that determines the sensitivity of the device. As we know, in biosensing, the biological samples have to be delivered to the sensor in an aqueous solution. This solution needs to mimic the physiological environment in which the samples are normally found in order to keep them viable. These solutions are variates of phosphate-buffered saline (PBS), which is a water-based solution containing a mix of salts (NaCl, KCl, Na_2HPO_4, and KH_2PO_4) at different concentrations maintained at a pH of 7.4. (Chen, 2011).

In strong buffer solutions containing high salt concentrations, the reaction between the bioreceptor and the analyte that causes the change in NW conductance in the FET sensor can be screened by the high ionic strength of the buffer, reducing the signals obtained from the sensor. In other words, the electrical charges resulting from the events that take place at the NW surface can be screened by the counter ions from the buffer solution, leading to an undetectable signal. This screening effect is exponentially enhanced by the distance between the bioreceptor-analyte complex and the sensor surface and is related directly to the Debye length. (Chen, 2011) Debye length is given by the following formula:

$$\lambda_D = \sqrt{\frac{\varepsilon_0 \varepsilon_r k_B T}{2 N_A e^2 I}}, \quad (1)$$

where ε_0 represents the permittivity of a vacuum, ε_r is the relative permittivity of the medium, k_B is the Boltzmann constant, N_A is Avogadro's number, e stands for elementary charge, T is the absolute temperature, and I represents the ionic strength of the buffer solution in molar units (Chen, 2011; Stern, 2007).

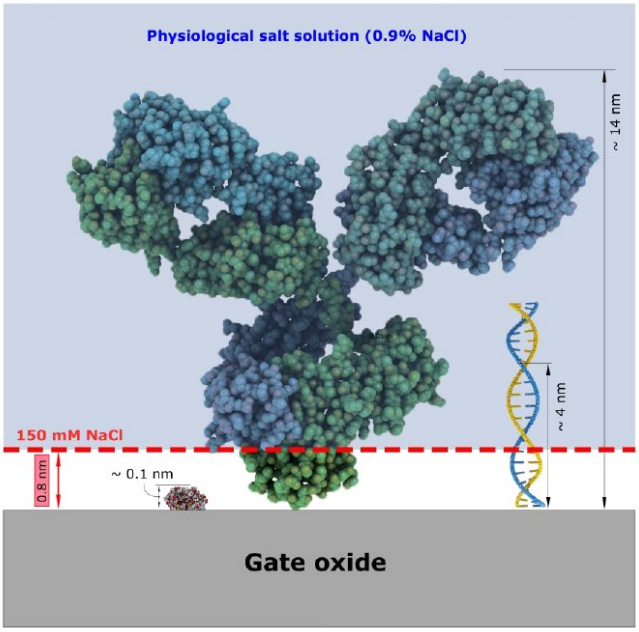

Figure 7. *Representation of different biomolecules (from left to right: enzyme, antibody, double stranded DNA) in buffer solution and in contact with the gate oxide, and their Debye length screening levels. (Afrasiabi, 2016)*

In Figure 7 is shown the Debye length (λ_D) for different strengths of the buffer solution. It is very important to choose the right buffer solution, because in practice the Debye length is closely related to the sensitivity and the LOD of the sensor. Based on formula (1), the values of λ_D are 0.7 nm for 1x PBS, 2.4 nm for 0.1x PBS, and 7.4 nm for 0.01x PBS (Chen, 2011). As can be observed from Figure 7, the charging events that take place outside the Debye length boundaries (red dashed line) are screened due to the high ionic strength of PBS (1x PBS) or to the biomolecule size (antibody). This leads to undetectable signals. Therefore, only the binding events that take place within the Debye length influence the signal of the FET sensor. A solution to this problem is to use diluted buffer solutions with a lower ionic strength that could reduce the charge screening. However, in real biological samples, such as blood or serum, such dilution is not possible, thus producing commercial devices for POC applications may be challenging. (Afrasiabi, 2016.)

3.5.2 Effect of nanowire diameter

The SiNW size, specifically the diameter (< 50 nm), affects the sensitivity of the FET sensors (Elfström, 2007; Chen, 2011). Elfström *et al.* demonstrated in 2007 the dependency between NW size and sensitivity and showed that the surface charge effect increased as the diameter or width of the NW decreased. Additionally, the study indicated

that large NWs with widths > 150 nm lose their detection sensitivity, as do micrometer-sized wires. (Elfström, 2007.)

For a better understanding of this idea, Figure 8 represents two wires with different diameters: one in the µm range and the other in the nm range.

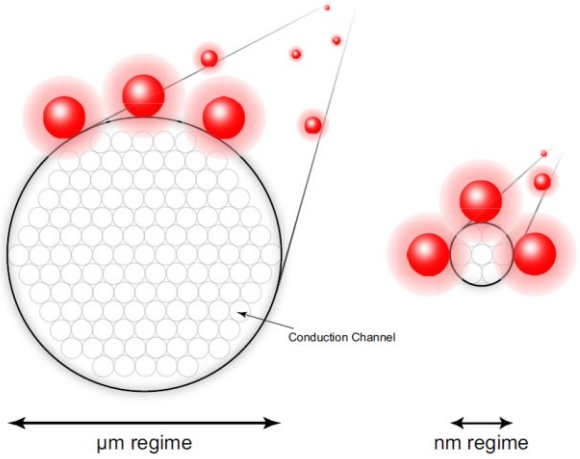

Figure 8. *Schematics of NW size effect on the conductance change in the wire.* ***Left****: a thick wire surrounded by electrical charges (red balls). The electrical field exerted by these charges affect only the exterior part of the wire, while the interior could still be unaffected.* ***Right****: a thin wire with dimensions in nm scale. When the wire diameter is reduced to nm scale (right) the external electrical field induced by charges reach the whole cross-section of the NW, being able to strongly influence its conductance. (Grieshaber, 2008.)*

Comparing to the thinner wires, the thick ones have a lower surface-to-volume ratio. Thus, when external charges approach the thick NW, their exerted electrical field affects only the surface of the wire, with the possibility of leaving the center unaffected, whereas in a thin wire the electrical field can reach through the wire's entire cross-section. In conclusion, conductivity changes in nanowires are much greater than in microwire-based FETs. (Chen, 2011.) Since the overall sensitivity of an SiNW-FET device depends strongly on the NW diameter, the NWs should be carefully designed.

4. SURFACE FUNCTIONALIZATION OF SiNW-FET BIOSENSORS FOR miRNA DETECTION

Through functionalization, the surface properties of a material or a device are altered – for example, by introducing chemical functional groups to the surface – to achieve a specific goal (Wang, 2012). This chapter presents some of the possible functionalization schemes for a SiNW-FET biosensor for miRNA detection. The chapter considers two important aspects: 1) the underlying material that must be modified is silicon, and 2) the DNA probe has an amine (-NH_2) at the 5´-end, thus the covalent attachment of the DNA probes is done through reaction with the amine group. Therefore, this chapter opens in Section 4.1 with some general concepts related to the chemical modification of a silicon surface (here SiNW), and continues with four functionalization methods proposed in this thesis for immobilization of DNA probes (DNAps) on the sensor NW surface: (3-aminopropyl)triethoxysilane (APTES)–glutaraldehyde (GA)–DNAp (Section 4.2), APTES–L-ascorbic acid (AA)–DNAp (Section 4.3), (3-glycidoxypropyl)trimethoxysilane (GPTMS)–DNAp (Section 4.4), and 1,1´-carbonyldiimidazole (CDI)–DNAp (Section 4.5).

4.1 General aspects

A reliable biosensing application based on SiNW-FETs, or any other biomeasurement device, must have a well-defined bioreceptor attachment schemes to provide chemical stability, to ensure proper interfacial electrical properties, and to allow the biomolecular recognition of the analyte of interest. The attachment schemes, also called surface functionalization, should allow a controlled immobilization of bioreceptors on the SiNWs, which is an important element in obtaining a device with high sensitivity and selectivity. (Coffinier & Boukherroub, 2014; Nimse, 2014.) The choice of a suitable immobilization procedure is determined by the physicochemical properties of both the bioreceptor probe (e.g., a DNA probe) and the underlying surface (Nimse, 2014). The success of DNA immobilization is related to the way the crosslinkers (molecules that connect adjacent molecules through chemical bonds) and other layers are deposited, specifically to how their structures allow the DNA probe to successfully react with the available surface reactive groups. Generally, the immobilization of a DNA probe or any other biological receptor on a surface is defined as the attachment of molecules to a surface resulting in

reduction or loss of mobility (Nimse, 2014). Multiple factors should be taken in consideration when choosing a surface immobilization chemistry, such as probe density, uniformity, long-term stability in aqueous environments, and charge screening effects (by controlling the distance between the probe and surface of the sensor) (Goddard & Erickson, 2009).

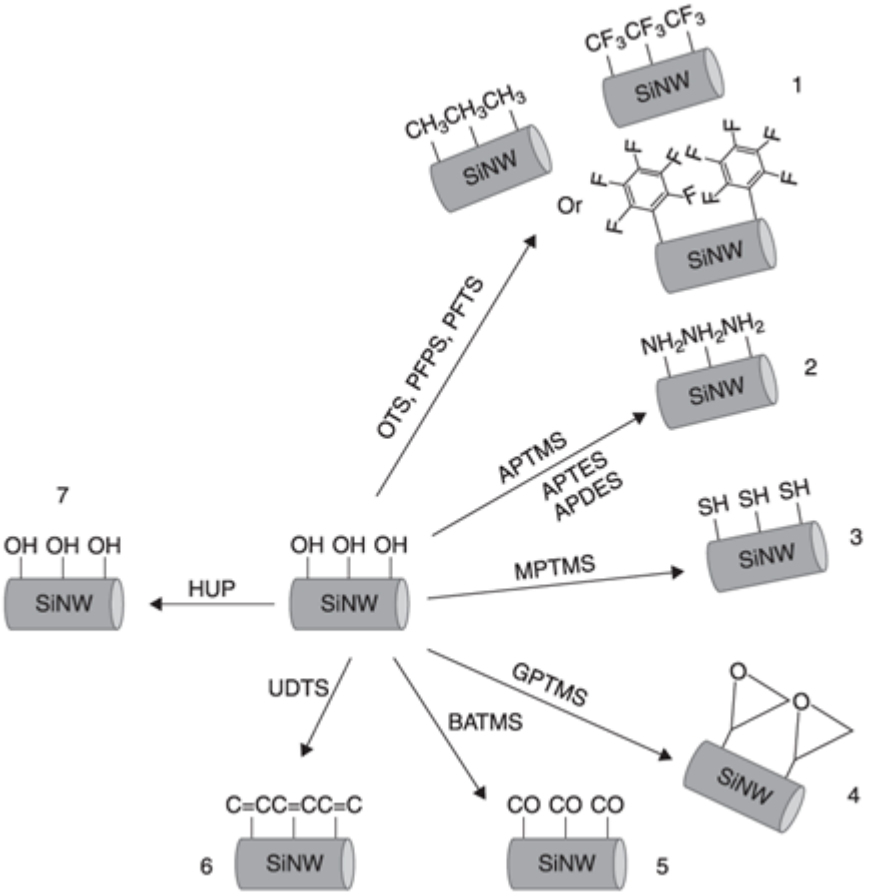

Figure 9. *Possible schemes for modification of silicon oxide surface of SiNWs, based on: (1) OTS (octadecyltrichlorosilane), PFTS (perfluorodecyltrichlorosilane), PFPS (perfluorophenyltrichlorosilane), (2) APTMS (aminopropyltrimethoxysilane), APTES (aminopropyltriethoxysilane), APDES (aminopropyldiethoxysilane) introducing amine groups, (3) MPTMS (3-mercaptopropyltrimethoxysilane), (4) GPTMS (3-glycidoxypropyltrimethoxysilane), (5) BATMS (3-(trimethoxysilyl) butyl aldehyde), (6) UDTS (10-undecenyltrichlorosilane). (Coffinier & Boukherroub, 2014.)*

Depending on the reactive group desired on the SiNW surface, there are multiple functionalization schemes, such as those depicted in Figure 9. The following sections present some of the schemes that would allow immobilization of an amine-terminated DNA probe.

As previously mentioned, for immobilization of DNA probes on a SiNW surface, the solid substrate (here silicon) needs to be modified with an appropriate functional layer. These

modifications are done to activate the surface by introducing different tail groups. Generally, a SiNW has a native oxide layer around it, thus subsequent chemical modifications can be performed on this native oxide layer. (Coffinier & Boukherroub, 2014.)

4.2 (3-Aminopropyl)triethoxysilane (APTES)–Glutaraldehyde (GA)–DNA probe functionalization scheme

Most of the chemical modification of the SiNW-FETs for biosensor applications are done through a silanization reaction, however, only a few organosilanes of the vast variety have been used. Silanization is a reaction that involves linking of molecules on an oxide layer through siloxane bonds (Si-O-Si). One of the functionalization methods often proposed is based on the silanization with APTES (see Figure 10) and GA (Lin 2009; Lu, 2014a; Lu, 2015; Noor, 2014; Zhang, 2009).

The functionalization steps will be explained based on the scheme presented in Figure 10 and Figure 21. Silanes, such as APTES, covalently bind to the oxygen plasma-treated surface of a SiNW by transferring a proton from the surface hydroxyl group (-OH) to a silane leaving group, eliminating an alcohol. Prior to silanization it is important that the surface be cleaned with an oxidant, which eliminates all organic residues that can hinder further reactions and increases the number of the available hydroxyl groups. The most used oxidizing methods are oxygen plasma and Piranha solutions. (Coffinier & Boukherroub, 2014.) Next, the surface is treated with APTES. Typically, 2% APTES in ethanol solution is used, and the treatment times vary from 30 minutes (Lin, 2009) to several hours, followed by an ethanol washing step. To remove the ethanol residues, the surface is dried and cured in oven at 80–120 °C. The heat curing plays the additional role of stabilizing and cross-linking the APTES layer.

The deposition of APTES monolayers having their amine groups oriented away from the surface is a complex process which depends on different reaction conditions, such as the presence of water (Acres, 2012), temperature (Chiang, 1982), reaction time (Vandenberg, 1991; Moiseev, 2006.), and APTES concentration (Wang, 2006). The presence of water in the reaction can lead to horizontal polymerization, and the resulting silanol moieties can react with each other through a condensation reaction forming siloxane bonds that are not reactive (Acres, 2012). Thus, the solvents used with APTES should be anhydrous. Generally, the reaction temperature is at room temperature, but drying of APTES surfaces at different temperatures was shown to have different effects on the layer conformation.

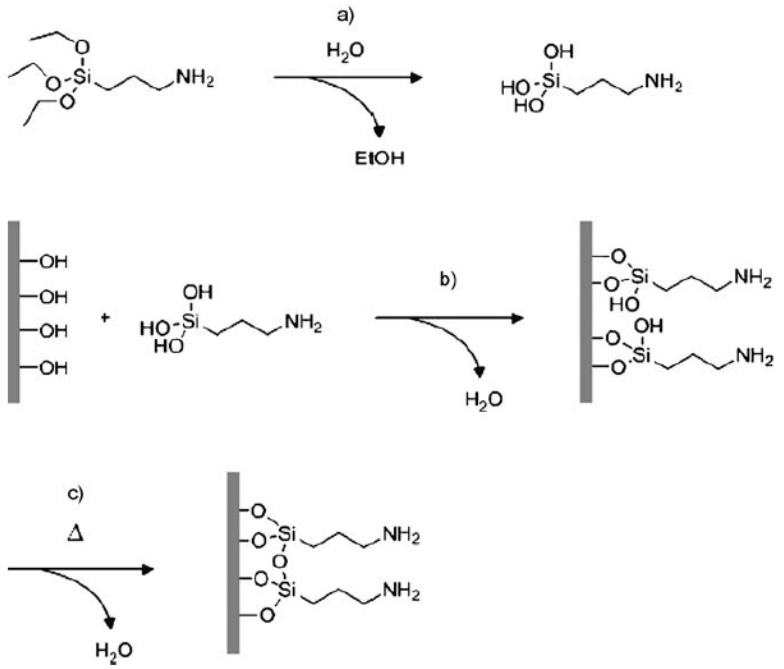

Figure 10. *The silanization process with APTES: (a) hydrolysis of the siloxanes that happens in solution or on the substrate surface, (b) condensation with surface silanol groups, (c) cross-linking due to thermal curing. (Jankheijm, 2008)*

While APTES surfaces air-dried at room temperature form two siloxane bonds, those cured at high temperature in an oven form three siloxane bonds with the underlying material surface. (Chiang, 1982.) In addition to previously mentioned factors, the reaction time of APTES also affects its structure and orientation. At short reaction times, between 20 minutes and 1 hour, APTES can produce monolayers, whereas by increasing the reaction time one can obtain multilayers, though with the disadvantage of the formation of islands of different thicknesses, leading to nonuniform coverage. (Vandenberg, 1991; Moiseev, 2006.) The concentration of APTES solution is also an important factor that should be considered; a 2% concentration was found optimal for further functionalization (Wang, 2006). Alternatives to APTES, aminopropyltrimethoxysilane (APTMS) or aminopropyldiethoxymethylsilane (APDMS) can be also used (Coffinier & Boukherroub, 2014; Goddard & Erickson, 2009). The main difference between them relates to the silanization procedures employed, such as liquid- or gas-phase silanization.

As the surface silanol groups have been converted into amine groups ($-NH_2$), the surface can be further reacted with a GA solution (e.g., 2.5% GA in PBS). One of the carbonyl groups of GA can react with the primary amines of APTES, forming a Schiff base (imine formation), while the other is available as a tail group for subsequent reactions. Thus, the DNA with amine modification at the 5´-end can now be covalently attached to the surface via a GA crosslinker. (Lin 2009; Lu, 2014a; Lu, 2015; Noor, 2014; Zhang, 2009.) A time-dependent loss of surface functionality was associated with Schiff base formation,

and some studies proposed the addition of sodium cyanoborohydride ($NaBH_3CN$) to reduce the imines into secondary amines (Elnathan, 2012; Dorvel, 2013).

4.3 (3-Aminopropyl)thriethoxysilane (APTES)–L-ascorbic acid (AA)–DNA probe functionalization scheme

In 1999, Tiller *et al.* proposed an immobilization method of enzymes on amine-terminated polymeric surfaces through an L-ascorbic acid (AA) crosslinker (Tiller, 1999), while Leivo *et al.* used AA for attachment of collagen on silanized polydimethylsiloxane (PDMS) surfaces (Leivo, 2017). Based on their studies and observations, the second proposed scheme is the covalent immobilization of DNA probes on SiNWs by means of an AA crosslinker.

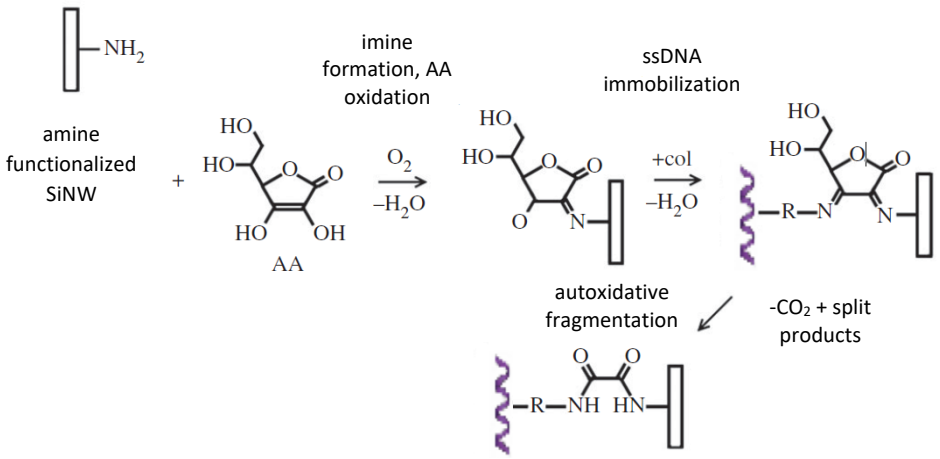

Figure 11. *Amine-terminated SiNWs reaction with AA used as crosslinker for amine terminated single-stranded DNA (ssDNA) immobilization scheme. (reproduced from Leivo, 2017)*

The functionalization process involves four steps as the method presented in Section 4.2, the first two of which are a cleaning step of the SiNW surfaces to remove contaminants and an oxygen plasma treatment for obtaining hydroxyl groups (-OH) that will subsequently react with APTES. The amine-terminated surface obtained after APTES silanization is then incubated with AA solution for approximately 30 minutes (Tiller, 1999). Leivo *et al.* proposed two AA solutions that can be prepared by dissolving 200 mg/ml AA powder in PBS or by dissolving 20 mg/ml AA powder in methanol (Leivo, 2017). The AA will bridge the binding of amine-terminated DNA probes on the sensor surface, acting as a crosslinker, as GA did above. The reaction scheme between AA and silanized surfaces is presented in Figure 11. This was described by Tiller *et al.* as reacting AA with enzymes, assuming that the enzyme immobilization involves compounds similar to those used in

the reaction of AA with n-butylamine (Tiller, 1999). Thus, the reaction scheme of AA with the amine-terminated DNA probes is based on the same assumptions, and to the writer's knowledge, has not yet been reported for miRNA biosensors.

After the reaction of the NH_2 groups of the silanized SiNW and reaction with AA, a dehydroascorbic acid derivative is formed by oxygen-dependent autoxidation. For preparation of AA solutions N,N-dymethyl acetamine (DMA), dimethyl sulfoxide (DMSO), ethanol, or methanol can be used (Tiller, 1999; Leivo, 2017). After exposing the surface to the AA solution, a washing step with ethanol or methanol and water is necessary for eliminating the solvent, the excess AA, and the products resulting from autoxidation. Subsequently, the AA-modified NWs are ready to react with the amine-terminated DNA probes. However, the structures newly formed are not stable and form oxalic acid diamide as an end product (Tiller, 1999).

Ascorbic acid was chosen as a crosslinker, as in the case of Leivo *et al.*, for its biocompatible properties. Since the tested SiNW FET sensors are meant to be integrated in future in *in vitro* platforms for the measuring of cell activity, thus being in close contact with the cells, biocompatibility is an important factor, and as Leivo *et al.* noted (Leivo, 2017), the GA-treated surfaces are cytotoxic. However, it is also important to keep in mind that the formation of unstable end products of AA with the materials bearing NH_2 groups could be a problem for sensor applications, by means of signal interference or instability in aqueous measurements.

4.4 (3-Glycidoxypropyl)trimethoxysilane (GPTMS)–DNA probe functionalization scheme

The functionalization methods presented in Section 4.2 and Section 4.3 use crosslinkers GA and AA, respectively, for immobilization of DNA probes on the NW surface. Since the increase of the deposited layers' thickness might affect the performance of a SiNW-FET device by influencing the Debye length which leads to a charge screening effect, one option for bringing the DNA probe closer to the surface is to eliminate the crosslinker layer. One such method is presented in Figure 9(4) and is based on epoxide chemistry.

GPTMS is, as is APTES, a silane, but it makes possible a direct and covalent coupling of the aminated DNA probes on the NW surface. The coupling mechanism is based on the epoxide ring opening reaction between the epoxy terminal groups of GPTMS with the amine ($-NH_2$) groups of aminated DNA probes, as presented in Figure 12. (Coffinier & Boukherroub, 2014; Dubrovsky, 1995; GhoshMoulick, 2009; Kamra, 2015; Goddard & Erickson, 2009.)

Prior to any modification, the surfaces of the SiNWs should be cleaned as was explained in Section 4.2 so as to obtain silane layers of high quality. The surface can be activated through oxygen plasma treatment so that enough silanol groups (Si-OH) are available to react with GPTMS. Goddard and Erickson used a 2% GPTMS in anhydrous toluene solution, containing 0.2% triethylamine, for 1 hour to silanize the surface. The subsequent washing step was done with toluene, isopropanol, and methanol in order to remove all the silane residues (Goddard & Erickson, 2009). As with all silanes, the GPTMS-modified surface was also cured in an oven to cross-link the formed layer. The curing temperatures varied from 80–120 °C and the times varied from 15 minutes to 2 hours depending on procedures.

By comparing the quality of deposited APTES and GPTMS layers, GhoshMoulick *et al.* showed through atomic force microscopy measurements that GPTMS layers were thinner than APTES layers, although the same deposition method was used (GhoshMoulick, 2009). Additionally, the density of DNA probes bound on the GPTMS surface was also higher than on APTES (Cloarec, 1999; GhoshMoulick, 2009). A higher density of bioreceptors on the sensor surface offers more available binding spots for miRNA and theoretically improves the signal obtained from the sensor.

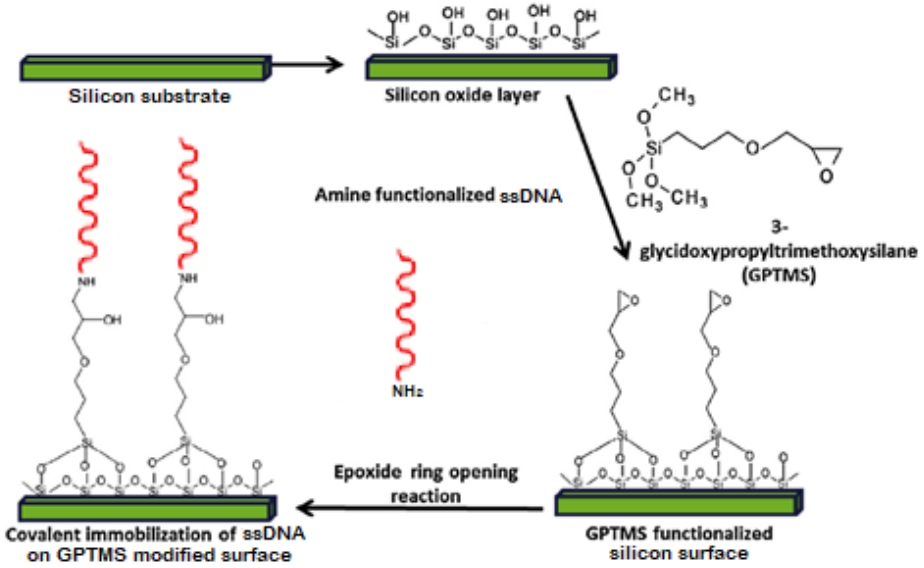

Figure 12. *A direct DNA probe attachment of amine-terminated ssDNA probes on a GPTMS functionalized surface via epoxide ring opening. (reproduced from Kamra, 2015)*

Although GPTMS has the advantages of direct grafting of DNA probes and better surface properties, the silanization process is often done in the gas phase (Ingerbrandt, 2011; GhoshMoulick, 2009), which involves a more complex and expensive setup than in the

liquid phase. However, GPTMS silanization in liquid is also possible and was employed in the study of Kamra *et al.* (Kamra, 2015).

The hydrophobicity of the surfaces induced by the GPTMS treatment (contact angle of 70.68° ± 0.28°) is caused by the presence of the hydrophobic alkane core (Goddard & Erickson, 2009) and may be problematic in certain applications. The design of the sensors used in this work, with the NW hanging inside a trench-like cavity (for more details about the design, see Figure 18 and Yang, 2018), combined with the hydrophobicity of the surface may reduce the access of the DNA probes to the NW (see Figure 30). This may cause a low density of immobilized probes and, subsequently, a low signal.

4.5 1,1´-Carbonyldiimidazole (CDI)–DNA probe functionalization scheme

The second method proposed for coupling the DNA probes to the nanowire without using a crosslinker is based on the study of Goddard and Erickson (Goddard & Erickson, 2009). After a cleaning with Piranha solution or oxygen plasma treatment, the SiNW activated surface bearing its hydroxyl groups was subsequently reacted with CDI, as in Figure 13. The procedure involved the immersion of silicon surfaces in a solution of 0.5 M CDI diluted in a dioxane solvent and shaken for two hours at 37 °C, followed by a washing step with acetone and water. The reaction of CDI-modified surfaces and the amine-modified DNA probes happens through the imidazole carbamate functional groups, leading to formation of carbamate linkages with the DNA probes.

In addition to the reduced time involved in preparing the surfaces as compared to the methods that involve crosslinkers, this CDI method offers another significant advantage. Surface wettability is an important factor when we discuss sensor surface modifications, and the imidazole carbamate functionalization increases only slightly the hydrophobicity of the surface (contact angle of 9.33° ± 0.48°) as compared to the hydrophilic surfaces obtained after Piranha or oxygen plasma treatment (contact angle of 4.85° ± 0.30°) (Goddard & Erickson, 2009). However, the CDI surface is also hydrophilic, as the oxygen plasma-treated surface. A proper wettability of the surface ensures good access of the liquid samples to the active area of the sensor, which is an important factor in the design of a miRNA biosensor.

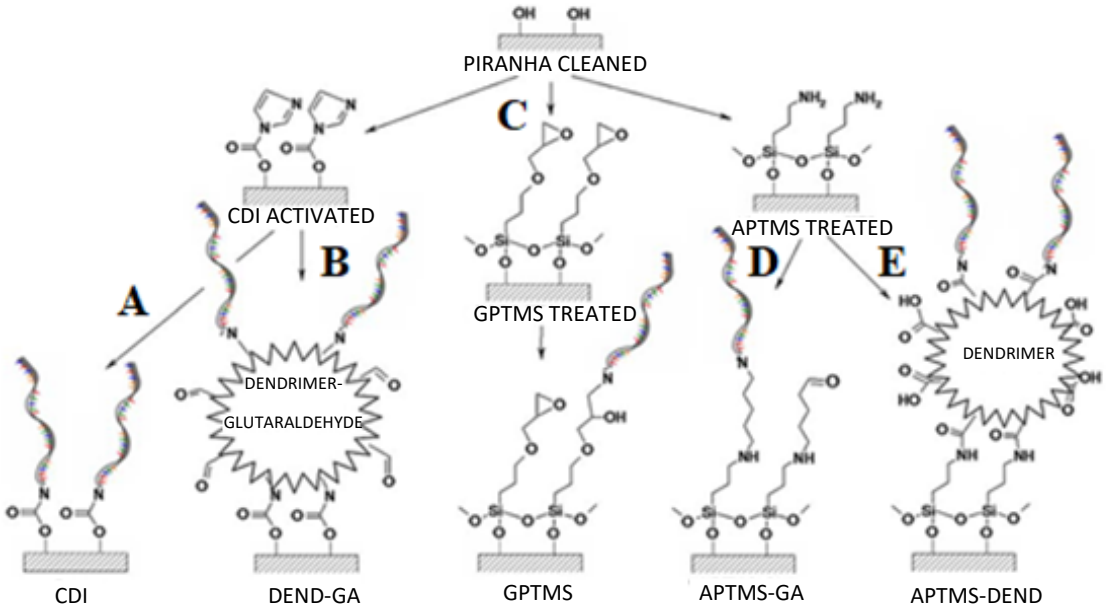

Figure 13. *Surface chemistry methods for SiNW: (A)CDI, (B) CDI–GA dendrimer, (C) GPTMS, (D) APTES–GA, (E) aminopropyltrimethoxysilane (APTMS) dendrimer. (reproduced from Goddard & Erickson, 2009)*

Goddard and Erickson evaluated in their study the density of the immobilized capture probes and the hybridization densities between the probes and analytes, and they observed that the CDI immobilization strategy allowed a higher hybridization density (0.072 pmol/cm^2) than the silane-based approaches such as APTMS (0.013 pmol/cm^2), although the density of immobilized probes was similar between the two approaches.

Table 2. *The contact angle and standard error values for different chemically modified surfaces. (from Goddard & Erickson, 2009)*

Surface treatment	**Contact angle (°)**
Piranha-cleaned silicon	4.85 ± 0.30
CDI treatment	9.33 ± 0.48
GPTMS treatment	70.68 ± 0.28
APTMS treatment	43.78 ± 2.16
GA onto APTMS	58.45 ± 0.86

Additionally, the hybridization efficiency, which is described as the ratio of hybridized target probes to immobilized capture probes, indicated that CDI is superior to GPTMS and APTMS–GA methods. Therefore, the CDI functionalization approach could be a good alternative to traditional silane-based approaches. The immobilization of DNAps

through CDI is a new approach, the method being previously used only for biomolecule labeling and protein immobilization. (Goddard & Erickson, 2009.)

4.6 Discussion and comparison of the proposed methods

The success of miRNA biosensors depends directly on the chemistry used for immobilization of the DNAps. The success also depends on the functionality, accessibility, attachment density, and reproducibility of the DNAps.

To increase the number of reactive groups on the surface, and subsequently increase the number of attached DNAps, schemes involving different dendrimers (e.g., GA dendrimers; see Figure 13E) have also been proposed. Dendrimers are synthesized branched molecules having a repetitive structure. Hence, GA holds more reactive groups available to react with the DNAps. However, Goddard and Erickson's study found that the density of immobilized probes was not as high as expected, but interestingly it led to high hybridization efficiency. Similarly, the CDI scheme that showed a low density of immobilized DNAps presented a high level of hybridization efficiency, whereas the silane–GA methods, which had the highest immobilized probe density, had one of the lowest hybridization efficiency levels. (Goddard & Erickson, 2009.)

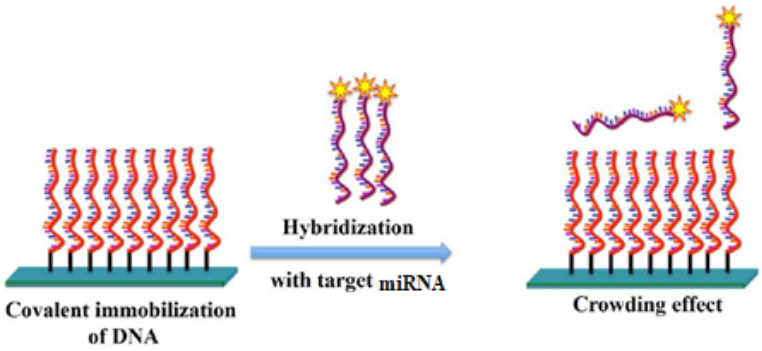

Figure 14. *The crowding effect caused by the closely packed ssDNAp hinders the hybridization event that must take place with the incoming miRNA analyte. This problem might be increased by the repulsion force developed between the negatively charged DNAp and miRNA molecules. (reproduced from Nimse, 2014)*

It is generally thought that a high density of immobilized DNAp implies better sensitivity of the sensor, but it was observed that a closely packed surface does not allow participation of the probes in hybridization reactions due to the phenomenon of crowding (see Figure 14). Because of the crowding effect, incoming miRNA molecules do not have space to get close to the single-stranded DNAps. Additionally, the high density of probes on the surface results in high background noise, and non-specific interactions decrease the signal intensity. (Nimse, 2014.) Therefore, a surface with an optimal DNAp density

could ensure high hybridization yield. This crowding effect might be the reason for the high hybridization efficiency of methods such as CDI, which had the lowest surface density of immobilized DNAps.

Other factors to consider when choosing a functionalization scheme are the uniformity and thickness of deposited layers, the long-term stability in aqueous solution, the charge screening effect, biocompatibility, and hydrophobicity of the resulting surfaces. Based on these factors, Table 3 presents the advantages and disadvantages of the proposed functionalization schemes for a SiNW-FET for miRNA detection.

Table 3. *Comparison between the proposed functionalization methods of a SiNW-FET biosensor for miRNA detection*

Functionalization method	Advantages	Disadvantages
APTES – GA – DNAp	• Stable in aquous solutions • Studied → known parameters that influence the reaction • GA improves the stability of the deposited APTES layer	• Use of crosslinker • Longer sensor functionalization times (due to crosslinker step) • DNAp further away from surface →possibility of charge screening effect • GA is cytotoxic • Possibility of APTES multilayer and isle formation
APTES – AA – DNAp	• AA is biocompatible	• AA degrades in aqueous solution • End products resulted might interfere with the sensor signal • Possibility of APTES multilayer and isle formation
GPTMS – DNAp	• Thinner layer than with APTES can be obtained • No need of crosslinker • Shorter time for sensor functionalization • GPTMS is less cytotoxic than GA (Shirosaki, 2013)	• GPTMS surface is highly hydrophobic (contact angle 70.63°)
CDI – DNAp	• No need for crosslinker • Less hydrophobic surface (contact angle 9.33°) than with GPTMS, GA or APTES • Higher hybridization efficiency than GPTMS and APTES – GA methods	• Less stable than silane-GA scheme

Through optimization of the reaction parameters, the quality of the deposited layers can be increased. For example, by choosing the right reaction time duration with APTES, the formation of multilayers and islands can be avoided. However, problems related to cytotoxicity and stability in aqueous environments might not be avoided unless different molecules are chosen.

These immobilization methods offer the possibility for covalent attachment of a variety of amine-modified materials, not only for aminated DNA probes as presented here, which extends the methods' applicability.

Among the proposed functionalization schemes, the APTES–GA–DNAp approach was previously studied by several groups, the reaction parameters are generally known, and successful results were obtained. Additionally, the accessibility and the low costs of the reactants make this functionalization scheme the most attractive for first experiments. However, the other proposed methods, specifically CDI–DNAp and GPTMS–DNAp, should be also practically assessed in the future, as the lack of crosslinkers reduces the time needed for functionalization of the sensors.

5. REGENERATION OF SINW-FET BIOSENSOR SURFACES

This chapter surveys the regeneration methods for miRNA SiNW-FET sensors. Regeneration refers to the unbinding of the miRNA analyte molecules from their bioreceptor probes (DNA, PNA, or LNA) in order to reuse the sensor. Section 5.1 presents some of the general concepts about what biosensor regeneration is and the regeneration principles of miRNA biosensors. The following sections introduce different regeneration methods that have been grouped into four categories: thermal regeneration (Section 5.2), regeneration based on chaotropic agents (Section 5.3), acid/base regeneration (Section 5.4), and introduction of a method that has not been reported in connection with biosensors, namely, enzyme-based regeneration (Section 5.5). It is important to mention that even if some of these regeneration schemes have already been reported in studies of SiNW-FETs biosensors, most of the methods proposed in this chapter are adapted from other types of biosensors.

5.1 General aspects

The antagonist process of hybridization is the denaturation or melting of DNA or DNA-RNA duplexes. The process of DNA denaturation refers to disruption of the double helix and dissociation into two single strands (Alberts, 2002). During this event, the hydrogen bonds that hold together the two strands by complementary base pairs are broken (see Figure 15). This can be performed by heating or by exposure of the nucleic acid duplexes to chemicals. When discussing specifically a miRNA biosensor, regeneration would refer to the ability of DNAp and miRNA hybridization to reoccur between the immobilized DNA probe and the target miRNA, after the hydrogen bonds between nucleotide bases of the formed duplex are broken, leaving the DNA probe intact and available for subsequent hybridization.

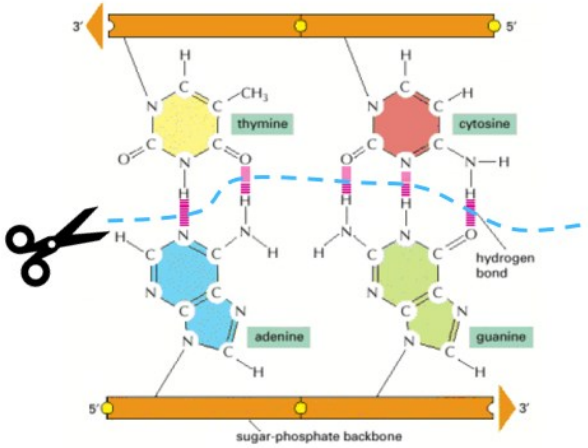

Figure 15. *Principle of nucleic acid sensor regeneration based on disruption of hydrogen bonds formed between the complementary base pairs of a single-stranded DNA probe and target miRNA. (reproduced from Alberts, 2002)*

Regeneration of biosensors is beneficial in many respects, such as lowering testing costs by allowing repeated use of the sensor. Through this approach, the sensor-to-sensor variation is eliminated, which is useful when we repeatedly evaluate the same level of analyte. When a biosensor regeneration method is considered, the molecular interactions between the bioreceptor and the target analyte are very important. (Goode, 2014.)

Throughout the literature, several regeneration strategies for different types of biosensors (e.g., optic, acoustic, and electrochemical) have been proposed. In Table 4 are collected the main reagents used in biosensor regeneration, together with the new proposed method, the enzyme-based regeneration method. In the next sections, the main methods that could be suitable for regeneration of a SiNW-FET for miRNA detection are discussed.

According to Dupont-Filliard, in DNA biosensors there are two possible regeneration paths: a complete removal of the DNAps from the surface or, by denaturation of the DNA–miRNA duplex, leaving the DNAps on the sensor surface (Dupont-Filliard, 2004). The complete elimination of the DNA probe from the surface might be challenging as the DNAp layer might not be fully removed, and the “leftovers” or residues might interfere in further reactions. Due to these uncertainties, the methods proposed refer only to denaturation of DNAp–miRNA duplexes.

Table 4. *Regeneration methods for biosensors*

Regeneration approach	Chemical agents	Application	Analyte	Reference
Acids	HCl Nitric acid Acetic acid	SiNW-FET, acoustic ssDNA sensor; SPR;	miRNA, proteins	Mannelli, 2003; Jokilaakso, 2013b
Alkaline agents	NaOH	SPR, acoustic sensors	DNA, antibodies	Ulianas, 2014; Yao, 2009; Lazerges, 2006; Jokilaakso, 2013b;
Thermal regeneration		SiNW FET, fluorescence-based DNA aptamer	miRNA, drug detection	Jokilaakso, 2013b; Hilton, 2011
Chaotropic agents	Urea	Immunosensors, SiNW-FET DNA/miRNA sensors	miRNA, DNA, HCG (human chorionic gonadotropin) hormone	Lu, 2011; Yang, 2009; Yao, 2009;
	DMSO	Optical biosensor	Human serum albumin	Tedeschi, 2003; Yao, 2009
	Formamide	Acoustic biosensor	Oligonucleotide	Tedeschi, 2005
	EDTA	Immunosensor	IgE	Yao, 2009
	Guanidinium thiocyanate (GTC)	SPR	Biotinylated bait	Knoglinger, 2018
	Guanidine hydrochloride Potassium thiocyanate	Microarrays	Pathogenic antibodies	Meyer, 2015
Detergents	SDS	Optical immunosensors, Quartz-crystal microbalance	Human cardiac troponin T, C-reactive protein	Mattos, 2012; Albrecht 2008; ForteBio, 2009
Enzymes	Helicases RNase H			
Glycine		Optical Immunosensors		Yao, 2009; ForteBio, 2009

5.2 Thermal regeneration

Changing of temperature often affects the structure and behavior of biomolecules such as oligonucleotides and proteins. In the case of oligonucleotides, the base pair decoupling due to an increase in temperature is called melting or denaturation (Garibyan & Avashia, 2013). At ambient temperatures, the double-stranded DNA is held together by the hydrogen bonds between the base pairs. The number and the type of base pairs involved influence the dissociation or melting temperature, with the guanine-cytosine (GC) content having the greatest influence. Theoretically, by increasing the temperature, we increase the kinetic energy that can overcome the base pairing and help to separate the strands.

The phenomenon of thermal DNA denaturation has been studied extensively in recent years. The temperature at which half of the DNA double helix is denatured is known as the melting temperature of DNA (T_m). This has been determined through changes in absorbance of 260-nm UV light by the DNA-containing solution. (Blanco & Blanco, 2017;

Sigma-Aldrich, 2019a.) This temperature is influenced by multiple factors, such as the length of DNA (the longer the DNA sequence, the higher the melting temperature), the nucleotide sequence composition, and the ionic strength of the buffer (Khandelwal & Bhyravabhotla, 2010). The GC nucleotide pairs are kept together by three hydrogen bonds and adenine-thymine (AT) pairs by two (see Chapter 2.3), thus a higher GC content in the DNA sequence has a higher resistance to denaturation and increases the melting temperature (Blanco & Blanco, 2017).

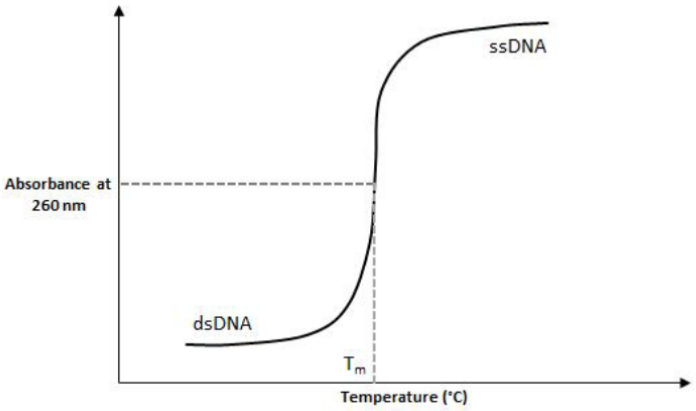

Figure 16. *DNA melting temperature (T_m) that corresponds to the temperature at which 50% of DNA is denatured. This was determined through changes in absorbance of 260-nm UV light by the DNA-containing solution (Sigma-Aldrich, 2019a)*

Since the T_m is very important in various biotechnology techniques, such as PCR, Southern blotting, and in situ hybridization, specifically in primer design, many research groups proposed different methods to predict T_m. The initial method for T_m calculation was based on the GC content of the sequence and later included the effect of the salt concentration of the solution.

The basic method for calculation of T_m is based on the Marmur Doty formula and is generally used for oligonucleotides with short sequences (14 or fewer) (Sigma-Aldrich, 2019a):

$$T_m = 2(A + T) + 4(C + G) - 7, \quad (2)$$

where T_m is the melting temperature in °C; A, T, C, and G refer to the number of adenine, thymine, cytosine, and guanidine nucleotides in the sequence, respectively; and -7 is a correction factor.

For longer sequences (15–120 nucleotides), the nearest neighbors method offers more accurate T_m values, as it takes into consideration thermodynamic factors and cation concentration in addition to sequence composition (Sigma-Aldrich, 2019a):

$$T_m = \frac{\Delta H}{A+\Delta S+Rln(\frac{C}{4})} - 273.15 + 16.6log[Na^+], \quad (3)$$

where T_m is the melting temperature in °C, *ΔH* is the enthalpy change in kcal/mol, *A* is a constant of -0.0108 kcal/(K·mol) and refers to the helix initiation during annealing/melting, *ΔS* is the entropy change in kcal/(K·mol), *R* is the gas constant of 0.00199 kcal/(K·mol), *C* is the concentration of oligonucleotides in M or mol/L, and [Na+] is the sodium ion concentration in M or mol/L.

Thermal regeneration of oligonucleotide-based biosensors has been previously reported (e.g., Jokilaakso, 2013b), but it has its limitations. It is very important to mention that, while a DNA molecule denatures at temperatures higher than the ambient temperature, the renaturation process (also known as annealing or hybridization), which refers to the reverse process when the separated single strands hybridize again, is thermodynamically favorable under ambient conditions. Therefore, accurate control of the temperature is required. The temperature of denaturation, however, is difficult to predict and control, often requiring expensive, time- and energy-consuming devices (e.g., thermal cyclers, as in PCR applications) (Syed, 2013). In addition to these drawbacks, the biological components, such as the DNA immobilized probes, the underlying layers, and the electronic components, must withstand the increased temperatures that might be required for separation of miRNA strand from the ssDNA probe.

5.3 Regeneration based on chaotropic agents

A chaotropic agent is a molecule that can disrupt the hydrogen bonding between water molecules, altering the stability of other molecules in solutions, such as proteins or nucleic acids, by reducing the hydrophobic effect (Salvi, 2005). These chemical agents work by lowering the melting temperature of the DNA molecule by competing for hydrogen donors and acceptors with the pre-existing nitrogenous base pairs (Ito, 2017; Wang, 2014).

One widely used chaotropic agent is urea. In a few studies, urea was used as a regeneration agent for immunosensors based on cyclic voltammetry detection. The concentration of urea solution varied from 4 M (Yang, 2009) to 8 M (Lu, 2011), and the regeneration was successful for approximately five cycles. Additionally, the use of urea resulted in no disturbance in the detected signal or in the underlying layers (Lu, 2011; Yang, 2009).

Other types of chaotropic agents include dimethyl sulfoxide (DMSO), formamide, ethylenediaminetetraacetic acid (EDTA), and potassium thiocyanate. Most of these agents have been used in molecular biology for denaturation of DNA. By extension, they could be used in miRNA biosensor regeneration. Tadeschi *et al*. successfully used a 1:1 (v/v) solution of formamide-water on an oligonucleotide-based sensor for regeneration of the sensor surface without loss of performance (Tadeschi, 2005). However, in the study of Wang *et al.*, a solution with 60% concentration of DMSO was shown to be more efficient in denaturation of DNA than formamide at room temperature (Wang, 2014). Therefore, DMSO is also a good candidate for regeneration of miRNA biosensors, being able to lower more efficiently the T_m.

5.4 Acid/base-based regeneration

Several research groups have reported biosensor regeneration methods based on high- or low-pH buffers. Generally, for increasing the pH of solutions, sodium hydroxide (NaOH) is used (Ulianas, 2014; Xu, 2017; Jokilaakso, 2013b), while hydrochloric acid (HCl) is used for decreasing the pH (Jokilaakso, 2013b). By modifying the pH of the environment, the enthalpic state of the system is altered due to changes between the analyte and bioreceptor charges that maintain the structure of, for example, the DNAp–miRNA duplex (Goode, 2014).

The choice between acid or base regeneration depends strongly on the substrate material. For example, gold substrates can be easily regenerated with NaOH buffer solutions, as has been demonstrated in optical and acoustic biosensors, but on a silicon substrate, as in the case of a SiNW-FET sensor, NaOH is not recommended, as the Na ions can leak through the oxide-insulating layer and destabilize the electric measurement (Jokilaakso, 2013b). However, HCl could be used as an agent for the surface regeneration of SiNW-FETs. Jokilaakso *et al.* stated that a solution of 1 mM HCl was superior to NaOH for thermal regeneration, allowing reuse of the sensor for ten cycles of regeneration–hybridization (Jokilaakso, 2013b).

Before conducting regeneration based on an acid or base solution, however, it is important to evaluate whether altering the pH of the environment interferes with the sensor signal. For example, in electrochemical biosensors, pH regeneration may affect the signal baseline. Additionally, it is important to take into consideration the possible effects of the solutions on the bioreceptor, to ensure that it will not be damaged. Although the method has its disadvantages, acid/base-based regeneration is low-cost and has been

widely reported on, which makes it a good starting point for biosensor regeneration. (Goode, 2014.)

5.5 Enzyme-based regeneration

Enzymes are specialized proteins that catalyze, or speed up, a chemical reaction. To the author's knowledge, regeneration methods for miRNA biosensors based on enzymes have not yet been reported. Therefore, this section introduces two classes of enzymes that may be suitable for a miRNA biosensor regeneration. This possibility is suggested by their analogous use in other biological processes, such as DNA replication.

In the process of DNA replication, which takes place when a cell divides, a large number of proteins act to unwind the DNA double helix and, subsequently, to synthesize a new DNA molecule. The types of enzymes that are capable of opening the DNA double helix in this way by breaking the H bonds between the bases are of interest. Two classes of enzymes have been identified: helicases and ribonucleases H (RNase H).

Helicases are a class of enzymes that use adenosine triphosphate as an energy source to unwind two annealed nucleic acids, such as DNA, RNA, or DNA–RNA complex (Patel & Donmez, 2006, Singleton, 2007, Wu, 2012). Helicases have different specificity depending on the substrate used, RNA or DNA, and they show different directionality of translocation (3′–5′or 5′–3′). They work by binding to a single-stranded region of an oligonucleotide to initiate the separation of strands. Once they attach to the strand, they translocate in either the 3′–5′ or 5′–3′ direction. (Patel & Donmez, 2006.) In previous research, Singleton *et al.* classified and described the families and subfamilies of helicases based on translocation directionality and whether they involve a double- or single-stranded nucleic acid (Singleton, 2007). The right enzyme should be carefully chosen based on these factors.

In the SiNW-FET sensor functionality design presented in this thesis, a DNA probe is covalently attached to the NW surface by its aminated 5′-end (see Figure 21), and during regeneration of the sensor, the bound miRNA molecule should be removed for subsequent sensor reuse. Thus, an enzyme with 5′–3′ directionality is needed to remove the miRNA strand. Singleton *et al.* identified a potential group of helicase enzymes, called the SF1B subfamily, with 5′–3′ directionality (Singleton, 2007).

Another class of enzymes that can work in regeneration of a miRNA biosensor are the ribonucleases H (RNase H). They have been identified as having a role in the DNA replication and repair process, and they can cleave the RNA of an RNA–DNA hybrid by

hydrolysis of the RNA strand to produce a 5´ phosphate-terminated oligonucleotide and a single-stranded DNA (Cerritelli & Crouch, 2009; Kanaya, 2009).

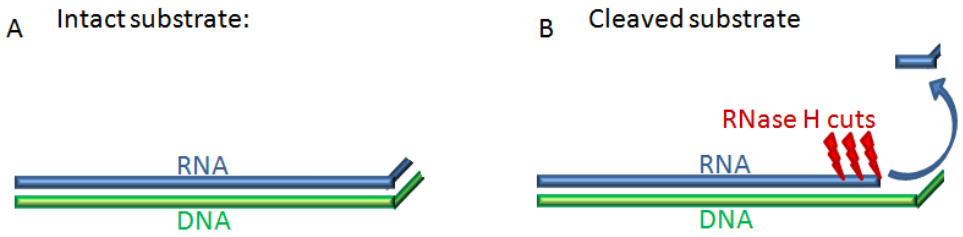

Figure 17. *The scheme of action of RNase H on the hybridized DNA–RNA duplex: (A) the formed DNA–RNA duplex is intact, and (B) action of RNase H enzyme on the RNA strand leading to its cleavage, leaving the DNA strand intact. (reproduced from Corona & Tramontano, 2015)*

Although a suitable enzyme for degrading the miRNA strand is identified, other aspects should be considered in regeneration of a miRNA biosensor as well. The DNA strand should not be affected by the enzymes, leaving it intact for other hybridization cycles. Additionally, a total removal of the enzyme from the sensor is required to eliminate any possible disturbances in the signal. All these aspects, together with the basic regeneration described by Goode *et al.*, make the process very complex, but they open more possibilities for biosensor regeneration.

5.6 Discussion on biosensor regeneration

In this section, the advantages and disadvantages of the regeneration methods previously discussed are presented. Additionally, the impact of the bioreceptor probe type on miRNA biosensor regeneration is also discussed. Finally, the criteria for reporting a successful regeneration are presented.

Although the melting temperature of, for example, a DNA double strand can be easily determined through different methods (see Formula (2) and (3) in section 5.2), little has been published on the thermal regeneration of RNA/DNA biosensors. The duplex separation by means of temperature change (or thermal denaturation) is widely used in qRT-PCR applications where the equipment allows accurate control of the temperature, which may be very difficult otherwise. The high costs of the equipment and the possibility of degradation of the sensor surface and electrical components due to the potential for excessively high temperatures are major drawbacks of this method. In contrast, an acid-based regeneration is much cheaper, with some studies reporting its successful use for SiNW-FETs for miRNA detection (Jokilaakso, 2013a). However, altering the pH of the

sensor environment can cause baseline shifts of the sensor and possible degradation of the oligonucleotide probes. Similar problems can be caused by other chemical agents as well, such as the chaotropic agents. In contrast, enzymes can be chosen for their precise action towards DNAp–miRNA duplex separation, avoiding damage to the underlaying layers. However, the presence of these enzymes can interfere with the signal, and eliminating them from the sensor surface may be very difficult.

An important aspect in the regeneration is the type of bioreceptor probe. In the previous sections, the regeneration possibilities of a miRNA biosensor with a DNA probe were discussed. However, synthetic PNA and LNA probes could be used as well. The possibilities of regeneration might differ due to their intrinsic properties. For example, PNA molecules have been reported to be electrically neutral, thus allowing a stronger binding with a miRNA molecule. The stronger binding is caused by the absence of the repulsion force normally developed between the negatively charged DNA and miRNA molecules. Thus, the bonds formed between PNA and miRNA molecules might be more difficult to break. In case of thermal regeneration, the temperature required to break the hydrogen bonds should be generally higher than with natural DNA, since the PNA molecule and the DNA–PNA duplexes are more thermally stable. Similarly, LNA probes might introduce similar drawbacks, since LNA has also been reported to have a high thermal stability. Additionally, both PNA and LNA molecules have been reported to be resistant to enzymatic degradation (Exiqon, 2009; Zhang & Apella, 2010), thus it may not be possible to apply enzyme regeneration of miRNA biosensors where PNA or LNA probes are used. To the author's knowledge, the regeneration of biosensors using synthetic oligonucleotides such as PNA and LNA has not yet been reported.

Wide studies have been done in the field of miRNA biosensors, but the regeneration aspects have not yet been much evaluated. Often, the publications from these studies feature only brief sections lacking detailed information and data, hence it is important to question how the success of a regeneration process can be evaluated and reported. According to Goode *et al.*, there is not yet established in the literature a criterion for determining a successful biosensor regeneration, leaving room for debate. The difficulty in comparing data sets makes it challenging to validate whether a regeneration procedure was successful. Thus, Goode *et al.* proposed basic criteria for evaluation of regeneration (see Table 5) and found that only ~60% of the reported regeneration studies met these criteria. Therefore, all biosensor regeneration studies should be reported on using a standard set of criteria as the one proposed by Goode *et al.* (Goode, 2014).

Table 5. *Basic criteria for evaluation of biosensor regeneration (from Goode, 2014)*

Attribute	Criteria
Signal loss between interrogation cycles	<5%
Number of continual cycles achieved	>10
Restoration of baseline signal	<±5%
Biosensor/transducer reconstruction	Avoided
Signal loss profile	Linear in order to allow accurate calibration
Regeneration conditions	Explicitly listed with time of incubation and full buffer components

The methods presented in previous sections (5.2, 5.3, 5.4, 5.5) may theoretically be usable in regeneration of a miRNA SiNW-FET, but their potential effects and efficiency should be practically assessed. Although, regeneration is not experimentally tested in this thesis work, the theoretical grounds discussed offer possibilities for further research.

6. MATERIALS AND METHODS

This chapter introduces the materials, including the devices (Section 6.1) and the chemical reagents (6.2), and the methods used in the experimental part of the thesis. The methods proposed for the study of SiNW-FETs for miRNA detection follow this strategy: electrical testing of sensors, testing of the effects of various influential parameters, conversion of sensors into biosensors by applying a chosen functionalization strategy, and finally measurement of miR-218. Section 6.3 presents the methods for characterizing provided SiNW-FET sensors. Section 6.4 proposes the testing of several parameters that might alter the signals and give false positive results during miRNA detection, such as temperature, illumination, sensor surface hydrophobicity and effects of crystalized PBS salts over the surface.

Maintaining the viability of the miRNA and DNA molecules is crucial for reliability of the experiments, therefore Section 6.5 introduces procedures for preparation of the PBS and miRNA/DNA samples. Section 6.6 describes the chemical functionalization method employed for immobilization of single-stranded DNA probes on the surface, which make possible the detection of miRNA.

6.1 Devices used in experiments

For this thesis, 15 p-type SiNW-FET sensors were obtained from Shanghai Institute of Microsystem and Information Technology. After the initial testing, 9 devices were found operational and were further utilized in the experiments. The As shown in Figure 18, the devices have an active sensing area of approximately 1 mm^2 (the black central square), including the grid/gate, source, and drain electrodes, and an array of 120 well-ordered NWs. The batch of 15 sensors obtained, however, contained different sensors with slightly varying size of the sensitive area and number of the NWs in the arrays.

The grid/gate, source, and drain electrodes are extended with gold lead wires to four pin electrodes that allow the connection of the sensor to measurement devices or breadboards. The overall size of the devices is approximately 81 mm^2.

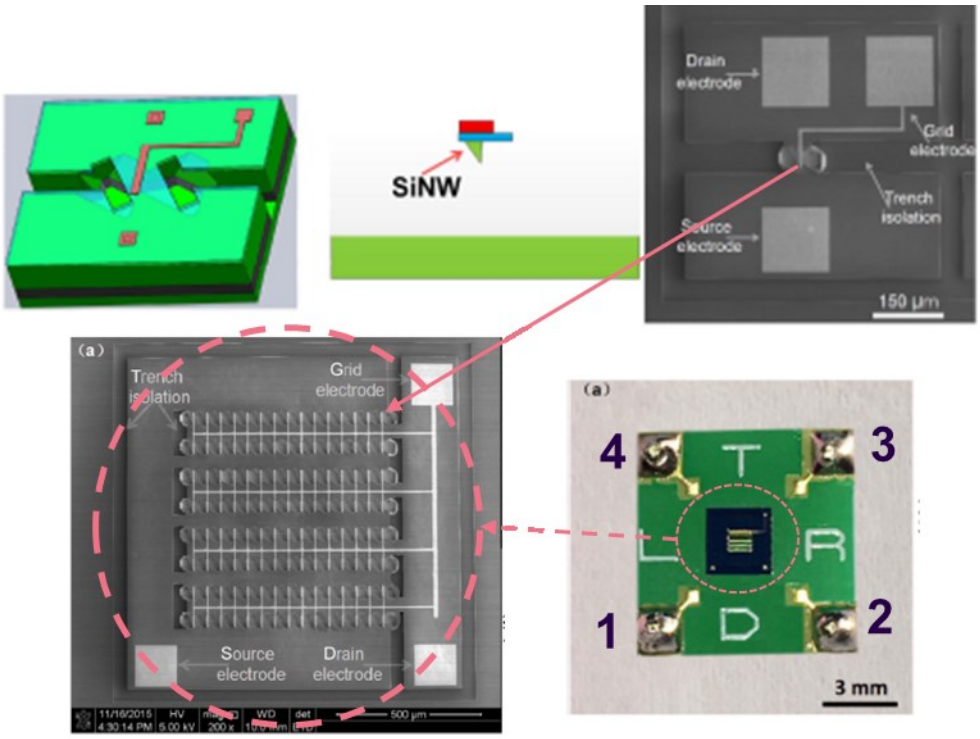

Figure 18. *Schematics and pictures of the SiNW-FET sensors used in the experiments.* ***Up left****: schematic of a single NW, top view;* ***up middle****: schematic of a single NW, side view (NW hanging underneath the surface inside a trench-like cavity;* ***up right****: SEM picture of a SiNW-FET with one NW.* ***Down left:*** *SEM image of a SiNW-FET array with 120 NW;* ***down right****: image of the SiNW-FET device, where (1) is the source pin, (2) is the drain, (3) is the grid/gate electrode, and (4) is a pin only for fixing purposes. (reproduced from Yang, 2018)*

Table 6. *Sensor count and the types of tests performed*

Test	Sensor
FET characterization in air	S5
FET characterization in liquid	S5
Resistive characterization in air	S1–S14
Resistive characterization in liquid	S1–S14
Hydrophobicity	S1, S2, S5
Hydrophilicity	S1, S2, S12
Droplet evaporation from non-functionalized surface	S1, S2, S5
Droplet evaporation from functionalized surface	S9, S11, S13
Temperature effect	S12
Illumination effect	S2
miRNA	S6, S7, S12, S15*

*Sensor S15 was not electrically characterized because it was used in a preliminary test.

For electrical characterization of the sensors as FETs, a Keysight semiconductor parameter analyzer was used, and the setup is shown in Figure 19.

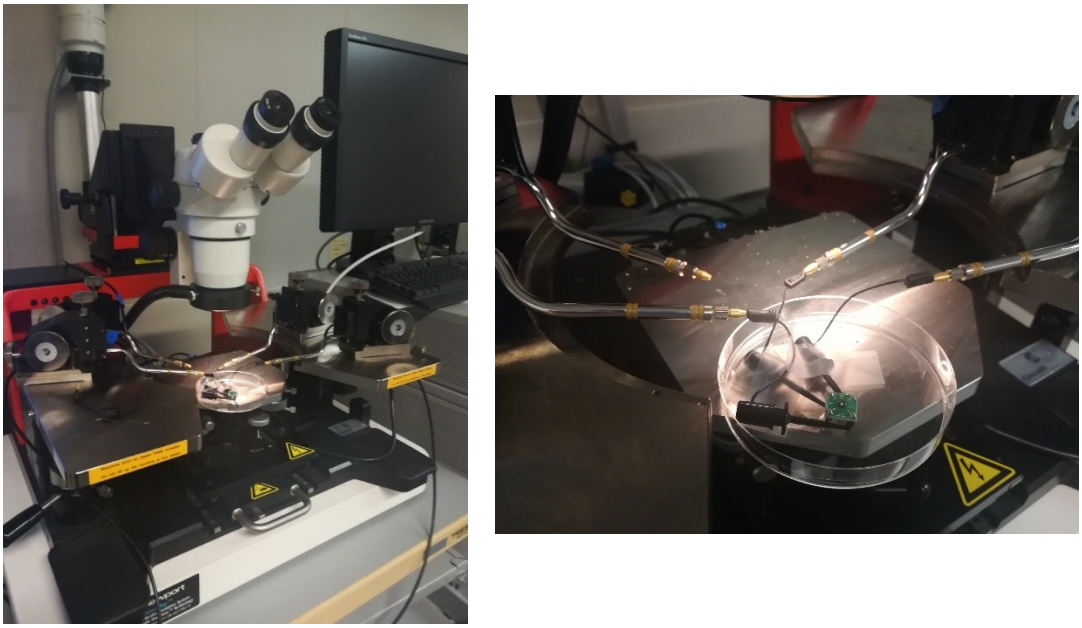

Figure 19. *Connection of the SiNW-FET devices to the Keysight semiconductor analyzer setup for SiNW-FET transistor characterization*

Devices and equipments used:

- SiNW-FETs (Shanghai Institute of Microsystem and Information Technology). During measurements, the sensors were inserted in a Faraday that offer sheltering from electromagnetic noise.
- IviumStat.h electrochemical analyzer (IviumStat.h, IUVIUM Technologies, Eindhoven, The Netherlands); ChronoAmperometry mode.
- Keysight semiconductor analyzer (Keysight B1500A, Keysight Technologies, USA).
- Plasma treatment device (Plasma Surface Technology, Diener Electronics, Ebhausen, Germany). Used for oxygen plasma treatment of SiNW-FETs. Parameters: 75 W, 15 min.
- Direct-Q Water purification system (Direct-Q 3, 5 & 8 System, Millipore, Merck, Germany) with Biopak ultrafilter for production of nuclease-, protease- and bacteria-free water (Biopak Polisher, Merck).
- Hot plate (AREX-6 Digital Advanced CerAlTop Hot Plate Stirrer, Velp Scientifica, Italy).
- Faraday cage (In house made).

6.2 Chemical reagents and DNAp/miRNA samples

The chemical reagents used for cleaning and functionalization of the SiNW-FET sensors and PBS preparation were as follows:

- Ethanol (ETAX Aa, 99.5%, Altia OY, Finland).
- APTES (3-Aminopropyl)triethoxysilane, 99%, Sigma Aldrich).
- GA (Grade II Glutaraldehyde, 25% in H_2O, Sigma Aldrich).
- Single-stranded DNA oligonucleotide probes (Sigma Aldrich) in dry form; HPLC purification.
- miR-218 in the form of small interfering RNA (siRNA) (ThermoFisher Scientific) in dry form; purification: desalted.

Based on the known miRNA sequence (see Table 7) retrieved from miRBase (miRBase, 2019), the complementary DNA probe was designed to have an amine (NH_2) termination at the 5´-end (see Table 7).The miRNA and DNA oligonucleotides are custom made. The samples were delivered in powder form and stored at -20 °C in freezer. The purification method used for DNAp was HPLC, and for miR-218 samples the type of purification was desalted.

Table 7. *The nucleotide sequences of the miR-218 and DNA probes*

Sample type	Sequence
miR-218	5´- UUG UGC UUG AUC UAA CCA UGU – 3´
DNA probe	5´ - [Amine] ACA TGG TTA GAT CAA GCA CAA - 3'

6.3 Electrical characterization of SiNW-FET devices

To evaluate and understand the performance of these SiNW-FETs the devices were characterized in two ways: as a FETs and as a resistive device, which are explained as follows.

6.3.1 FET characterization

The SiNW-FET transfer characterization and measurements of gate current leakages were performed with a Keysight semiconductor analyzer (see Figure 19) by connecting the gate (G), source (S), and drain (D) electrodes of the sensor to the measurement device. The I_D-V_G and I_G-V_G curves were simultaneously measured by swiping the gate voltage (V_G) between 0 and 0.5 V and measuring the drain current (I_D) while the drain voltage (V_D) was maintained at a constant level (0 to -0.5 V, with a 0.1 V step). The same measurement procedure was followed for characterization in both air and liquid environments. The latter measurement was performed by drop casting a 20 µl droplet of PBS solution on top of the sensor, assuring full coverage of the active area. Next, the transistor characterization was performed to evaluate the levels of current leakages.

6.3.2 Resistive characterization

To avoid the use of the gate electrode as in normal transistors, further characterization was performed with the sensors in the resistive device mode, meaning that the gate electrode was not operated, and the I_D through the NW was measured while swiping the V_{DS} between 0 and 0.5 V (0.025 V step, 30 s/step). The source and drain electrodes of the sensors were connected to an IviumStat.h electrochemical analyzer operated in ChronoAmperometry mode, making 25 mV step-wise changes in the V_{DS} while drain current (I_D) was measured through the NW (see Figure 20).

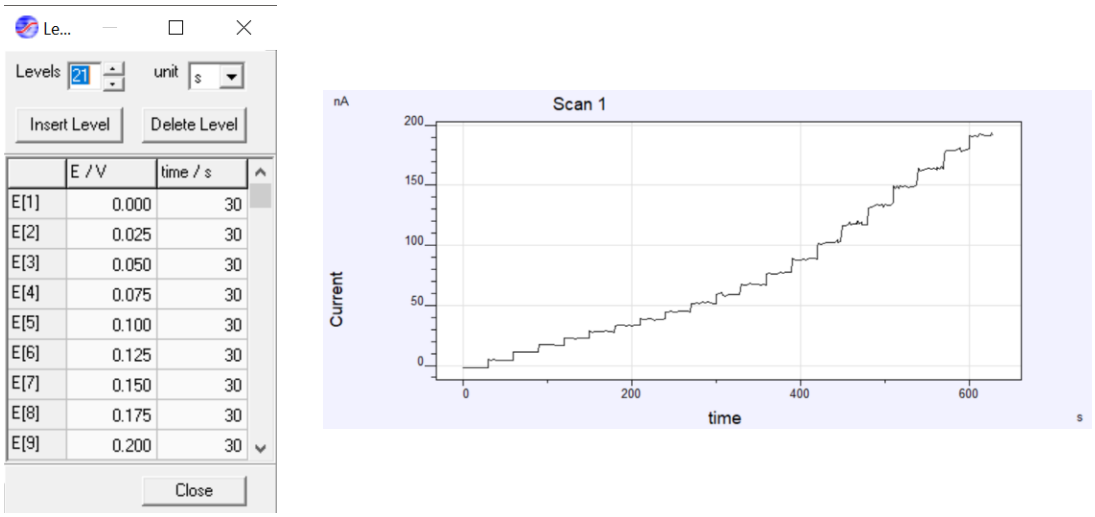

Figure 20. *Example of the input step voltages (left) and the output current obtained with IviumStat.h(right).*

These measurements were performed for each of the fourteen devices included in the final tests, and based on the data obtained, the sensors with good functionality were chosen for further measurements. Sensor S15 was used not included in the characterization tests because it was used in a preliminary test.

6.4 Disturbance tests

Generally, it is desired that a biosensor be sensitive only to the biological interactions that take place at its surface and not to other internal or external influences. However, in practice, the devices are not ideal but are susceptible to various types of influences.

6.4.1 Hydrophobicity and hydrophilicity of sensor surface

In its unmodified state, the active surface area of the sensor is hydrophobic. Thus, the access of aqueous solutions to the inside of the cavity where the NW are suspended (for

more details about the design see Figure 18) may be hindered as a result of hydrophobicity of the sensor surface. To evaluate hydrophobicity versus hydrophilicity effects, a constant V_{DS} was applied (0.4 V) while the I_D through the NW was monitored with the IviumStat.h during the drop casting of five PBS droplets (5 µl/droplet) at intervals of 5 minutes. The difference between the hydrophobic and hydrophilic tests was that in the latter the surface was rendered hydrophilic by exposure to an oxygen plasma for 15 minutes at 75 W.

6.4.2 PBS droplet evaporation

The droplet evaporation test was performed to evaluate whether the PBS solution, specifically the salts it contained, had an effect on the sensor operation during successive uses. For these tests, two types of surfaces were employed: a non-functionalized surface (not chemically modified), and a functionalized surface to which the functionalization scheme described in Section 6.5 had been applied. For each surfaces type, a 2.5 µl PBS droplet was drop cast onto the sensor surface, and the drain current I_D was monitored until the droplet's full evaporation. The measurement was performed with the IviumStat.h, setting the V_{DS} at 0.4 V.

6.4.3 Effect of temperature

To measure the effect of the temperature on the sensor behavior, the sensor was placed on a hot plate and introduced in a Faraday cage so as to avoid electrical interference from the environment (i.e., electromagnetic noise). The I_D of the sensor was monitored with the IviumStat.h by keeping the V_{DS} at a constant value while the temperature of the hot plate was increased (starting from room temperature of 21.7 °C and increasing to 36 °C, with a step of 2 °C). Since the Faraday cage was closed, the temperature inside the cage was assumed to be the temperature of the hot plate.

6.4.4 Effect of illumination

Preliminary tests with the SiNW-FETs showed high levels of interference caused by changes in environment illumination. Therefore, in these tests the sensors were connected to the IviumStat.h device by feeding a constant V_{DS} (0.4 V), and the I_D was measured while illumination was changed over six steps: from full illumination (four ceiling lights on), through three decreasing steps (three lights on, two lights on, one light on), to dark mode (all lights off), and back to full illumination.

6.5 Preparation of miRNA and DNA probe samples

The cleaning of the equipment and containers used for preparation and handling of samples, the preparation of PBS solution, and the resuspension of the miRNA and DNA samples are important steps to assure viability of the samples. Therefore, the procedures followed these steps are presented below.

Procedure for cleaning the equipment and containers used in sample preparation:

1. Preparation of Piranha solution by mixing of 5:1:1 (v/v/v) deionized (DI) and nuclease-free water, hydroxylamine (NH_2OH), and hydrogen peroxide (H_2O_2) in a bottle or container.
2. Place the bottle with the solution on a hot plate (with the cap loose) and heat it to approximately 80 °C until the reaction starts.
3. Close the bottle and slowly shake it for a few seconds to wash the walls and cap with the solution.
4. Loosen the cap and return the bottle to the hot plate for several minutes, then repeat steps 2 and 3 for approximately 10 minutes to ensure elimination of all organic contaminants.
5. Add the Piranha solution to an open beaker or bottle and leave it to cool before final disposal.
6. Thoroughly rinse the cleaned bottles with DI water and leave to dry in a clean location (e.g., under a laminar hood) to avoid contamination.

Procedure for preparing the PBS solution:

1. To the cleaned bottle add 1 PBS tablet and 50% nuclease-free DI water and place it in an ultrasonic bath for 15 minutes until the tablet is fully dissolved.
2. Adjust the water to the final volume and stir it for several minutes.
3. Filter the resulting PBS with a syringe through a 0.22 µm filter.
4. Store the final solution in a clean bottle in a refrigerator.

miRNA and DNA oligonucleotides resuspension:

1. Thaw the tube of dried oligonucleotides that were previously stored at -20 °C.
2. Centrifuge the tube before opening it to avoid loss of the material from the vial cap.
3. Transfer the vial in a clean environment such as under a laminar hood (do not open it before this point) after ensuring a proper cleaning of laminar hood surfaces and pipettes with 80% ethanol solution.
4. Use a laboratory coat and long gloves that properly cover the skin. Skin particles can contaminate the environment with nucleases.
5. Clean the gloves with 80% ethanol solution as well, and do not touch anything outside the laminar hood.
6. Use only sterile and nuclease-free pipette tips and tubes to avoid contamination with enzymes and sample degradation.
7. Resuspend the oligonucleotides in the PBS solution previously prepared in 100 µM or 10 µM master stock concentrations.
8. Store the master stock solutions in a freezer at -20 °C for prolonged viability.
9. The samples to be used can be stored for a short period of time in a refrigerator.

6.6 SiNW-FET sensor functionalization and measurement setup

The surface of the SiNW must be modified with a complementary single-stranded DNA probe molecule for the biosensor to be able to recognize and detect the specific miR-218 analyte molecule. For the experimental part of this work, the covalent attachment of the DNAp based on APTES and GA was chosen and is represented in Figure 21 (for details see Chapter 4.2).

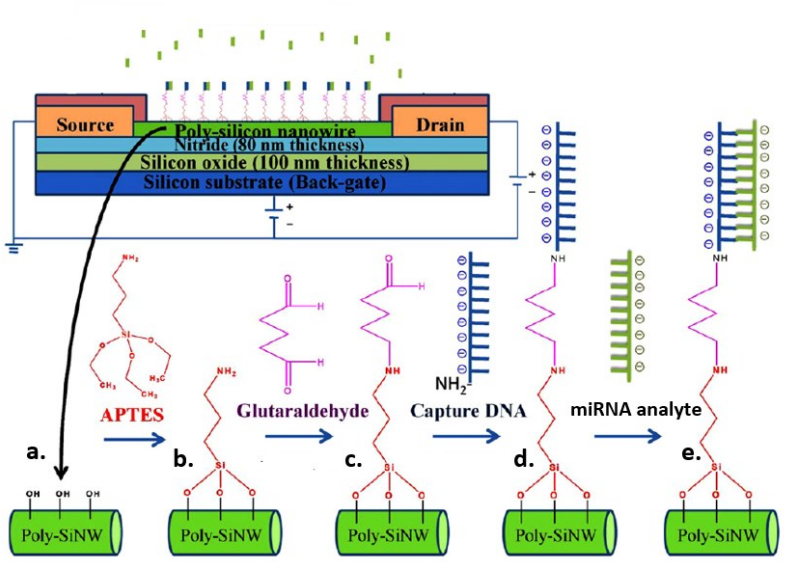

Figure 21. *SiNW-FET functionalization scheme based on APTES–GA–DNAp. (re-produced from Lin, 2009)*

Before any modification of the SiNW surface, the sensors were cleaned with ethanol or isopropyl alcohol solutions to eliminate contaminants, followed by rinsing with nuclease-free DI water and drying. To chemically modify the surface of the NW, different reactive groups have to be present on the surface to ensure a covalent binding of the subsequent layers. Normally, silicon surfaces have a native oxide layer, but to ensure enough hydroxyl groups (-OH) on the surface, the sensors were treated with oxygen plasma for 15 minutes at 75 W (Figure 21a). Additionally, the oxygen plasma ensured a further cleaning of the surface.

The plasma-treated sensors were then incubated with a solution of 2% APTES in ethanol for two hours for formation of amine reactive groups (Figure 21b), followed by a washing step with ethanol and drying. The treatment with APTES was extended from one hour, as generally recommended for obtaining monolayers, to two hours for the liquids to properly reach the NW found in the cavity. The sensors were then thermally cured in an

oven at 120 °C for 15 minutes to eliminate the surplus ethanol and to cross-link and stabilize the silane layer.

In the next step, the silanized surfaces were reacted with a 2.5% GA solution in PBS for two hours for formation of aldehyde reactive groups on the surface (Figure 21c). Compared to DI water, GA dilution with PBS maintains the stability of the GA molecules. To eliminate the surplus GA, the incubation was followed by a thorough washing step with PBS and a subsequent drying.

After the deposition of APTES and GA layers, the sensor was ready for immobilization of the single-stranded DNA probes on the surface. The covalent attachment is a result of the reaction of the aldehyde groups with the amine ends of the DNA probes. Thus, the sensors were further incubated with a 0.5 µM DNA complementary probe solution for two hours (Figure 21d). The concentration of the DNA probes was limited to 0.5 µM to avoid the crowding effect. As described below, the sensors were washed with PBS to eliminate the unbound DNA probes and were then dried.

Procedure for functionalization of a SiNW-FET surface:

1. Wash the sensors with isopropyl alcohol and ethanol to remove possible contaminants.
2. Rinse the sensors with nuclease-free DI water, and dry the surfaces in airflow (low pressure).
3. Apply an oxygen plasma treatment on the sensors for 15 minutes at 75 W, to ensure formation of hydroxyl groups.
4. After step 3, immediately incubate the sensors with a 2.5 % solution of APTES diluted in ethanol for two hours in a clean container, for amine group formation. Assure that the sensors are protected from evaporation of APTES.
5. Wash the sensors thoroughly with ethanol to eliminate surplus APTES, then dry the surfaces in airflow at low pressure.
6. Cure the sensors in an oven at 120 °C for 15 minutes to eliminate surplus ethanol and stabilize the APTES layer.
7. Cool the sensors before next steps.
8. Incubate the sensors with a solution of 2.5 % GA diluted in PBS for two hours for aldehyde group formation. Protect the surface from evaporation and contamination.
9. Wash the sensors with PBS and dry them in airflow at low pressure.
10. For immobilization of the DNAp on the surface, incubate the sensors with 5 µl of 0.5 µM DNAp solution for two hours.
11. Wash the sensors with PBS to remove surplus DNAps and dry the surface in airflow.
12. Avoid contamination of the sensors between the functionalization steps by always wearing gloves when handling the sensors and by working under a laminar hood.
13. Before experiments, store the sensors in a clean container.

After the attachment of the DNAp to the SiNW the sensors were prepared for miRNA measurement. The sensors' source and drain electrodes were connected to the Ivium-Stat.h device, a constant V_{DS} voltage was fed through the NW, and changes in the I_D

current through the NW were monitored as miR-218 was introduced on the surface (see Figure 22). The miRNA samples were introduced on the surface by drop casting 5 µl miRNA onto the active area of the sensor. Due to the negative charges possessed by the phosphate backbones of the DNA and miR-218 molecules, their hybridization (Figure 21e) event alters the NW conductivity, and this altered the conductivity is detected by the measurement system as a change in the current I_D.

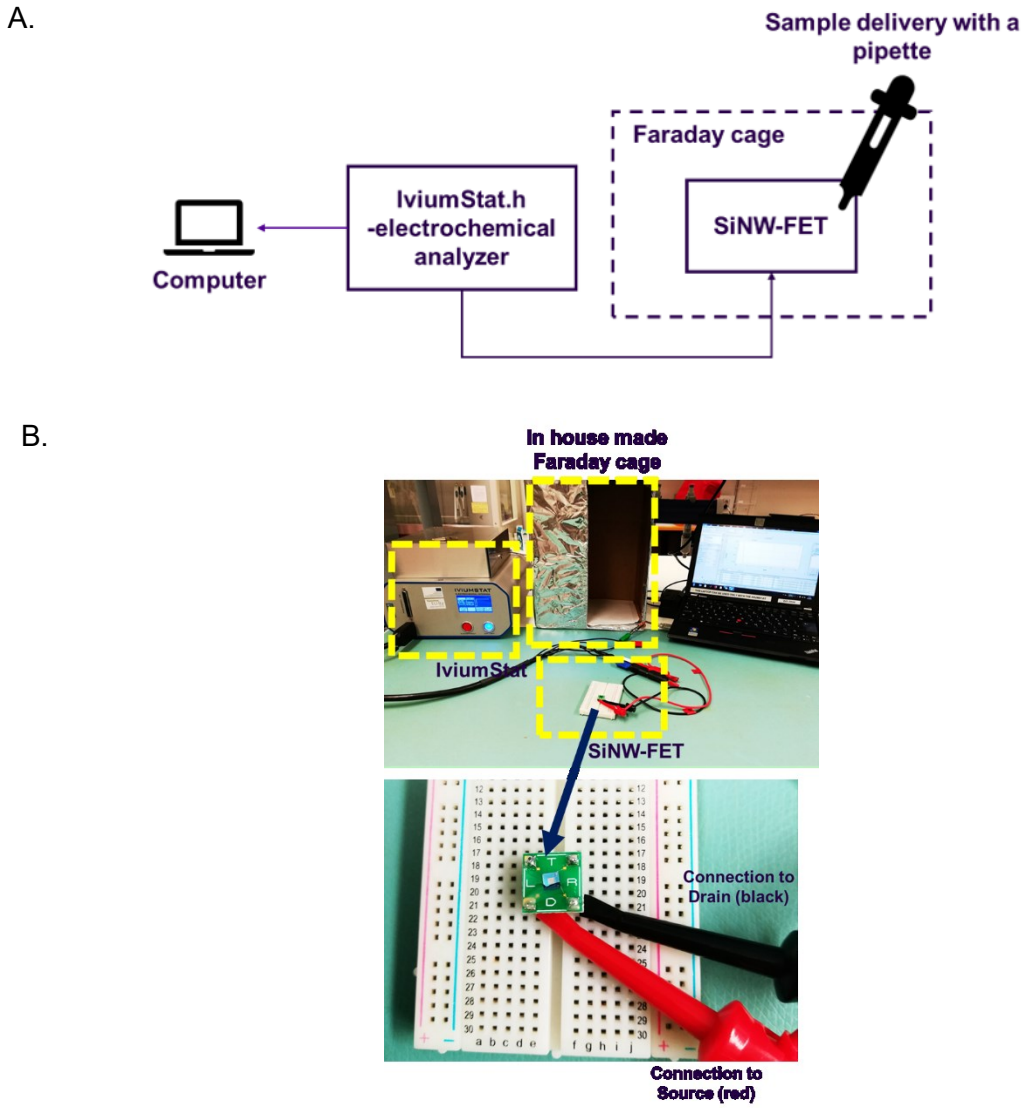

Figure 22. *Schematics of the measurement setup (A) including the Ivium-Stat.h electrochemical analyzer, the SiNW-FETs placed inside a Faraday cage, the sample delivery pipette, and the computer where the signals can be tracked and recorded. Picture of the laboratory setup (B) showing the IviumStat.h, the in house made Faraday cage, the SiNW-FETs and the computer; (down) zoom in picture of the SiNW-FET and the connections to source and drain electrodes.*

7. RESULTS AND DISCUSSION

This chapter presents the results and discusses of this thesis work. Section 7.1 introduces the results obtained from electrical characterization of SiNW-FET devices. Since the sensors are generally susceptible to different disturbances, Section 7.2 introduces and discusses the effects of hydrophobicity and hydrophilicity of the sensor surface (Section 7.2.1), the effects of PBS droplet evaporation (Section 7.2.2), the effects of temperature (Section 7.2.3), and the effects of illumination on the sensor signal (Section 7.2.4). The functionalization method applied to the SiNW-FETs and the results of the miRNA experiments are presented in Section 7.3.

7.1 Electrical characterization of SiNW-FET devices

Generally, before using a SiNW-FET sensor in a biomeasurement it is important that the sensor is electrically characterized so that its behavior and possible drawbacks are better understood. The SiNW-FET devices used in this thesis work are reported to present some drawbacks, such as high current leakages at the grid/gate electrode. Thus, until this problem is solved, the operation of the gate electrode is recommended to be avoided. Basically, this involved using the sensor as a resistive device such that, by applying a constant drain-source voltage (V_{DS}) on the SiNWs, the drain-source current (I_{DS}) could be measured. However, to experimentally confirm the effect of using the gate electrode, the leakage currents at the gate electrode were measured to evaluate their magnitude and possible effects (see Figure 23 and Figure 24). The devices were characterized in both air and liquid media, because sensor performance can vary in different media. Additionally, since the miRNA measurements were done in PBS, the performance of the devices in liquid was important to evaluate.

For measuring the I_D-V_G characteristic the value of source-drain voltage (V_{DS}) is fixed and the drain-source current (I_D) is measured while different gate voltages (V_G) are applied. The blue curves presented in Figure 23 and Figure 24 represent the I_D-V_D characteristics. For the plots in Figure 23, the measurement was done in air, whereas for Figure 24, measurements were done in a liquid environment (PBS).

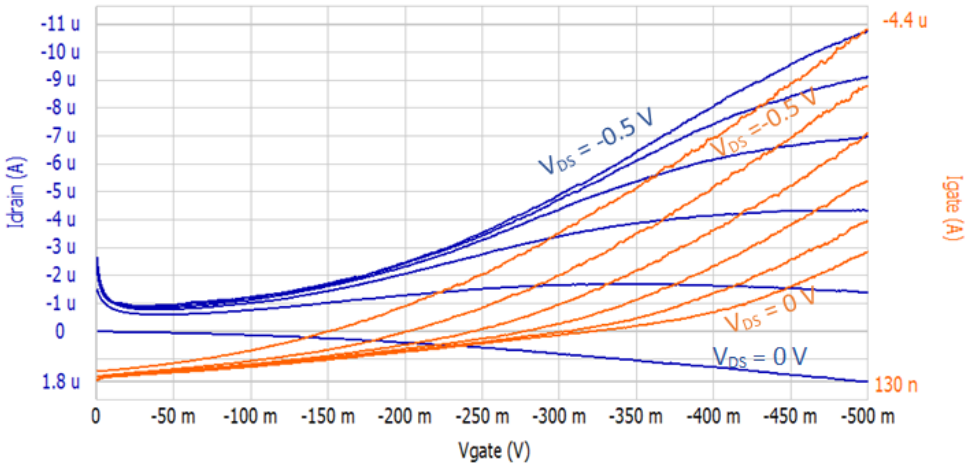

Figure 23. *Drain current (I_D) versus gate voltage (V_G) (blue) and gate leakage current (I_G) versus gate voltage (V_G) (orange) characteristics of the SiNW-FET in air, at a drain voltage (V_D) swiped between 0 and -0.5 V (with a 0.1 step)*

Additionally, for each medium (air and liquid), the gate leakage current (I_G) was measured against the gate voltage (V_G) (the orange curves). The minus sign for V_G, I_D, and I_G is given only to indicate the change of measurement probe polarity, and It can be ignored. Only the sign of V_{DS} is required to be negative in this measurement, as the device is a p-type SiNW-FET and requires negative voltages for operation.

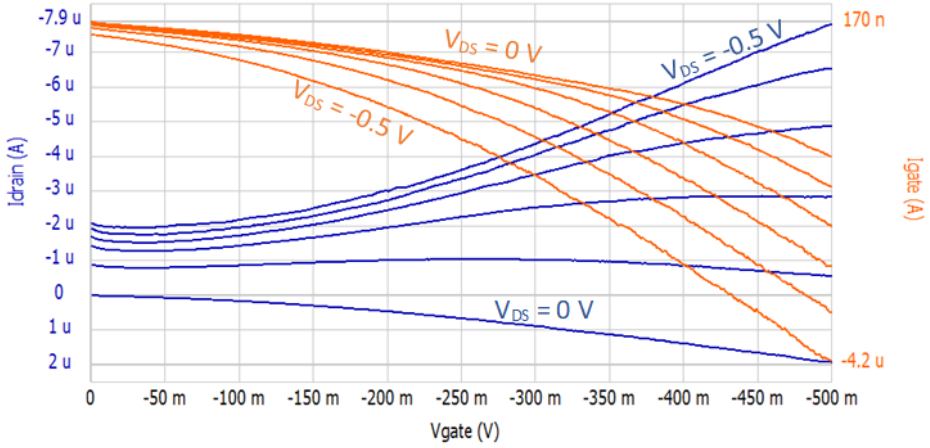

Figure 24. *Drain current (I_D) vs. gate voltage (V_G) (blue) and gate leakage current (I_G) vs. gate voltage (V_G) (orange) characteristics of the SiNW-FET in liquid media, at a drain voltage (V_D) swiped between 0 and -0.5 V (with a 0.1 step)*

Figure 25 presents the typical output and transfer characteristics of an organic field-effect transistor (Klug, 2010). Based on the measured I_D-V_G and I_G-V_G curves of the SiNW-FETs and on the characteristic curves of a FET possessing a normal behavior presented in Figure 25, we can evaluate the performance of the SiNW-FET used in this work.

A. B.

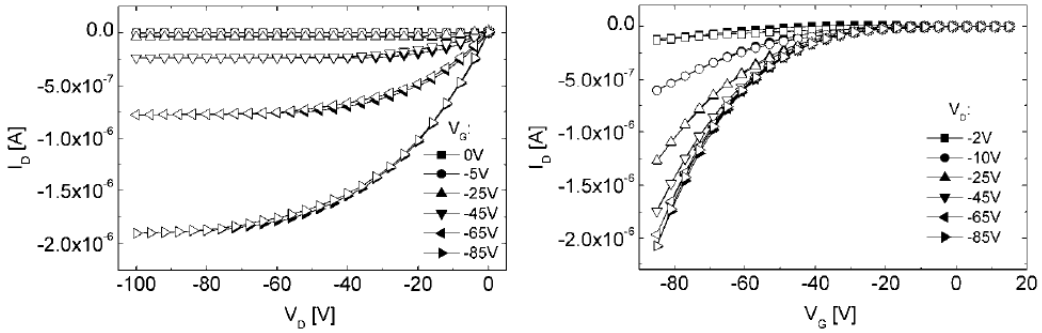

Figure 25. *Typical characteristic curves of an OFET: output (I_D-V_D) (A), and transfer (I_D-V_G) characteristics (B) (Klug, 2010)*

By comparing the maximum gate leakage current (I_G) and the drain current (I_D) values, we can observe that in the air the sensors have approximately 40% leakage current, while in liquid the leakage increases to 53%. This indicates that, for example, from a drain current of 7.9 µA, 4.2 µA is lost as leakage from the gate electrode when the measurement is performed in a liquid medium (this can be interpreted in a similar fashion for air measurement). This indicates leakage current at the gate electrode is more predominant in liquid than in air. These levels of the leakage currents are much higher than the levels normally accepted (ideally, I_G should be 0, and in practice < 10%), thus these devices present major drawbacks that may have a significant effect on the measurements. Additionally, in Figure 23 and Figure 24 it can be observed that at V_{DS} = 0 V and V_{DS} = -0.1 V, the absolute values of the drain current (I_D) decreases at high V_G, which is in contrast to the normal behavior of a normal FET (see Figure 25B). This behavior was observed by Klug (Klug, 2010) and was associated with gate leakage currents. There may be other reasons for this behavior of the used SiNW-FET sensors, but further analysis is not the scope of this thesis.

Based on these observations, the SiNW-FET sensors were used in the next tests as resistive devices. This means leaving the gate electrode unused to avoid the influence of the high gate leakage currents. However, it is important to keep in mind that even if no voltage is applied at the gate electrode, it is still physically present in the device. Therefore, in practice two strategies can be adopted for the non-operated gate electrode in order to avoid unpredicted changes in the gate voltage levels: to disconnect the gate or to connect the gate to ground.

Disconnected gate. A disconnected gate electrode (sometimes called a floating gate), leads to random changes of its voltage level, which is generally caused by the effects of electromagnetic noise. However, by protecting the measurement setup with a Faraday cage, we can assume that V_G is defined by the leakage current I_G and is kept at a constant random value during the measurement. The Faraday cage has the role of protecting the measurement system from external sources of noise, thus we can consider that it stabilizes the measurement.

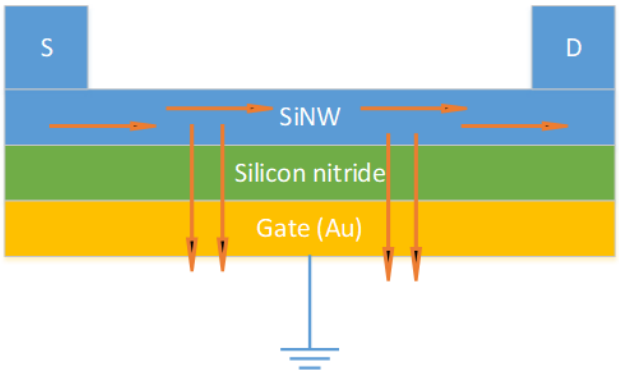

Figure 26. *Schematic of a SiNW-FET device with the gate electrode connected to ground, and the currents (red arrows) flowing through the NW. The NW is connected between the source (S) and drain (D) and is separated from the gold gate electrode by a silicon nitride layer insulating layer. If defects are present in the silicon nitride layer, the I_{DS} current will be leaking towards ground.*

Gate connected to ground. Another option to operate the devices would involve the connection of the gate electrode to the ground such that its fluctuating level of voltage would not affect the measurement (see Figure 26). Normally, during manufacturing of FET devices, it is desirable that the insulating layer of the gate electrode be thin to increasing the gate capacitance and consequently achieve a greater field effect. Thus, one might assume that if during the manufacturing process the insulation layer (here silicon nitride) has defects (holes), when the gold layer of the gate electrode is deposited, the gold might fill the defects and come in contact with the NW, leading to high leakage currents. If the gate electrode were connected to the ground, the drain-source current would leak to the ground through the insulating layer defects, decreasing the overall signal of the device (see Figure 26). Consequently, for testing of the SiNW-FET sensors, the gate electrode was not connected to ground and left “floating”.

In order to conclude whether these SiNW-FET devices could be used as resistive devices in liquid measurements, they were further characterized. For each of the devices, the I-V curves were measured. In Table 8 and Table 9 are presented the mean resistances of the NWs, the standard deviation of the resistances, and the R^2 values, which

indicate the closeness of fit to the measurement data, when the devices were characterized in air, and in liquid medium. However, the resistive characterization in liquid medium is the one of importance here, since the miRNA measurements are done in a liquid environment (PBS). The I-V characterization in air was also performed to show the performance differences of the sensors in different media. It was observed that generally the sensors exhibiting a non-linear behavior in air presented similar behavior in liquid, which might indicate problems originated with the manufacturing process. Figure 28(A–E) shows the I-V plots of sensors with a non-linear behavior, and Figure 27(blue) presents the I-V characteristic plot of a sensor with normal (linear) resistive behavior.

Table 8. *Mean resistance and standard deviation of the resistance of sensors characterized in air, and the R squared value (R^2) indicating the closeness of linear fit to the measured values.*

Sensor	Mean resistance [MΩ]	Standard deviation of resistance [MΩ]	R^2	Observations
S1	0.4866	±0.1207	0.9879	
S2	1.3005	±1.5291	0.9737	
S3	0.0935	±0.0223	0.9862	Saturation at V ≥ 0.45 V
S4	0.0661	±0.0288	0.7643	Saturation at V ≥ 0.2 V
S5	1.7246	±0.2303	0.9998	
S6	0.1337	±0.0221	0.918	
S7	0.2344	±0.0556	0.9966	
S8	0.3525	±0.0822	0.9976	Saturation at V ≥ 0.4 V
S9	0.3875	±0.0892	0.9981	
S10	0.7865	±0.2299	0.9443	
S11	1.9058	±0.4396	0.9984	
S12	1.4196	±0.3732	0.9933	
S13	1.9203	±0.5101	0.9998	
S14	2.41	±0.1963	0.9449	

Table 9. *Mean resistance and standard deviation of sensors characterized in liquid (PBS), and R squared value (R^2) indicating the closeness of linear fit to the measured values.*

Sensor	Mean resistance [MΩ]	Standard deviation of resistance [MΩ]	R^2	Observations
S1	0.7731	±0.2642	0.9879	
S2	0.3952	±0.0332	0.908	
S3	0.4264	±0.1649	0.9018	Saturation at V ≥ 0.4 V
S4	0.0399	±0.0149	0.6737	Saturation at V ≥ 0.2 V
S5	3.6892	±1.1511	0.9527	
S6	1.3851	±0.5715	0.9255	
S7	0.1894	±0.0536	0.9822	
S8	0.3580	±0.1195	0.9427	Saturation at V ≥ 0.425 V
S9	0.3325	±0.1080	0.962	
S10	0.7357	±0.2484	0.7663	
S11	1.2687	±0.3164	0.9943	
S12	1.1196	±0.2872	0.9912	
S13	0.3289	±0.0768	0.9965	
S14	0.5674	±0.2648	0.8252	

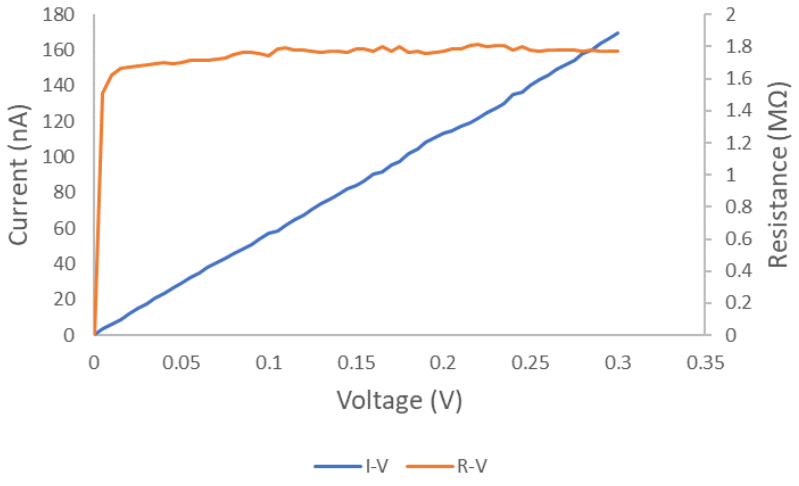

Figure 27. *Example of a linear characteristic plot of a resistive device. The current vs. voltage (blue) and resistance vs. voltage (red) plots of S17 measured in air.*

A resistor or a resistive device should have a reasonably linear characteristic curve within a certain range of current and voltage, as it is an ohmic device. Therefore, over the entire range of voltages applied to the NW (0–0.5 V), the sensors should have a fairly linear characteristic plot, such as S17 presented in Figure 27. The linearity of the characteristic

curves was verified by applying a linear fitting, and R^2 was computed to show how close the fitting was to the measurement data. The closer the value of R^2 is to 1, the better is the linear fit to the measurement data. In contrast, lower values of R^2 (e.g., 0.7663) indicate that the plots of measured data do not have linear behavior.

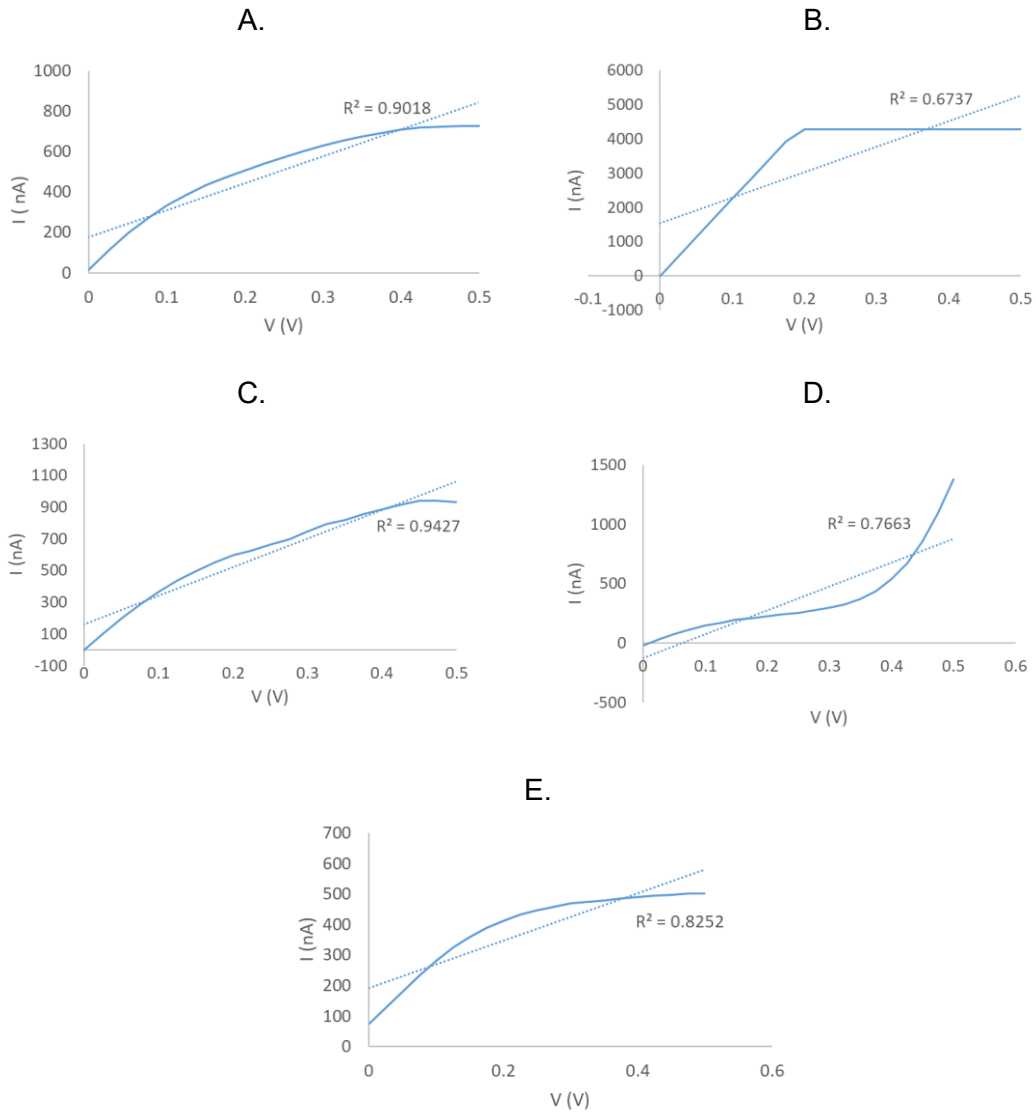

Figure 28. *Examples of sensors plots with a non-linear characteristic behavior measured in liquid media. All these sensors were excluded from further experiments. (A) S3, (B) S4, (C) S8, (D) S10, and (E) S14.*

The plots of S3 (Figure 28A), S4 (Figure 28B), S8 (Figure 28C), S10 (Figure 28D), and S14 (Figure 28E) are examples of the characteristic curve of the devices with non-linear behavior. In addition to their non-linear behavior, devices S3, S4, S8, and S14 showed no changes in the current levels at higher voltages, thus indicating saturation. Saturation at such low voltage levels might indicate that the NW structures were damaged, and these devices were not reliable for future experiments. Therefore, based on the data

from Table 9 and the shape of the characteristic plots, S3, S4, S8, S10, and S14 were excluded from further testing.

The resistance (*R*) of the NWs was computed from the I-V characteristic curves as the voltage to current ratio. In Figure 27(orange), the R-V plot is presented. Figure 29 presents the values of the NW resistances for sensors measured in air (see Table 8) and in liquid medium (PBS) (see Table 9). Generally, the devices have very different NW resistances, indicating different intrinsic characteristics and sensor-to-sensor variations. Due to the sensor-to-sensor variations, if the same experiment were to be performed on each sensor, the comparison of the results might be quite challenging since the sensors are not identical. Additionally, in liquid measurements the resistance measured should decrease, while for S1, S3, S5, and S6 the resistance increases (see Figure 29). The reason for this behavior is not actually known, but it might be related to the physical presence of the gate electrode in the device. Comparing to S1 that was already excluded from experiments due to non-linear resistive behavior, S3, S5, and S6 possess a linear behavior and were further used in tests.

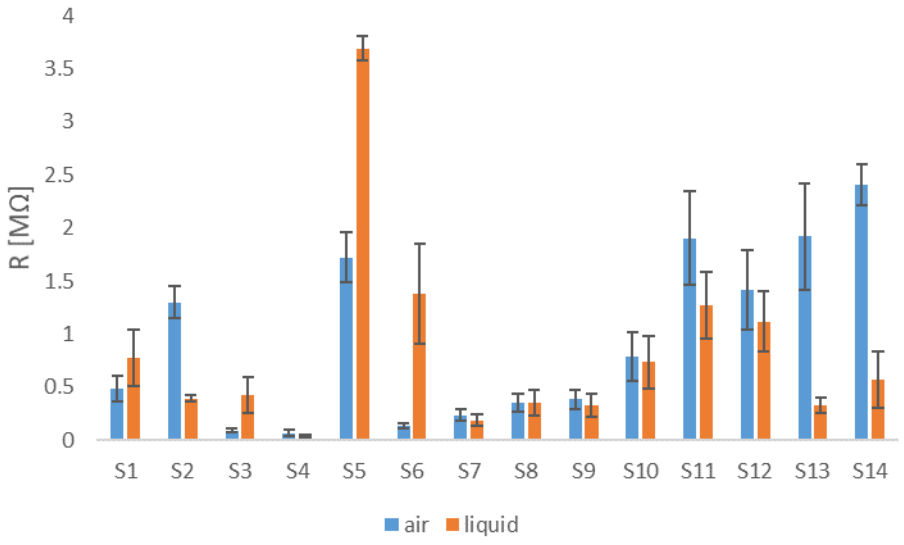

Figure 29. *The mean resistance (MΩ) and the standard deviation of R (MΩ) for sensors S1–S14 measured in air and liquid (PBS) media*

7.2 Disturbance tests

It is important to differentiate the signal produced by the biological event from other possibly induced signals. This is an important aspect when reporting the results of a biosensor in order to avoid false positive results. Elimination of all possible sources of signal interferences requires a thorough testing and analysis of different variables, but given

the limits of this thesis work, only the most potentially significant sources were analyzed. The choice of testing here was based on observations made during preliminary testing.

7.2.1 Hydrophobicity and hydrophilicity of sensor surface

The surface of the non-functionalized sensors is naturally hydrophobic, but with oxygen plasma treatment, the surface can be rendered hydrophilic. Additionally, the surfaces of the sensors were hydrophobic after the APTES–GA–DNAp functionalization process. Thus, considering the architecture of the sensor with the NW found underneath the surface, hanging inside a trench-like cavity (see Figure 30), it is important to study whether the liquid delivered to the sensor surface properly reach the NWs.

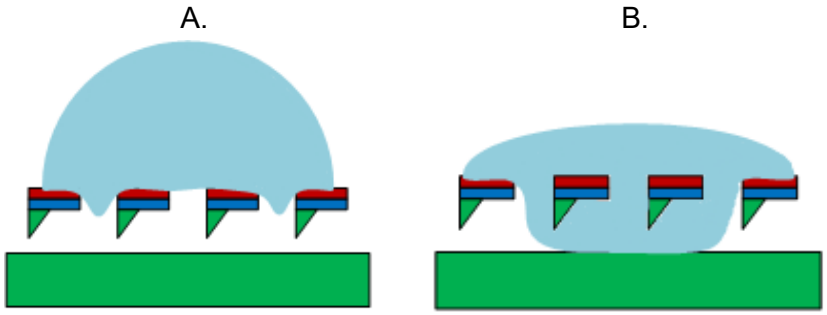

Figure 30. *Representation of a liquid droplet on top of a hydrophobic surface (A) and hydrophilic surface (B). Underneath the surface the NWs are suspended. The red section is the gold layer, the blue layer is silicon nitride, and the green triangles are the silicon NWs. Drawing based on the design of the sensors from Yang, 2018.*

A series of tests were done by introducing multiple PBS droplets with a volume of 5 µl/droplet, at 5 minutes intervals, onto a series of non-modified sensors with hydrophobic surfaces, and onto hydrophilic surfaces. The 5 µl volume of the droplet was chosen to assure proper coverage of the sensor's active area. Additionally, the 5 minutes intervals between droplet injections were chosen so that the liquid does not have time to evaporate. The devices were visually checked to made sure that after the first PBS injection the liquid was always present on the sensor surface. During the 25 minutes experiment the 25 ul PBS accumulated on the surface could not evaporate.

The hypothesis was that if the level of current continued to change upon addition of subsequent PBS droplets on the sensor surface, it might be evidence that the liquid was gradually entering the cavity and reaching the NWs, which would be expected for a hydrophobic type of surface. For a hydrophilic surface was assumed that the liquids enter the cavity easier and reach the NWs more quickly, thus the current stabilizes upon addition of subsequent PBS droplets on the sensor surface.

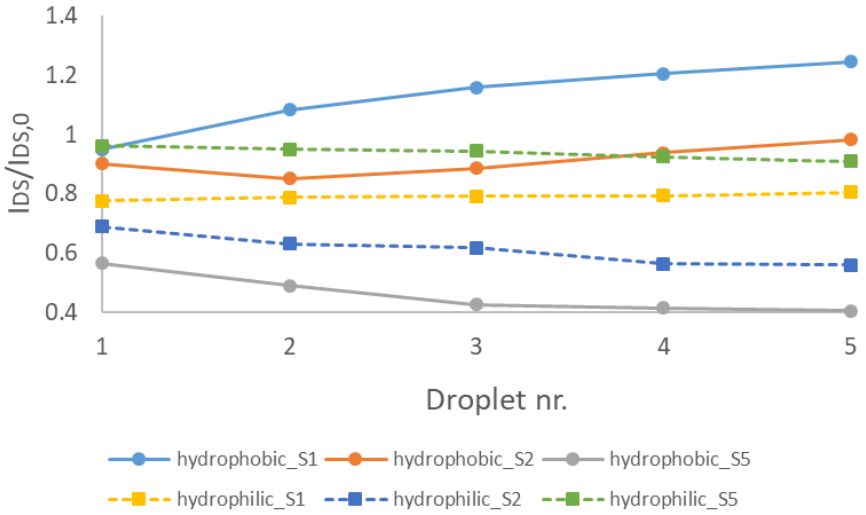

Figure 31. *Effect of multiple droplets injection on the sensor current level for a series of three hydrophobic and three hydrophilic surfaces*

Considering that a hydrophobic surface has a low surface energy, proper liquid access to the NW might be hindered. By rendering the surface hydrophilic, we assume that the liquid more readily reaches the NWs. Figure 31 shows that the change of current level upon multiple injections of PBS on the hydrophobic surfaces is greater than on hydrophilic surfaces. The hydrophilic surfaces reach a relatively stable current level after fourth or fifth droplet. This likely indicates that the liquids reach and cover the NWs more quickly when the surfaces are rendered hydrophilic.

The surface chemistry based on APTES–GA–DNAp was observed to make the sensor surface hydrophobic, thus the liquid measurements with this sensor design and functionalization scheme were quite challenging. A sensor with the NWs positioned on top of the surface would solve the problems of liquid access.

7.2.2 PBS droplet evaporation

The droplet evaporation test was performed to determine whether the PBS droplet, specifically the salts contained in solution, have any effect on the sensor. We assumed that if the current level returned to the initial air level after the liquid evaporated, it would indicate that the PBS salts did not have any effect on the sensor. The tests were done on a series of three non-functionalized sensors, where the NW surface was not chemically modified and is hydrophobic, and three functionalized sensors, chemically modified with the APTES–GA–DNAp functionalization scheme. As previously mentioned, the surfaces functionalized with the APTES–GA–DNAp scheme were hydrophobic.

Since the measurements were performed on different devices, to enable direct comparison of their plots, the data sets were first leveled to the same starting point by computing $I_{DS}/I_{DS,0}$, where I_{DS} is the data set and $I_{DS,0}$ is the I_{DS} value at t = 0 (see Figure 32).

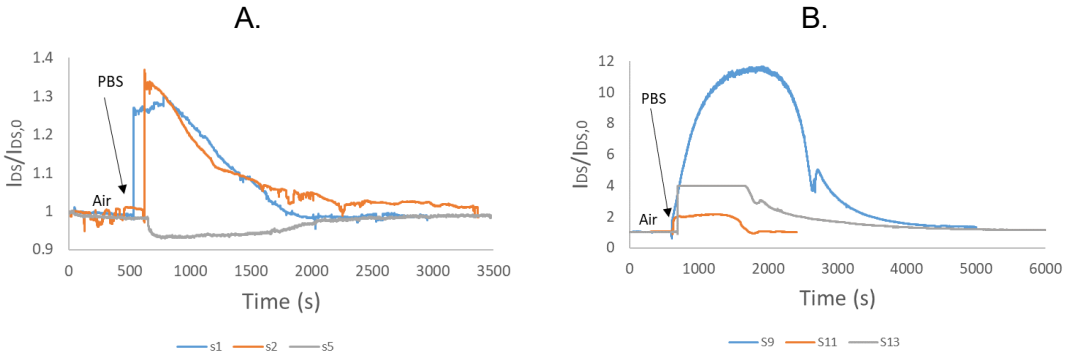

Figure 32. *Current vs. time measurement of droplet evaporation of (A) three different non-functionalized sensors (S1, S2, S5), and (B) three different functionalized sensors (S9, S11, S13).*

Figure 32 presents the behavior of three sensors during the droplet evaporation experiment on non-functionalized (A) and functionalized (B) devices. Despite the consistent behavior of all the three sensors during and after evaporation, with the current levels returning to their initial levels recorded in air (see Figure 32A), device S5 presents abnormal behavior, with the NW's resistance increasing in a liquid environment whereas it should decrease, as liquid media normally increases the current transfer. This behavior of S5 was already observed during resistive characterization testing in liquid medium. However, is it important to keep in mind that even though the SiNW-FET is operated as a resistive device where the gate electrode is not used, the gate is still physically present, and this presence might cause the behavior seen in device S5.

The evaporation times (see Table 10) were on average longer on the functionalized surfaces (~ 46 minutes) than on the non-functionalized surfaces (~27 minutes), which might be caused by the absorption of PBS by the self-assembled layers on the sensor surface. From data presented in Table 10 and Figure 33, we can observe that PBS droplet evaporation has a more random behavior on the functionalized devices. The high current values of the functionalized surfaces comparing to the non-functionalized surfaces (Figure 33) are caused by the changes resulted from functionalization of the surfaces. Through functionalization the negatively charged DNAp molecules were attached on the surface, thus their charges might alter the baseline currents.

Table 10. *Droplet evaporation parameters of three non-functionalized (S1, S2, S5) and three functionalized (S9, S11, S13) sensors*

		S1/S9	**S2/S11**	**S5/S13**
Non-functionalized	Initial air level	0.995 ± 0.004	0.994 ± 0.013	0.986 ± 0.004
	Return air level	0.986 ± 0.004	1.019 ± 0.005	0.985 ± 0.004
	Droplet evaporation time [min]	27	28	26
Functionalized	Initial air level	1.329 ± 0.027	1.383 ± 0.032	3.066 ± 0.043
	Return air level	1.791 ± 0.022	2.246 ± 0.016	3.364 ± 0.023
	Droplet evaporation time [min]	50	19	70

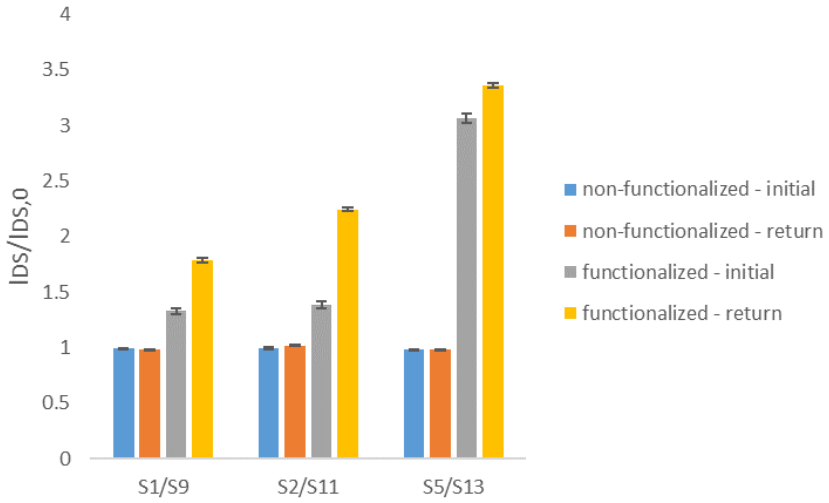

Figure 33. *Comparison of the initial and returned current levels in air for a series of three non-functionalized and three functionalized sensors. On x axis is the sensor number, and y axis represents the current.*

The difference in current levels before and after evaporation may indicate that the PBS has an effect on underlying self-assembled layers of the sensor surface, possibly caused by crystallization of salts upon evaporation. Therefore, for subsequent uses of the same devices, the sensors should be washed with DI water to eliminate the salts and carefully dried in airflow.

7.2.3 Effect of temperature

It is well-established that electronic devices and components are susceptible to temperature effects. To evaluate the magnitude of this effect, the output current of the SiNW-FETs was measured while the temperature of the environment was changed (see Figure 34).

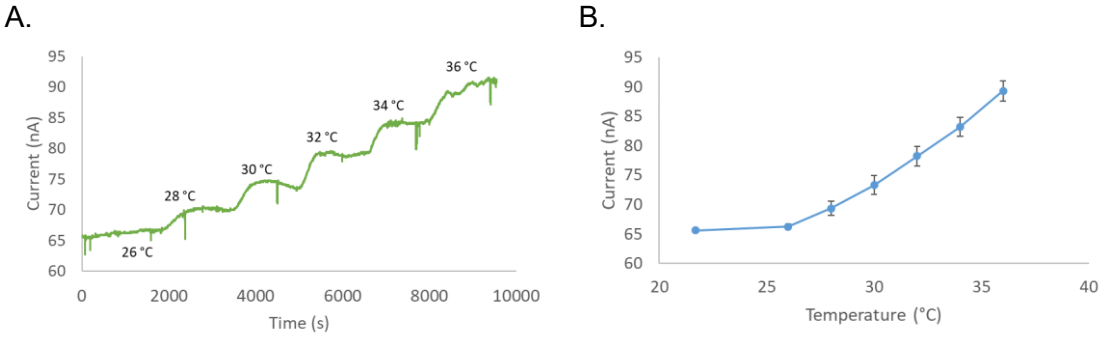

Figure 34. *Effect of temperature over the current output of S12: current output measurement over time with an increment in temperature of the environment (left), and current output for different temperature steps (right).*

Table 11. *The average current values and standard deviation of S12 during measurement under different temperatures*

Temperature (°C)	Current I (nA)	Standard deviation of current (nA)
21.7	65.5916	±0.2061
26	66.2674	±0.3638
28	69.3232	±1.2009
30	73.2906	±1.6150
32	78.2151	±1.6683
34	83.1990	±1.6489
36	89.3033	±1.7472

The results presented in Table 11 indicate that at lower temperatures the change in current and the noise are negligible, <1 nA for a 4 °C change (from 21.7 to 26 °C), while for temperatures higher than 26 °C the current output and the noise in the system increase gradually reaching a maximum of ~6 nA at 36 °C. Normally, the temperature of the laboratory environment in which the experiments are performed is kept constant at a level near 22 °C, thus the effect of temperature over the experiments can be considered negligible. Additionally, the buffer and the miRNA solutions are also at room temperature before experiments.

7.2.4 Effect of illumination

During experiments it was observed that the change in the environment illumination affected the sensor signal, so further investigations were done. All three measurements were performed on the same device (S2). While measurements 1 and 2 were done in the same day, measurement 3 was performed in a different day. In preliminary tests it

was observed that the current baseline level of the same sensor was changing in different days, possibly due to electromagnetic noise that charges differently the gate of the SiNW-FET.

The illumination effect is shown in sensor's signal as a peak decrease with a fast recovery time (e.g., Figure 35G). To prove the provenance of the high amplitude peaks on the signal, the current response of the sensors was measured while the illumination was changed (see Table 12), thus confirming that the high peaks shown in in Figure 35(G) result from the hand shadowing effect.

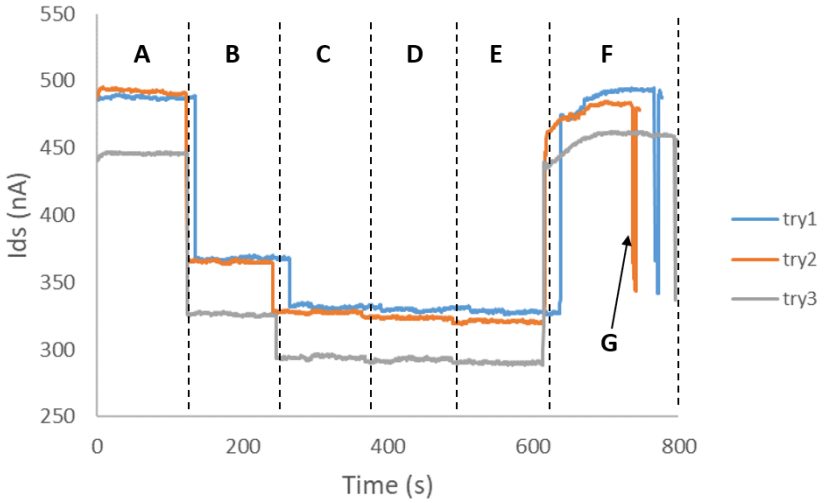

Figure 35. *The effect of changing the illumination on S2: (A) full illumination, (B) three ceiling lights on, (C) two ceiling lights on, (D) one ceiling light on (E) dark, (F) back to full illumination, and (G) is the hand shadowing effect.*

These peaks have a fast return to the current baseline level upon removal of the hand; thus, the peaks do not affect the measurement and can be easily identified in the signal. However, a change in the background illumination influences the signal baseline (as it happens in Figure 35), thus during the experiments it was important to keep a constant illumination.

Table 12. *Mean and standard deviation of the current during measurement of illumination effect on S2 signal.*

	Try 1		Try 2		Try 3	
Illumination level	**Mean I (nA)**	**Standard deviation of I (nA)**	**Mean I (nA)**	**Standard deviation of I (nA)**	**Mean I (nA)**	**Standard deviation of I (nA)**
A	487.570	±0.861	492.374	±1.295	446.005	±0.463
B	367.770	±0.873	365.380	±0.805	326.207	±0.917
C	331.751	±1.145	327.838	±0.718	294.298	±0.986
D	329.737	±1.003	323.745	±0.594	292.379	±1.051
E	327.890	±0.832	321.018	±0.713	290.140	±0.651
F	493.461	±0.407	482.855	±0.668	460.672	±0.838

7.3 SiNW-FET surface functionalization and miRNA detection

For preparation of the sensors, the APTES–GA–DNAp functionalization scheme was employed to immobilize the single-stranded DNA probes on the NW surface. Subsequently, the current of the SiNW was measured in real-time upon the injection of miR-218 while feeding a constant V_{DS}.

To shelter the sensors and minimize electromagnetic noises, the measurement system was placed in a Faraday cage. Additionally, the Faraday cage, as explained in Section 7.1, helps maintain the stability of the gate voltage, V_G, since the gate of the SiNW-FET is not operated as in a normal FET. The measurements were performed at the ambient room temperature, at constant illumination, and the sensors were placed inside the Faraday cage.

In the initial steps, multiple droplets of PBS with a volume of 5 µl/droplet were introduced onto the SiNW-FETs sensors to act as a buffer while maintaining a V_{DS} at 0.4 V (Figure 36). Sensors S12 (Figure 36A), S6 (Figure 36C), and S7 (Figure 36D), were then given approximately 25 minutes for the conductance of the SiNWs to settle to a relatively constant value. For each sensor, multiple injections of PBS were provided in order to observe whether there was a step response.

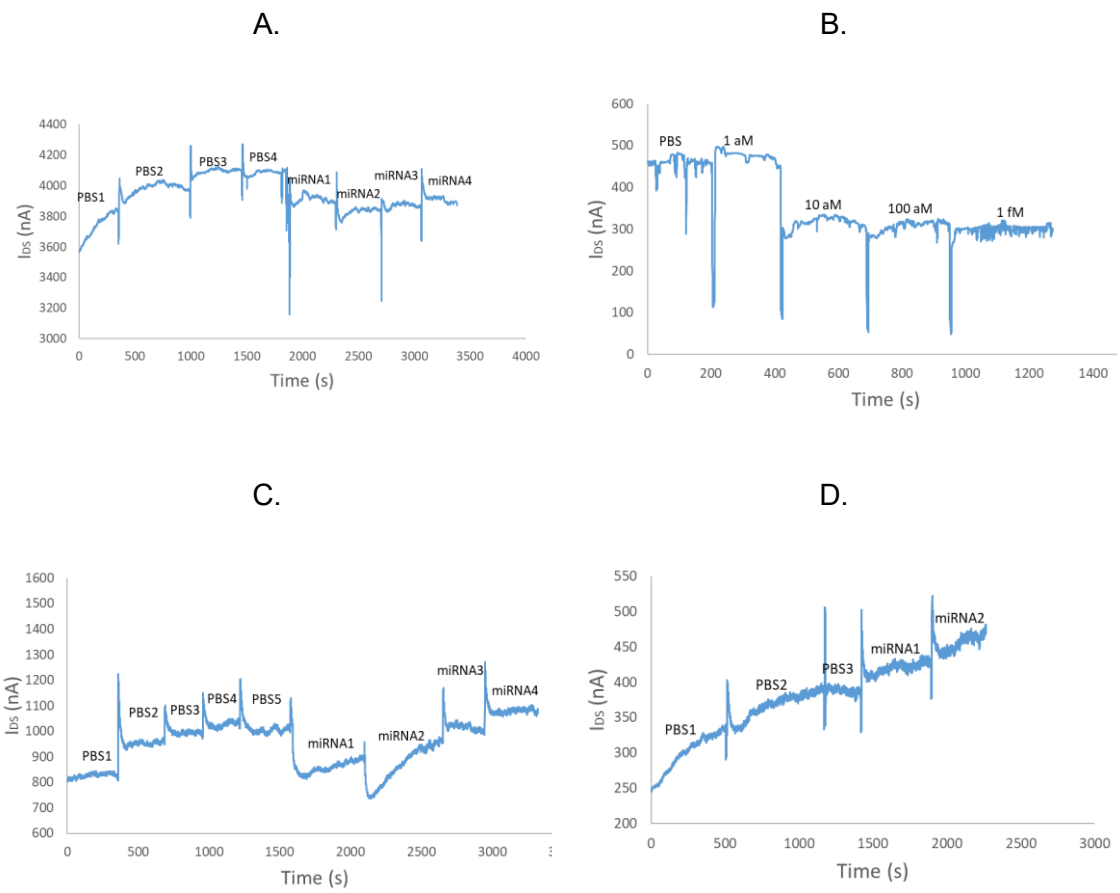

Figure 36. *The change of current through the NW during time for multiple injections of PBS and miR-218 on four different SiNW-FET devices: (A) S12, (B) S15, (C) S6, and (D) S7*

As discussed in Section 7.2.1, the hydrophobicity of the surface, which was also observed after the functionalization of the sensor, might delay the access of the aqueous solutions in the NWs cavity, causing a step response. While sensors S6 and S12 showed a stabilization of the NW conductance level, sensor S7 indicated an upward drift. Although the sensors were identically functionalized, the chemical reactions might have not occurred in identical fashion (e.g., because of surface contaminants), thus the drift of the sensor S17 might be the result of a poorly functionalized surface, of surface degradation, or even of damage to the NWs. Compared to sensors S6, S17, and S12, sensor S15 showed a faster stabilization of the NW conductance of only ~3 minutes.

After stabilization of the conductance in PBS, the miR-218 samples were delivered to the sensors (over the PBS that was already on the surface). Volumes of 5 µl/injection of 10 fM concentration of miR-218 (fresh samples) were repeatedly delivered to the sensor surface for sensors S6, S7, and S12, while for sensor S15, miR-218 was titrated from 1 aM up to 1 fM. Figure 36 shows a decrease in the current level measured over time upon introduction of the first sample of miR-218 for sensors S6, S12, and S15, which might be

a result of the hybridization event taking place between the single-stranded DNA probes and the miRNA. In contrast, sensor S7 shows an increase in the signal, but given its strong drift, it can be excluded from further comparisons.

Table 13. *The current levels and standard deviation of four different SiNW-FETs (S12, S15, S7, S6) for PBS and for multiple miR-218 injections, and the current peak amplitude resulted upon injection of miR-218 over the PBS buffer.*

		Current level [nA]				
Sensor		**PBS**	**miRNA1**	**miRNA2**	**miRNA3**	**miRNA4**
S12	I [nA]	4092.875	3913.034	3843.123	3876.863	3889.049
	Standard deviation	± 5.786	± 15.532	± 7.637	± 9.952	± 5.873
	Current decrease [nA]		179.841	69.911	33.740	12.186
S15	I [nA]	459.504	480.978	327.073	314.666	301.503
	Standard deviation	± 6.745	± 1.039	± 4.303	± 7.843	± 6.033
	Current decrease [nA]		21.473	153.905	12.407	13.163
S6	I [nA]	1003.025	877.927	948.264	1002.953	1079.048
	Standard deviation	± 9.931	± 9.090	± 13.112	± 9.615	± 7.290
	Current decrease [nA]		125.099	70.337	54.689	76.095
S7	I [nA]	388.580	423.250	463.635		
	Standard deviation	± 3.372	± 5.000	± 4.057		
	Current decrese [nA]		34.670	40.385		

*For sensors A. B and C each droplet has a miR-218 concentration of 10 fM.
*For sensor D miRNA1, miRNA2, miRNA3, and miRNA4, refer to concentrations of 1 aM, 10 aM, 100 aM, respectively 1 fM.

Normally, the current levels in a p-type FET device should increase when a negative voltage is applied, but in case of the used SiNW-FETs the current decreases as it can be observed in Figure 36(A, B, C). This discrepancy of the signal directionality was observed in multiple experiments and might be a cause of the unused gate electrode.

The maximum current change for S12, S15, and S6 was calculated as the difference between the stabilized current baseline in PBS and the current level after injection of the miR-218 (see Table 13). The current signal decreases of S12 and S6 shown in Figure 36 might indicate the detection of a 10 fM miR-218 concentration, while the signal of S15 shows detection down to 10 aM. The fast saturation of the S12 and S15 surfaces may be caused by poor DNAp attachment or, on the opposite, by the DNAp crowding effect. In contrast to S12 and S15, S6 current increases after injection of the second miR-218 droplet. This behavior of S6 cannot be clearly explained.

8. CONCLUSIONS

Decreasing the sizes of materials to nanometer-scale results in properties different from those manifested at macroscale. It is evident that materials' physical and chemical properties are strongly affected by the high surface-to-volume ratios and quantum size effects at nanometer scale. Additionally, the size similarity of the nanomaterials (i.e., SiNWs) to biomolecules offers an advantage in biosensing applications. Hence, the design of the source-drain channel as a silicon nanowire in FET structures offers the possibility of a label-free and ultra-sensitive mechanism for the detection of biomolecules. As has been proved by several groups (Gao, 2013a; Gao, 2013b; Lu, 2014a; Lu, 2014b; Shen, 2013; Zhang, 2009; Zhang, 2011), SiNW-FETs enable detection of low concentrations of miRNA biomarkers at levels similar to the amounts found in biological samples, such as cell culture medium or body fluids.

The goals of this thesis were to identify and apply one of the methods suitable for immobilization of complementary DNA probes onto the NW structures of SiNW-FETs for use in detection of miR-218, one of the biomarkers found to be upregulated during osteogenic differentiation, and to evaluate the capability of these tailored sensors to detect miRNA. Additionally, identification of regeneration methods for miRNA SiNW-FET biosensors gives researchers information about the reusability potential of these sensors, which would allow multiple sampling and cost reduction. The evaluation of the SiNW-FET sensors performance and of the functionalization scheme gives important information about possibility of integrating these types of sensors into *in vitro* cell platforms.

The first part of this study involved a theoretical approach focused on identifying of possible functionalization schemes for immobilizing of the DNA probes on the SiNW surfaces, and the regeneration strategies that would allow breaking of the hydrogen bonds in the miRNA–DNAp duplex formed through hybridization, leaving the DNA probe available for subsequent hybridizations. Four chemical functionalization schemes for DNAp immobilization were proposed: two schemes that involve silanization with APTES and attachment of the single-stranded DNA probes by means of either GA or AA crosslinkers, and two schemes that allow a direct covalent attachment of the DNA probes to GPTMS- or CDI-modified NWs. The AA-based functionalization is a novel method that has not yet been reported in the literature for design of miRNA biosensor. Due to biocompatibility properties of AA, the APTES–AA functionalization method might be suitable for sensors that come in direct contact with cells.

Additionally, to enable the reusability of the SiNW-FET sensors, approaches to thermal, chemical, and enzyme-based regeneration were identified. Thermal regeneration would allow DNAp–miRNA separation by means of heat, while chemical regeneration could involve chaotropic agents, such as urea, or acids, such as HCl. While the thermal and chemical approaches were mentioned in some studies, the approach based on enzymes was not found associated with biosensor applications in the literature and represent a novel approach proposed in this thesis. Two classes of enzymes were identified as capable of breaking the DNAp–miRNA duplex: the helicases specifically the SF1B family and the RNase H enzymes. Although in theory these enzymes could be beneficial in surface regeneration, their efficiency should be experimentally assessed, since their activity may interfere with sensors signals and removing the enzymes from the system could be a challenging process. Since applications and information about miRNA SiNW-FET regeneration is scarce, this theoretical ground covered in this thesis offers valuable information for future research. Based on their costs and accessibility, the regeneration methods based on HCl and urea could be first applied in regeneration of a miRNA SiNW-FET biosensor. The limited time and devices available for this work did not allow practical testing of the other functionalization scheme or the regeneration strategies, therefore, they could be included in future studies.

In the beginning of experimental part of the thesis, the performance of the SiNW-FETs was evaluated. The evaluation identified a series of challenges related to performance of these sensors and the properties of the functionalized surface: the high gate leakage currents of the SiNW-FET sensors; the sensor design's having the NWs build inside a cavity, hanging under the surface; and the resulting hydrophobic surface after the APTES–GA–DNAp functionalization scheme.

To prevent the problems related to the high leakage currents of the SiNW-FET gate electrode, the operation was adapted to a strategy of using the sensors as resistive devices by leaving the gate electrode non-operational. By sheltering the sensors with a Faraday cage, it was assumed that the gate leakage currents stabilize the gate voltage and the sensors can be considered stable.

The novel design of the SiNW-FETs used in this thesis proposed by Yang *et al.* (Yang, 2018) have the NW structure under the surface, hanging inside a trench-like cavity. The design, together with the hydrophobicity of the surface resulting from the APTES–GA–DNAp functionalization, leads to concerns about whether the aqueous solution has sufficient access to the NW and that miRNA detection is not hindered. Thus, this device may be problematic in liquid measurements, and for future experiments, devices in which the NWs are designed on the sensor surface may solve these issues.

Next, the APTES–GA functionalization scheme was applied for immobilization of DNA probes of NWs surfaces and miRNA measurements were performed. The measurements indicated possible promising results for miRNA detection down to concentrations of 10 fM and 10 aM. However, it is important to be critical and to be aware of the possibility of obtaining false positive results caused by effects other than miRNA activity. In addition to the problems identified above, a poorly functionalized surface may also cause false positive results. To exclude all the uncertainty factors, more research is needed.

Thus, a clear conclusion about whether miRNA was detected cannot be made. Nevertheless, the proposed functionalization and regeneration approaches, the protocols for miRNA handling and miRNA experiments, and the observations from the tests offer valuable information for future research.

REFERENCES

Acres, R. G., Ellis, A. V., Alvino, J., Lenahan, C. E., Khodakov, D. A., Metha, G. F., & Andersson, G. G. (2012). Molecular structure of 3-aminopropyltriethoxysilane layers formed on silanol-terminated silicon surfaces. The Journal of Physical Chemistry C, 116(10), 6289-6297.

Afrasiabi, R. (2016). Silicon nanoribbon FET sensors: fabrication, surface modification and microfluidic integration (Doctoral dissertation, KTH Royal Institute of Technology).

Alberts, B., Johnson, A., Lewis, J., Raff, M., Roberts, K. and Walter, P. (2002). Molecular Biology of the Cell. Garland, New York.

Albrecht, C., Kaeppel, N., & Gauglitz, G. (2008). Two immunoassay formats for fully automated CRP detection in human serum. Analytical and bioanalytical chemistry, 391(5), 1845.

Almeida, M. I., Reis, R. M., & Calin, G. A. (2011). MicroRNA history: discovery, recent applications, and next frontiers. Mutation Research/Fundamental and Molecular Mechanisms of Mutagenesis, 717(1), 1-8.

Bantz, K. C., Meyer, A. F., Wittenberg, N. J., Im, H., Kurtuluş, O., Lee, S. H., Lindquist, N. C., Oh, S. H., & Haynes, C. L. (2011). Recent progress in SERS bio-sensing. Physical Chemistry Chemical Physics, 13(24), 11551-11567.

Bartel, D. P. (2004). MicroRNAs: genomics, biogenesis, mechanism, and function. Cell, 116(2), 281-297.

Bergveld, P. (1970). Development of an ion-sensitive solid-state device for neurophysiological measurements. IEEE Transactions on Biomedical Engineering, (1), 70-71.

Bergveld, P. (1972). Development, operation, and application of the ion-sensitive field-effect transistor as a tool for electrophysiology. IEEE Transactions on Biomedical Engineering, (5), 342-351.

Bhalla, N., Jolly, P., Formisano, N., & Estrela, P. (2016). Introduction to biosensors. Essays in Biochemistry, 60(1), 1–8.

Bhome, R., Del Vecchio, F., Lee, G. H., Bullock, M. D., Primrose, J. N., Sayan, A. E., & Mirnezami, A. H. (2018). Exosomal microRNAs (exomiRs): Small molecules with a big role in cancer. Cancer Letters, 420, 228-235.

Blanco, A., & Blanco, G. (2017). Nucleic acids. In Medical Biochemistry. Academic Press, 121-140.

Caras, S., & Janata, J. (1980). Field effect transistor sensitive to penicillin. Analytical Chemistry, 52(12), 1935-1937.

Cerritelli, S. M., & Crouch, R. J. (2009). Ribonuclease H: the enzymes in eukaryotes. The FEBS Journal, 276(6), 1494-1505.

Chen, K. I., Li, B. R., & Chen, Y. T. (2011). Silicon nanowire field-effect transistor-based biosensors for biomedical diagnosis and cellular recording investigation. Nano Today, 6(2), 131-154.

Chen, X., Ba, Y., Ma, L., Cai, X., Yin, Y., Wang, K., Guo, J., Zhang, Y., Chen, J., Guo, X., Li, Q., Li, X., Wang, W., Zhang, Y., Wang, J., Jiang, X., Xiang, Y., Xu, C., Zheng, P., Zhang, J., Li, R., Zhang, H., Shang, X., Gong, T., Ning, G., Wang, J., Zen, K., Zhang, J., & Zhang, C.Y. (2008). Characterization of microRNAs in serum: a novel class of biomarkers for diagnosis of cancer and other diseases. Cell Research, 18(10), 997.

Chen, Y. X., Huang, K. J., & Niu, K. X. (2018). Recent advances in signal amplification strategy based on oligonucleotide and nanomaterials for microRNA detection - a review. Biosensors and Bioelectronics, 99, 612-624.

Chiang, C. H., Liu, N. I., & Koenig, J. L. (1982). Magic-angle cross-polarization carbon 13 NMR study of aminosilane coupling agents on silica surfaces. Journal of Colloid and Interface Science, 86(1), 26-34.

Cloarec, J. P., Martin, J. R., Polychronakos, C., Lawrence, I., Lawrence, M. F., & Souteyrand, E. (1999). Functionalization of Si/SiO2 substrates with homooligonucleotides for a DNA biosensor. Sensors and Actuators B: Chemical, 58(1-3), 394-398.

Coffinier, Y., & Boukherroub, R. (2014). Surface modification of semiconducting silicon nanowires for biosensing applications. In Semiconducting silicon nanowires for biomedical applications, 26-61.

Cui, Y., & Lieber, C. M. (2001). Functional nanoscale electronic devices assembled using silicon nanowire building blocks. Science, 291(5505), 851-853.

Cui, Y., Wei, Q., Park, H., & Lieber, C. M. (2001). Nanowire nanosensors for highly sensitive and selective detection of biological and chemical species. Science, 293(5533), 1289-1292.

Deng, H., Liu, Q., Wang, X., Huang, R., Liu, H., Lin, Q., Zhou, X. & Xing, D. (2017). Quantum dots-labeled strip biosensor for rapid and sensitive detection of microRNA based on target-recycled nonenzymatic amplification strategy. Biosensors and Bioelectronics, 87, 931-940.

Dong, H., Zhang, J., Ju, H., Lu, H., Wang, S., Jin, S., Hao, K., & Zhang, X. (2012). Highly sensitive multiple microRNA detection based on fluorescence quenching of graphene oxide and isothermal strand-displacement polymerase reaction. Analytical Chemistry, 84(10), 4587-4593.

Dorvel, B., Reddy Jr, B., & Bashir, R. (2013). Effect of biointerfacing linker chemistries on the sensitivity of silicon nanowires for protein detection. Analytical Chemistry, 85(20), 9493-9500.

Driskell, J. D., Seto, A. G., Jones, L. P., Jokela, S., Dluhy, R. A., Zhao, Y. P., & Tripp, R. A. (2008). Rapid microRNA (miRNA) detection and classification via sur-face-enhanced Raman spectroscopy (SERS). Biosensors and Bioelectronics, 24(4), 917-922.

Dubrovsky, T., Tronin, A., Dubrovskaya, S., Vakula, S., & Nicolini, C. (1995). Immunological activity of IgG Langmuir films oriented by protein A sublayer. Sensors and Actuators-B-Chemical Biochemical Sensors, 23(1), 1-8.

Dupont-Filliard, A., Billon, M., Livache, T., & Guillerez, S. (2004). Biotin/avidin system for the generation of fully renewable DNA sensor based on biotinylated polypyrrole film. Analytica Chimica Acta, 515(2), 271-277.

Egholm, M., Buchardt, O., Nielsen, P. E., & Berg, R. H. (1992). Peptide nucleic acids (PNA). Oligonucleotide analogs with an achiral peptide backbone. Journal of the American Chemical Society, 114(5), 1895-1897.

Elfström, N., Juhasz, R., Sychugov, I., Engfeldt, T., Karlström, A. E., & Linnros, J. (2007). Surface charge sensitivity of silicon nanowires: Size dependence. Nano Letters, 7(9), 2608-2612.

Elnathan, R., Kwiat, M., Pevzner, A., Engel, Y., Burstein, L., Khatchtourints, A., Lichtenstein, A., Kantaev, R., & Patolsky, F. (2012). Biorecognition layer engineering: overcoming screening limitations of nanowire-based FET devices. Nano Letters, 12(10), 5245-5254.

Exiqon. Locked Nucleic Acid (LNA). (2009). Custom oligonucleotides for RNA and DNA research. Retrieved at: http://www.exiqon.com/lna-technology

Fang, C. S., Kim, K. S., Yu, B., Jon, S., Kim, M. S., & Yang, H. (2017). Ultrasensitive electrochemical detection of miRNA-21 using a zinc finger protein specific to DNA–RNA hybrids. Analytical Chemistry, 89(3), 2024-2031.

Fang, S., Lee, H. J., Wark, A. W., & Corn, R. M. (2006). Attomole microarray detection of microRNAs by nanoparticle-amplified SPR imaging measurements of sur-face polyadenylation reactions. Journal of the American Chemical Society, 128(43), 14044-14046.

ForteBio. (2009). Regeneration strategies for streptavidin biosensors on the Octet Platform. Retrieved from: http://www.biophysics.bioc.cam.ac.uk/wp-content/uploads/2011/02/TN_14_Streptavidin_regeneration.pdf

Gao, A., Lu, N., Dai, P., Li, T., & Wang, Y. (2013a). Label-free and ultrasensitive detection of microna biomarkers in lung cancer cells based on silicon nanowire FET biosensors. Transducers & Eurosensors XXVII: The 17th International Conference on Solid-State Sensors, Actuators and Microsystems, IEEE, 2439-2442.

Gao, X., Xu, H., Baloda, M., Gurung, A. S., Xu, L. P., Wang, T., Zhang, X., & Liu, G. (2014). Visual detection of microRNA with lateral flow nucleic acid biosensor. Biosensors and Bioelectronics, 54, 578-584.

Gao, Z., Deng, H., Shen, W., & Ren, Y. (2013b). A label-free biosensor for electrchemical detection of femtomolar microRNAs. Analytical Chemistry, 85(3), 1624-1630.

Garibyan, L., & Avashia, N. (2013). Research techniques made simple: polymerase chain reaction (PCR). The Journal of Investigative Dermatology, 133(3), e6.

Geißler, D., Charbonnière, L. J., Ziessel, R. F., Butlin, N. G., Löhmannsröben, H. G., & Hildebrandt, N. (2010). Quantum dot biosensors for ultrasensitive multiplexed diagnostics. Angewandte Chemie International Edition, 49(8), 1396-1401.

GhoshMoulick, R., Vu, X. T., Gilles, S., Mayer, D., Offenhäusser, A., & Ingebrandt, S. (2009). Impedimetric detection of covalently attached biomolecules on field-effect transistors. Physica Status Solidi (a), 206(3), 417-425.

Glick, B. R., Pasternak, J. J., Patten, C. L. (2010). Molecular Biotechnology: Principles and Applications of Recombinant DNA. 4th ed., Washington, DC, ASM Press.

Goddard, J. M., & Erickson, D. (2009). Bioconjugation techniques for microfluidic biosensors. Analytical and Bioanalytical Chemistry, 394(2), 469.

Goldhaber-Gordon, D., Montemerlo, M. S., Love, J. C., Opiteck, G. J., & Ellenbogen, J. C. (1997). Overview of Nanoelectronic Devices. Proceedings of the IEEE, 85(4), 521-540.

Goode, J. A., Rushworth, J. V. H., & Millner, P. A. (2014). Biosensor regeneration: a review of common techniques and outcomes. Langmuir, 31(23), 6267-6276.

Grieshaber, D., MacKenzie, R., Voeroes, J., & Reimhult, E. (2008). Electrochemical biosensors-sensor principles and architectures. Sensors, 8(3), 1400-1458.

Gupta, A., Mishra, A., & Puri, N. (2017). Peptide nucleic acids: Advanced tools for biomedical applications. Journal of Biotechnology, 259, 148-159.

Hamidi-Asl, E., Palchetti, I., Hasheminejad, E., & Mascini, M. (2013). A review on the electrochemical biosensors for determination of microRNAs. Talanta, 115, 74-83.

Hassan, M. Q., Maeda, Y., Taipaleenmaki, H., Zhang, W., Jafferji, M., Gordon, J. A., Li, Z., Croce, C. M., van Wijnen, A. J., Stein, J. L., Stein, G. S., & Lian, J. B. (2012). miR-218 directs a Wnt signaling circuit to promote differentiation of osteo-blasts and osteo-mimicry of metastatic cancer cells. Journal of Biological Chemistry, 277(50), 42084-92.

Hilton, J. P., Nguyen, T. H., Pei, R., Stojanovic, M., & Lin, Q. (2011). A microfluidic affinity sensor for the detection of cocaine. Sensors and Actuators A: Physical, 166(2), 241-246.

Homola, J. (2008). Surface plasmon resonance sensors for detection of chemical and biological species. Chemical Reviews, 108(2), 462-493.

Huang, C., Geng, J., & Jiang, S. (2017). MicroRNAs in regulation of osteogenic differentiation of mesenchymal stem cells. Cell and Tissue Research, 368(2), 229-238.

Husale, S., Persson, H. H., & Sahin, O. (2009). DNA nanomechanics allows direct digital detection of complementary DNA and microRNA targets. Nature, 462(7276), 1075-1078.

Ito, Y., Tsukagoshi, K., & Kobayashi, A. (2017). Denaturation of DNA in ternary mixed solution of water/hydrophilic/hydrophobic organic solvent. Journal of Analytical Sciences, Methods and Instrumentation, 7(02), 40-46.

Johnson, B. N., & Mutharasan, R. (2012). Sample preparation-free, real-time detection of microRNA in human serum using piezoelectric cantilever biosensors at attomole level. Analytical Chemistry, 84(23), 10426-10436.

Jokilaakso, N. (2013a). A Biotechnology Perspective on Silicon Nanowire FETs for Biosensor Applications (Doctoral dissertation, KTH Royal Institute of Technology).

Jokilaakso, N., Afrasiabi, R., Larsson, A., Björk, P., Schönberg, T., Linnros, J., & Eriksson Karlström, A. (2013b). Spot-on functionalization of SiO2 for multiplexed silicon nanowire-FET biosensors. Submitted

Kamra, T., Chaudhary, S., Xu, C., Johansson, N., Montelius, L., Schnadt, J., & Ye, L. (2015). Covalent immobilization of molecularly imprinted polymer nanoparticles using an epoxy silane. Journal of Colloid and Interface Science, 445, 277-284.

Kanaya, S. (2009). Ribonuclease H. The FEBS Journal, 276(6), 1481-1481.

Khandelwal, G., & Bhyravabhotla, J. (2010). A phenomenological model for predicting melting temperatures of DNA sequences. PloS One, 5(8), e12433.

Kilic, T., Erdem, A., Ozsoz, M., & Carrara, S. (2018). MicroRNA biosensors: Opportunities and challenges among conventional and commercially available techniques. Biosensors and Bioelectronics, 99, 525-546.

Kilic, T., Topkaya, S. N., & Ozsoz, M. (2013). A new insight into electrochemical microRNA detection: a molecular caliper, p19 protein. Biosensors and Bioelectronics, 48, 165-171.

Kilic, T., Topkaya, S. N., Ariksoysal, D. O., Ozsoz, M., Ballar, P., Erac, Y., & Gozen, O. (2012). Electrochemical based detection of microRNA, mir21 in breast cancer cells. Biosensors and Bioelectronics, 38(1), 195-201.

Kim, W. H., Lee, J. U., Song, S., Kim, S., Choi, Y. J., & Sim, S. J. (2019). A label-free, ultra-highly sensitive and multiplexed SERS nanoplasmonic biosensor for miRNA detection using a head-flocked gold nanopillar. Analyst, 144(5), 1768-1776.

Klug, A. (2010). Organic field-effect transistors: Process development, stability issues and sensor applications (Doctoral dissertation, Graz University of Technology).

Knoglinger, C., Zich, A., Traxler, L., Poslední, K., Friedl, G., Ruttmann, B., Schopp, A., Muller, K., Zimmermann, M., & Gruber, H. J. (2018). Regenerative biosensor for use with biotinylated bait molecules. Biosensors and Bioelectronics, 99, 684-690.

Labib, M. & Berezovski, M.V. (2015). Electrochemical sensing of microRNAs: avenues and paradigms. Biosensors and Bioelectronics, 68, pp.83-94.

Lautner, G., & Gyurcsányi, R. E. (2014). Electrochemical detection of miRNAs. Electroanalysis, 26(6), 1224-1235.

Lazerges, M., Perrot, H., Zeghib, N., Antoine, E., & Compere, C. (2006). In situ QCM DNA-biosensor probe modification. Sensors and Actuators B: Chemical, 120(1), 329-337.

Lee, R. C., Feinbaum, R. L., & Ambros, V. (1993). The C. elegans heterochronic gene lin-4 encodes small RNAs with antisense complementarity to lin-14. Cell, 75(5), 843-854.

Leivo, J., Virjula, S., Vanhatupa, S., Kartasalo, K., Kreutzer, J., Miettinen, S., & Kallio, P. (2017). A durable and biocompatible ascorbic acid-based covalent coating method of polydimethylsiloxane for dynamic cell culture. Journal of The Royal Society Interface, 14(132), 20170318.

Li, J., Lei, P., Ding, S., Zhang, Y., Yang, J., Cheng, Q., & Yan, Y. (2016). An enzyme-free surface plasmon resonance biosensor for real-time detecting microRNA based on allosteric effect of mismatched catalytic hairpin assembly. Biosensors and Bioelectronics, 77, 435-441.

Li, X., Wang, Y., Wang, L., & Wei, Q. (2014). A surface plasmon resonance as-say coupled with a hybridization chain reaction for amplified detection of DNA and small molecules. Chemical Communications, 50(39), 5049-5052.

Lin, C. H., Hung, C. H., Hsiao, C. Y., Lin, H. C., Ko, F. H., & Yang, Y. S. (2009). Polysilicon nanowire field-effect transistor for ultrasensitive and label-free detection of pathogenic avian influenza DNA. Biosensors and Bioelectronics, 24(10), 3019-3024.

Lodish, H., Berk, A., Darnell, J.E., Kaiser, C.A., Krieger, M., Scott, M.P., Bretscher, A., Ploegh, H., & Matsudaira, P., (2008). Molecular Cell Biology. Vol. 1, Macmillan.

Lu, L., Liu, B., Li, S., Zhang, W., & Xie, G. (2011). Improved electrochemical immunosensor for myeloperoxidase in human serum based on nanogold/cerium diox-ide-BMIMPF6/L-Cysteine composite film. Colloids and Surfaces B: Biointerfaces, 86(2), 339-344.

Lu, N., Dai, P., Gao, A., Valiaho, J., Kallio, P., Wang, Y., & Li, T. (2014a). Label-free and rapid electrical detection of hTSH with CMOS-compatible silicon nanowire transistor arrays. ACS Applied Materials & Interfaces, 6(22), 20378-20384.

Lu, N., Gao, A., Dai, P., Mao, H., Zuo, X., Fan, C., Wang, Y. & Li, T. (2015). Ultrasensitive detection of dual cancer biomarkers with integrated CMOS-compatible nanowire arrays. Analytical Chemistry, 87(22), 11203-11208.

Lu, N., Gao, A., Dai, P., Song, S., Fan, C., Wang, Y., & Li, T. (2014b). CMOS-compatible silicon nanowire field-effect transistors for ultrasensitive and label-free microRNAs sensing. Small, 10(10), 2022-2028.

Lundin, K. E., Højland, T., Hansen, B. R., Persson, R., Bramsen, J. B., Kjems, J., Koch, T., Wengel, J., & Smith, C. E. (2013). Biological activity and biotechnological aspects of locked nucleic acids. Advances in Genetics, 82, 47-107.

Mahdiannasser, M., & Karami, Z. (2018). An innovative paradigm of methods in microRNAs detection: highlighting DNAzymes, the illuminators. Biosensors and Bioelectronics, 107, 123-144.

Mannelli, I., Minunni, M., Tombelli, S., & Mascini, M. (2003). Quartz crystal microbalance (QCM) affinity biosensor for genetically modified organisms (GMOs) detection. Biosensors and Bioelectronics, 18(2-3), 129-140.

Mattos, A. B., Freitas, T. A., Silva, V. L., & Dutra, R. F. (2012). A dual quartz crystal microbalance for human cardiac troponin T in real time detection. Sensors and Actuators B: Chemical, 161(1), 439-446.

Meyer, V., Kober, C., Niessner, R., & Seidel, M. (2015). Regeneration of recombinant antigen microarrays for the automated monitoring of antibodies against zoonotic pathogens in Swine Sera. Sensors, 15(2), 2614-2628.

miRBase. The microRNA database. (May, 2019). Retrieved from: http://www.mirbase.org/

Mitchell, P. S., Parkin, R. K., Kroh, E. M., Fritz, B. R., Wyman, S. K., Pogosova-Agadjanyan, E. L., Peterson, A., Noteboom, J., O'Briant, K. C., Allen, A., Lin, D. W., Urban, N., Drescher, C. W., Knudsen, B. S., Stirewalt, D. L., Gentleman, R., Vessel-la, R. L., Nelson, P. S., Martin, D. B., & Tewari, M. (2008). Circulating microRNAs as stable blood-based markers for cancer detection. Proceedings of the National Academy of Sciences, 105(30), 10513-10518.

Moiseev, L., Ünlü, M. S., Swan, A. K., Goldberg, B. B., & Cantor, C. R. (2006). DNA conformation on surfaces measured by fluorescence self-interference. Proceed-ings of the National Academy of Sciences, 103(8), 2623-2628.

Nimse, S. B., Song, K., Sonawane, M. D., Sayyed, D. R., & Kim, T. (2014). Immobilization techniques for microarray: challenges and applications. Sensors, 14(12), 22208-22229.

Noor, M. O., & Krull, U. J. (2014). Silicon nanowires as field-effect transducers for biosensor development: A review. Analytica Chimica Acta, 825, 1-25.

Patel, S. S., & Donmez, I. (2006). Mechanisms of helicases. Journal of Biological Chemistry, 281(27), 18265-18268.

Patolsky, F., & Lieber, C. M. (2005). Nanowire nanosensors. Materials Today, 8(4), 20-28.

Patolsky, F., Zheng, G., Hayden, O., Lakadamyali, M., Zhuang, X., & Lieber, C. M. (2004). Electrical detection of single viruses. Proceedings of the National Academy of Sciences, 101(39), 14017-14022.

Peng, S., Gao, D., Gao, C., Wei, P., Niu, M., & Shuai, C. (2016). MicroRNAs regulate signaling pathways in osteogenic differentiation of mesenchymal stem cells. Molecular Medicine Reports, 14(1), 623-629.

Ramnani, P., Gao, Y., Ozsoz, M., & Mulchandani, A. (2013). Electronic detection of microRNA at attomolar level with high specificity. Analytical Chemistry, 85(17), 8061-8064.

Rayner, K. J., & Hennessy, E. J. (2013). Extracellular communication via microRNA: lipid particles have a new message. Journal of Lipid Research, 54(5), 1174-1181.

Rothberg, J.M., Hinz, W., Rearick, T.M., Schultz, J., Mileski, W., Davey, M., Leamon, J.H., Johnson, K., Milgrew, M.J., Edwards, M., Hoon, J., Simons, J.F., Marran, D., Myers, J.W., Davidson, J.F., Branting, A., Nobile, J. R., Puc, B. P., Light, D., Clark, T. A., Huber, M.,…, Bustillo, J. (2011). An integrated semiconductor device enabling non-optical genome sequencing. Nature, 475(7356), 348.

Salvi, G., De Los Rios, P., & Vendruscolo, M. (2005). Effective interactions be-tween chaotropic agents and proteins. Proteins: Structure, Function, and Bioinformatics, 61(3), 492-499.

Schenck, J. F. Field effect transistor for detection of biological reactions. U.S. Pa-tent 4, 238, 757, 1980.

Shakeel, S., Karim, S., & Ali, A. (2006). Peptide nucleic acid (PNA): a review. Journal of Chemical Technology & Biotechnology: International Research in Process, Environmental & Clean Technology, 81(6), 892-899.

Shen, W., Deng, H., Ren, Y., & Gao, Z. (2013). A label-free microRNA biosensor based on DNAzyme-catalyzed and microRNA-guided formation of a thin insulating polymer film. Biosensors and Bioelectronics, 44, 171-176.

Shirosaki, Y., Okayama, T., Tsuru, K., Hayakawa, S., & Osaka, A. (2013). In vitro bioactivity and MG63 cytocompatibility of chitosan-silicate hybrids. International Journal of Materials and Chemistry, 3, 1-7.

Sigma-Aldrich. (2019a). Oligonucleotide melting temperature. Retrieved from https://www.sigmaaldrich.com/technical-documents/articles/biology/oligos-melting-temp.html

Sigma-Aldrich. miRNA (microRNA) introduction. (2019b). Retrieved at: https://www.sigmaaldrich.com/life-science/functional-genomics-and-rnai/mirna/learning-center/mirna-introduction.html

Singh, R. P., Oh, B. K., & Choi, J. W. (2010). Application of peptide nucleic acid towards development of nanobiosensor arrays. Bioelectrochemistry, 79(2), 153-161.

Singleton, M. R., Dillingham, M. S., & Wigley, D. B. (2007). Structure and mechanism of helicases and nucleic acid translocases. Annu. Rev. Biochem., 76, 23-50.

Šípová, H., Zhang, S., Dudley, A. M., Galas, D., Wang, K., & Homola, J. (2010). Surface plasmon resonance biosensor for rapid label-free detection of microribonucleic acid at subfemtomole level. Analytical Chemistry 82(24), 10110-10115.

Stern, E., Wagner, R., Sigworth, F. J., Breaker, R., Fahmy, T. M., & Reed, M. A. (2007). Importance of the Debye screening length on nanowire field effect transistor sensors. Nano Letters, 7(11), 3405-3409.

Storey, N. (2009). Electronics: a systems approach, 4th ed. Pearson/Prentice Hall, New York; Harlow, England.

Syed, S. N., Schulze, H., Macdonald, D., Crain, J., Mount, A. R., & Bachmann, T. T. (2013). Cyclic denaturation and renaturation of double-stranded DNA by redox-state switching of DNA intercalators. Journal of the American Chemical Society, 135(14), 5399-5407.

Tedeschi, L., Citti, L., & Domenici, C. (2005). An integrated approach for the de-sign and synthesis of oligonucleotide probes and their interfacing to a QCM-based RNA biosensor. Biosensors and Bioelectronics, 20(11), 2376-2385.

Tedeschi, L., Domenici, C., Ahluwalia, A., Baldini, F., & Mencaglia, A. (2003). Antibody immobilisation on fibre optic TIRF sensors. Biosensors and Bioelectronics, 19(2), 85-93.

Tiller, J., Berlin, P., & Klemm, D. (1999). A novel efficient enzyme-immobilization reaction on NH2 polymers by means of L-ascorbic acid. Biotechnology and Applied Biochemistry, 30(2), 155-162.

Tsujiura, M., Ichikawa, D., Komatsu, S., Shiozaki, A., Takeshita, H., Kosuga, T., Konishi, H., Morimura, R., Deguchi, K., Fujiwara, H., & Okamoto, K., (2010). Circulating microRNAs in plasma of patients with gastric cancers. British Journal of Cancer, 102(7), 1174-1179.

Ulianas, A., Heng, L. Y., Ahmad, M., Lau, H. Y., Ishak, Z., & Ling, T. L. (2014). A regenerable screen-printed DNA biosensor based on acrylic microsphere–gold nanoparticle composite for genetically modified soybean determination. Sensors and Actuators B: Chemical, 190, 694-701.

Vandenberg, E. T., Bertilsson, L., Liedberg, B., Uvdal, K., Erlandsson, R., Elwing, H., & Lundström, I. (1991). Structure of 3-aminopropyl triethoxy silane on silicon oxide. Journal of Colloid and Interface Science, 147(1), 103-118.

Veigas, B., Fortunato, E., & Baptista, P. V. (2015). Field effect sensors for nucleic acid detection: recent advances and future perspectives. Sensors, 15(5), 10380-10398.

Wahid, F., Shehzad, A., Khan, T., & Kim, Y. Y. (2010). MicroRNAs: synthesis, mechanism, function, and recent clinical trials. Biochimica et Biophysica Acta (BBA)-Molecular Cell Research, 1803(11), 1231-1243.

Wang, J.H. (2012). Surface preparation techniques for biomedical applications. In Driver, M. (Ed.). In Coatings for biomedical applications. (pp. 144-175). Woodhead Publishing Limited, Cambridge, UK.

Wang, L., Feng, X., Hou, S., Chan, Q., & Qin, M. (2006). Microcontact printing of multiproteins on the modified mica substrate and study of immunoassays. Surface and Interface Analysis, 38(1), 44-50.

Wang, Q., Liu, R., Yang, X., Wang, K., Zhu, J., He, L., & Li, Q. (2016). Surface plasmon resonance biosensor for enzyme-free amplified microRNA detection based on gold nanoparticles and DNA supersandwich. Sensors and Actuators B: Chemical, 223, 613-620.

Wang, X., Lim, H. J., & Son, A. (2014). Characterization of denaturation and renaturation of DNA for DNA hybridization. Environmental Health and Toxicology, 29.

Wang, Z., Lee, S., Koo, K. I., & Kim, K. (2016). Nanowire-based sensors for bio-logical and medical applications. IEEE transactions on Nanobioscience, 15(3), 186-199.

Whang, D., Jin, S., Wu, Y., & Lieber, C. M. (2003). Large-scale hierarchical organization of nanowire arrays for integrated nanosystems. Nano letters, 3(9), 1255-1259.

Wu, Y. (2012). Unwinding and rewinding: double faces of helicase? Journal of Nucleic Acids.

Xu, S., Zhan, J., Man, B., Jiang, S., Yue, W., Gao, S., Guo, C. Liu, H., Li, Z., Wang, J. & Zhou, Y. (2017). Real-time reliable determination of binding kinetics of DNA hybridization using a multi-channel graphene biosensor. Nature Communications, 8, 14902.

Yang, G., Chang, Y., Yang, H., Tan, L., Wu, Z., Lu, X., & Yang, Y. (2009). The preparation of reagentless electrochemical immunosensor based on a nanogold and chitosan hybrid film for human chorionic gonadotrophin. Analytica Chimica Acta, 644(1-2), 72-77.

Yang, X., Gao, A., Wang, Y., & Li, T. (2018). Wafer-level and highly controllable fabricated silicon nanowire transistor arrays on (111) silicon-on-insulator (SOI) wafers for highly sensitive detection in liquid and gaseous environments. Nano Research, 11(3), 1520-1529.

Yao, C., Qi, Y., Zhao, Y., Xiang, Y., Chen, Q., & Fu, W. (2009). Aptamer-based piezoelectric quartz crystal microbalance biosensor array for the quantification of IgE. Biosensors and Bioelectronics, 24(8), 2499-2503.

Yildiz, U.H., Alagappan, P., & Liedberg, B. (2013). Naked eye detection of lung cancer associated miRNA by paper based biosensing platform. Analytical Chemistry, 85(2), 820–824.

Yin, H., Wang, M., Zhou, Y., Zhang, X., Sun, B., Wang, G., & Ai, S. (2014). Photoelectrochemical biosensing platform for microRNA detection based on in situ producing electron donor from apoferritin-encapsulated ascorbic acid. Biosensors and Bioelectronics, 53, 175-181.

Zhang, G. J. (2011). Silicon nanowire biosensor for ultrasensitive and label-free direct detection of miRNAs. Methods in Molecular Biology, 676, 111-121.

Zhang, G. J., Chua, J. H., Chee, R. E., Agarwal, A., & Wong, S. M. (2009). Label-free direct detection of MiRNAs with silicon nanowire biosensors. Biosensors and Bioelectronics, 24(8), 2504-2508.

Zhang, N., & Apella, D. H. (2010). Advantages of peptide nucleic acids as diagnostic platforms for detection of nucleic acids in resource-limited settings. Journal of Infectious Diseases, 201(Supplement_1), S42-S45.

Zhang, W. B., Zhong, W. J., & Wang, L. (2014). A signal-amplification circuit be-tween miR-218 and Wnt/β-catenin signal promotes human adipose tissue-derived stem cells osteogenic differentiation. Bone, 58, 59-66.

Zhang, X. Y., Zhang, L. D., Meng, G. W., Li, G. H., Jin-Phillipp, N. Y., & Phillipp, F. (2001). Synthesis of ordered single crystal silicon nanowire arrays. Advanced Materials, 13(16), 1238-1241.

Zhang, X., Dong, H., & Tian, Y. (2015). MicroRNA Detection and Pathological Functions. Springer, Berlin, Heidelberg.